Electrochemical Society

UNIV. OF MICHIGAN
APR 7 1954
EAST ENGINEERING
LIBRARY

UNIV. OF MICHIGAN
APR 7 1954

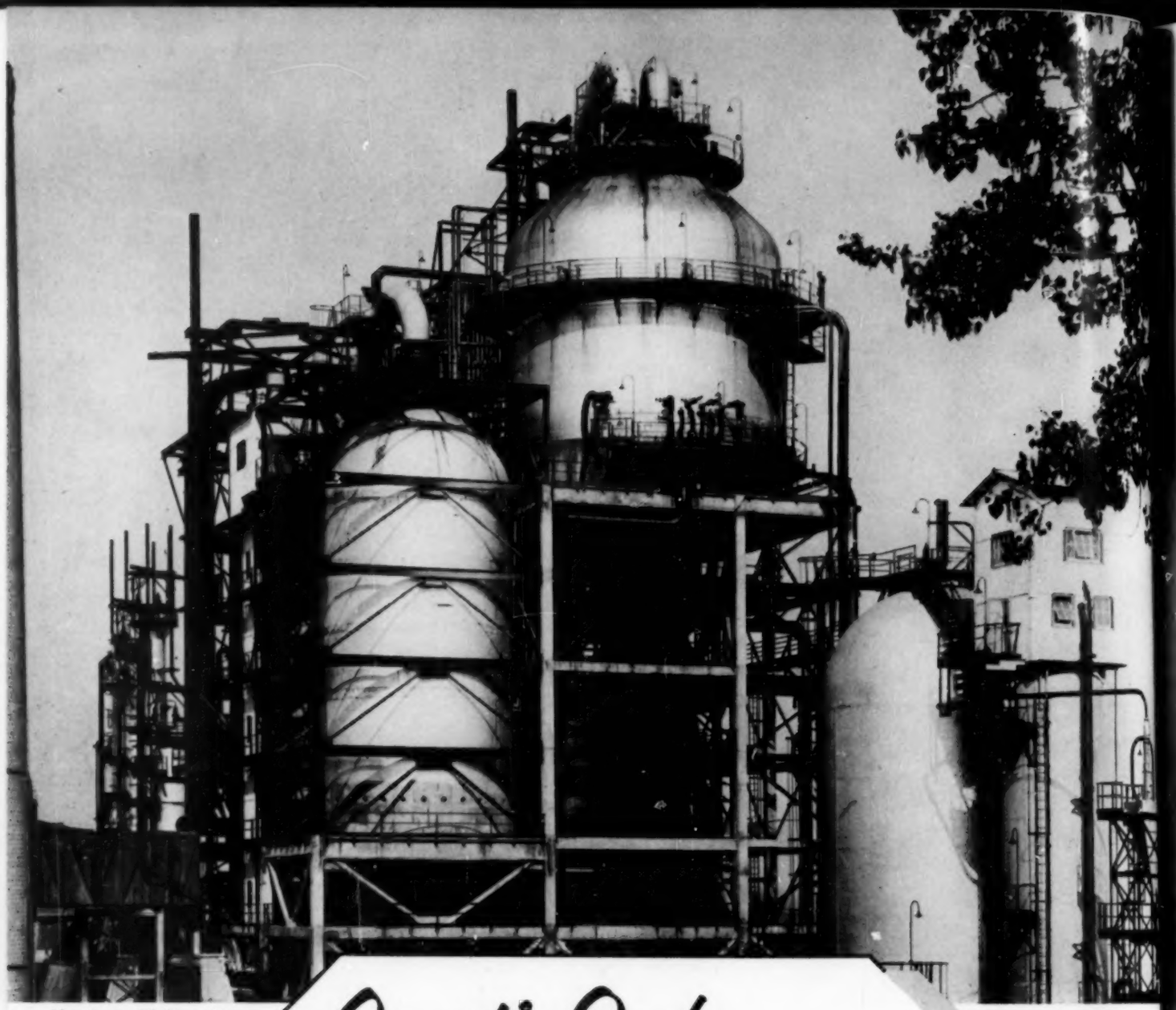

Photo Courtesy The Texas Company

Caustic Soda

. . . for the Petroleum Industry

Caustic Soda is an essential chemical used in petroleum refining.

Uniformly high quality GLC GRAPHITE ANODES are essential too—in helping the electrolytic industry meet the growing civilian and defense needs for caustic soda and chlorine.

ELECTRODE DIVISION

Great Lakes Carbon Corporation

Niagara Falls, N.Y. GLC Morganton, N. C.

Graphite Electrodes, Anodes, Molds and Specialties

Sales office: Niagara Falls, N.Y. **Other offices:** New York, N.Y., Oak Park, Ill., Pittsburgh, Pa.

Sales Agents: J. B. Hayes, Birmingham, Ala.; George O'Hara, Long Beach, Cal.; Great Northern Carbon & Chemical Co., Ltd., Montreal, Canada

Overseas Carbon & Coke Company, Inc., Geneva, Switzerland; Great Eastern Carbon & Chemical Co., Inc., Chiyoda-Ku, Tokyo

Rate of Oxidation of Three Nickel-Chromium Heater Alloys between 500° and 900°C[1]

EARL A. GULBRANSEN AND KENNETH F. ANDREW

Westinghouse Research Laboratories, East Pittsburgh, Pennsylvania

ABSTRACT

Rates of oxidation of three heater alloys of nominal composition 80% nickel-20% chromium were studied over the temperature range of 500° to 950°C and at a pressure of 7.6 cm of Hg of oxygen, using the vacuum microbalance method. Temper color films were obtained for all oxidations below 850°C, while gray or gray-green films were obtained at temperatures of 850°C and higher. No evidence was found for scaling or cracking of the oxide from the alloys on cooling at temperatures of oxidation up to 950°C.

The parabolic rate law was applied to the data. Reasonable agreement was found for temperatures above 650°C, while below this temperature the parabolic rate law constant varied with time. This time variation was explained in terms of composition changes in the oxide and growth of the oxide crystallite size.

The classical theory of diffusion was used to interpret effect of temperature on rate of oxidation, and heats, entropies, and free energies of activation for the over-all reaction were evaluated from the data.

Heats of activation varied from 38,150 cal/mole for alloy 12046 to 51,400 cal/mole for alloy 13246, while the entropies of activation varied from −15.8 entropy units (eu) for alloy 12046 to −3.5 eu for alloy 13246. On an absolute basis, alloy 12246 had the slowest rate of attack with oxygen under the given conditions. This was not in agreement with the results of A.S.T.M. life tests.

When compared to other metals, chromium reacted 4.1 times and nickel 12.6 times as fast with oxygen as alloy 13246.

Calculations were made on the entropy of vacancy formation assuming that the reaction follows a mechanism of positive ion diffusion through vacancies created by the solution of oxygen at the oxide-gas interface. This gives an entropy term of −7.5 eu which partially accounts for the negative entropy of activation observed. Agreement of the theoretical rate of reactions with experiment was within a factor of 10 for all of the alloys. This difference is discussed briefly.

INTRODUCTION

The high resistance to oxidation of the 80% nickel-20% chromium series of heater alloys is well known. One of the interesting developments in this series of alloys over the past 30 years has been the improvement in performance in cyclic oxidation tests. This is a result of changing the manganese and silicon contents as well as a result of addition of small quantities of zirconium, calcium, aluminum, cerium, etc., to the alloy. In spite of the great technical importance, no adequate scientific explanations have been put forward.

In a recent series of papers (1, 2, 3) from these laboratories, a systematic study was made of the crystal structures of oxide films using x-ray and electron diffraction methods on eight alloys of this nominal composition. It was shown that crystal structures of oxide films were a function of time and temperature of oxidation and the composition of the alloy, if manganese was present. For this series of alloys there appeared no direct correlation between performance in cyclic oxidation tests and composition and crystal structure of the oxide film.

It is the purpose of this paper to study the rate of oxidation of three alloys of the 80% nickel-20% chromium composition as a function of time and temperature and to relate the data to the parabolic rate law and the classical theory of diffusion.

Literature

No published work has been reported on the rate of oxidation of the 80% nickel-20% chromium alloys. Scheil and Kiwit (4) studied the oxidation of a series of iron-nickel-chromium alloys. They find the best alloys were characterized by presence of a scale of Cr_2O_3 alone, while poorer alloys gave scales characterized by the presence of oxides of iron. Lustman (2) subjected a series of 80% nickel-20% chromium alloys to cyclic as well as constant temperature oxidation tests at 1175°C. Continuous oxidation tests showed little difference in oxidation rates, while A.S.T.M. life tests showed a sixfold

[1] Manuscript received April 6, 1953. This paper was prepared for delivery before the Wrightsville Beach Meeting, September 13 to 16, 1953.

variation. Cyclic oxidation tests showed a fair correlation with A.S.T.M. useful life tests.

The A.S.T.M. useful life test (5) is a cyclic test conducted on wire specimens in air atmosphere at 1175°C. Useful life is defined as the time required for a 10% change in the electrical resistance of the wire.

The effect of minor constituents on lifetime tests has been described by Hessenbruch (6). The effect of small quantities of magnesium, calcium, zirconium, cerium, thorium, of the order of 0.1% or less, was to greatly improve the performance.

In a recent work, Buckle, Jacquet, and Poulignier (7) applied metallographic and oxidation studies to the determination of service temperatures of 80 nickel-20 chromium alloy turbine blades. Details of this study are not available to date.

Thermodynamic Predictions

Gulbransen and McMillan (3) considered in detail the thermodynamic equilibria of several surface reactions occurring on nickel-chromium alloys. Six types of reactions were shown to occur. These were: (*a*) direct oxidation of the several metal components, (*b*) solid phase reactions of one oxide with another metal, (*c*) formation of spinels with either Cr_2O_3 or Fe_2O_3, (*d*) formation of silicates between the oxides and SiO_2, (*e*) reaction of carbon from the metal with the surface oxide to form CO and reduced metal and, (*f*) vaporization of the metals.

Calculations showed that all oxides of the major and minor components of the alloy were stable to direct decomposition up to 1200°C, except in neutral or reducing atmospheres. Solid phase reactions of NiO with Cr, Si, Mn, and Ca were possible at all temperatures. Spinels could form between NiO, MnO, FeO and Cr_2O_3 and Fe_2O_3 but not with CaO and SiO_2. Reaction of carbon in the alloy with NiO was feasible at temperatures above 975°C. Formation of silicates was possible, while vaporization became important only at the higher temperatures under vacuum or inert and reducing atmospheres.

Gulbransen and McMillan (3) also considered the effect of minor components on composition and physical properties of the oxide and oxide-alloy interface.

Experimental

Method

A vacuum microbalance was used for all rate measurements. Its construction and use have been described (8, 9). The 0.0127-cm thick specimens have surface areas of 14 cm^2 and weigh 0.6840 gram. Sensitivity of the balance was 1 division (0.001 cm) per microgram and the weight change was estimated to ¼ of a division (0.25×10^{-6} gram).

Auxiliary apparatus containing the balance and specimen was evacuated to 10^{-6} mm of Hg or better. A quartz or mullite furnace tube (10) was used to contain the specimen and was sealed directly to the Pyrex glass apparatus.

Other auxiliary apparatus was used for the preparation of pure hydrogen and oxygen (8). Weight change during reaction was followed by observing a pointer on the balance beam by means of a micrometer microscope. Readings of the balance were taken in vacuo before reaction at the temperature, during the reaction in oxygen, and after the reaction in vacuo.

Samples

Specimens used in this study were specially prepared, analyzed chemically and spectrographically, the useful life tested, and were made available to us by the Driver Harris Company. The three alloys represent a 30-year improvement in the technology of heater alloy preparation. Alloy 12046 represents a modern high life heater alloy. Table I shows analyses of samples together with A.S.T.M. life tests.

Specimens were given the following surface preparation. Portions of the strip were abraded starting with number 1 grit paper and finishing through 4/0 paper. The last stage was carried out under purified kerosene to avoid oxidation. After abrading, samples were cleaned with soap and water, distilled water, petroleum ether, absolute alcohol, and stored in a dessicator.

A number of specimens were given an additional treatment by heating in hydrogen at 900°C for one-half hour before reacting with oxygen.

TABLE I. *Composition and life tests, nickel-chromium alloys*

Alloy	Composition %										Useful life (hr)	Test temp, °C
	C	Mn	Si	Cr	Ni	Fe	Zr	Ca	Mg	Al		
12046 New Ni-Cr Alloy V	0.08	0.01	1.39	19.91	Bal.	0.34	0.10	0.024		0.07	157	1175
12246 Old Ni-Cr Alloy V	0.08	0.01	0.30	19.98	Bal.	0.32	0.05	0.029		0.08	86	1175
13246 Old Ni-Cr Alloy V	0.12	1.70	0.30	19.98	Bal.	0.20	—		0.006		25	1175

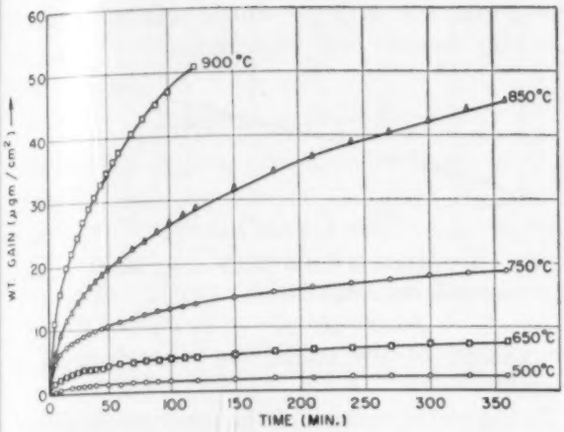

FIG. 1. Effect of temperature oxidation of 12046 Ni-Cr alloy, 7.6 cm of Hg of O_2 abraded through 4/0.

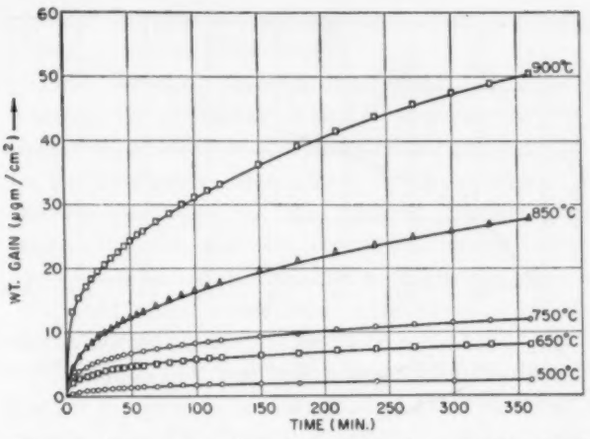

FIG. 2. Effect of temperature oxidation of 12246 Ni-Cr alloy, 7.6 cm of Hg of O_2 abraded through 4/0.

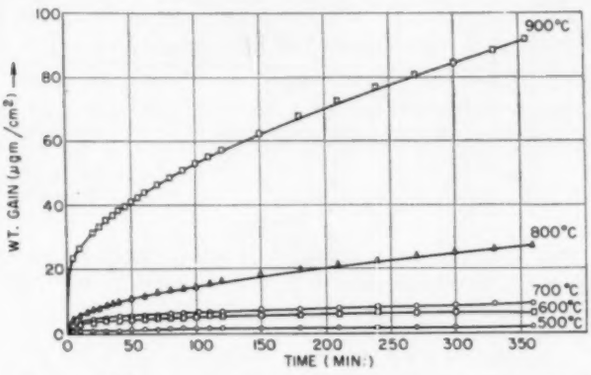

FIG. 3. Effect of temperature oxidation of 13246 Ni-Cr alloy, 7.6 cm of Hg of O_2 abraded through 4/0.

RESULTS

The reaction with oxygen was studied as a function of time and temperature and results are shown in Fig. 1 to 3. An oxygen pressure of 7.6 cm of Hg was used for all experiments. The weight change was plotted in $\mu g/cm^2$. The thickness of the resulting oxide in Angstroms was calculated from the crystal structure or density assuming a surface roughness ratio of unity. For Cr_2O_3 the relation was 1 $\mu g/cm^2$ equals 61 Å. However, other oxides observed in the film would have different thickness values per microgram of oxygen reacted. For purposes of convenience the value for Cr_2O_3 was used in this paper.

Time and Temperature

Fig. 1 to 3 show effect of time and temperature on the rate of oxidation for the three alloys over the temperature range of 500° to 900°C. Most of the experiments were run for a total of six hours. Thirty-hour experiments were made at the lower temperatures to test the variation of the parabolic rate law constant with time.

For all of the curves a rapid pickup of oxygen occurs in the first few minutes with the rate decreasing as the film thickens. Similar curves were found for other metals (11, 12).

Table II shows oxide film thickness vs. oxide

TABLE II. *Oxide film thickness vs. oxide color*

7.6 cm of Hg of O_2, 6 hr of reaction except where noted

Temp	Alloy 12046			Alloy 12246			Alloy 13246		
	Thickness		Color	Thickness		Color	Thickness		Color
	$\mu g/cm^2$	Å($\rho = 1$)		$\mu g/cm^2$	Å($\rho = 1$)		$\mu g/cm^2$	Å($\rho = 1$)	
450	2.48	152	Lt. straw						
500	6.2[a]	378	Pink	5.9[a]	360	Pink	4.56[a]	278	Pink
550	5.13	312	Straw	5.45	332	Pink	6.50[a]	396	Dk. blue
600	11.5[a]	701	Blue	8.86	540	Dark blue	8.01	490	Dk. blue
650	9.73	594	Blue	10.3	629	Blue	12.69[a]	774	Lt. blue
700							12.9	786	Lt. blue
750	20.6	1260	Straw	15.5	945	Straw-green	19.7	1200	Straw
800				22.6	1380	Straw-pink	31.2	1905	Green
850	50.4	3080	Gray	32.6	1990	Gray-green	58.1	3550	Gray
900	55.5	3380	Gray	50.4[b]	3065	Gray	92.1	5610	Gray

Lt.—light.
[a] 30-hr test.
[b] 2-hr test.

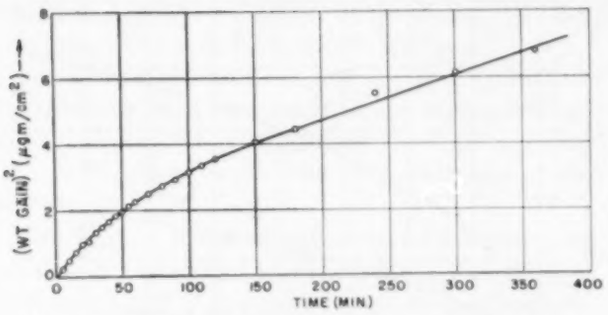

FIG. 4. Oxidation of 12246 Ni-Cr alloy, 500°C, 7.6 cm of Hg of O_2. Parabolic plot: 1–2 hr $K = 3.75 \times 10^{-16}$; 3–6 hr $K = 2.27 \times 10^{-16}$.

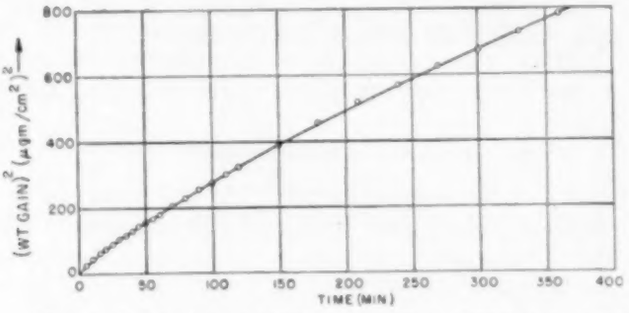

FIG. 5. Oxidation of 12246 Ni-Cr alloy, 850°C, 7.6 cm of Hg of O_2. Parabolic plot: 1–2 hr $K = 4.055 \times 10^{-14}$; 3–6 hr $K = 3.14 \times 10^{-14}$.

color for the three alloys as a function of temperature. Two series of temper colors were observed on the alloys. For alloy 12046, the first straw color was found at a thickness of 152 Å. This color appeared to be present also at a thickness of 312 Å. A second straw color was noted at 1260 Å. Above 2000 Å, all of the oxides were gray or green-gray. All of the oxides formed in this study were stable to cracking on cooling the alloy to room temperature. It should be noted that the temper colors produced were not only a function of the temperature but also of the time of oxidation and the composition of the alloy.

A comparison at 900°C of the total extent of oxidation showed alloy 12246 as the most resistant to oxidation. However, the differences between the rates of reaction of the three alloys were not large.

Parabolic Rate Law

Although many empirical rate laws have been suggested to explain the effect of time on the rate of oxidation, the parabolic rate law (13, 14) has been the most successful since its derivation was based on principles of formation and diffusion of ions in the oxide (14). The equation states $W^2 = Kt + C$. Here W is the weight gain, t is the time, and K and C are constants.

It was not expected that this rate law should hold for the initial part of the reaction or where the

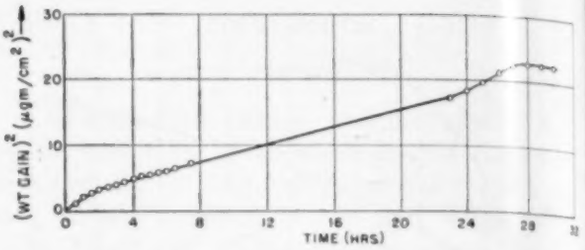

FIG. 6. Oxidation of 12046 Ni-Cr alloy, 500°C, 7.6 cm of Hg of O_2 abraded through 4/0.

composition of the oxide film was changing appreciably.

To test the agreement of the experiments with the parabolic rate law, plots were made of the square of the weight gain vs. time. Fig. 4 and 5 show two such plots for alloy 12246 at 500° and 850°C, respectively. It was noted that the slope of the plot decreases rapidly with time for the first two hours of reaction at 500°C and that there was a smaller change at 850°C. Decrease in value of the parabolic rate law constant K with time is illustrated in the captions on the figures for the 1–2 hr and 3–6 hr time periods. Larger changes in the value of K were noted if the initial slope at time zero was compared to the 24–30 hr value.

Fig. 6 shows a parabolic rate law plot for the oxidation of alloy 12046 at 500°C for 30 hr. For this experiment the parabolic rate law constant K (slope of plot) was essentially constant between 4 hr and 22 hr of reaction. The value of K then increased and levelled off to zero value. In several experiments on other alloys, a weight loss after 28 hr of reaction was actually observed. This type of behavior is similar to the first stage of a stepwise oxidation process observed by Caplan and Cohen (15) in a study of the oxidation of iron-chromium alloys.

Levelling off of the rate of reaction shown in Fig. 6 could be explained by a change in the composition of the oxide film. Gulbransen and McMillan (3) noted from electron diffraction studies that NiO was the oxide formed after a two-hour oxidation, while Cr_2O_3 was found after a thirty-hour oxidation.

The strong dependence of the parabolic rate law constant K on the time of oxidation, as shown in Fig. 4 and 6, was probably due to two factors: (*a*) a process of composition change, and (*b*) a growth in the crystallite size of oxide particles. This latter effect has been discussed in detail in another work (16). In brief, the argument was that diffusion occurred for an oxide film of small crystallites at the grain boundaries, while for larger crystallites this grain boundary area was small and diffusion occurred throughout the crystal lattice.

The parabolic rate law could be fitted approximately to the data above a temperature of 650°C,

while below this temperature it was not possible to make a reasonable fit for reasons previously noted.

Temperature Dependence

In earlier papers the authors have used the transition rate law theory (17) and the classical expression for the diffusion coefficient as expressed by Zener (18) to interpret the parabolic rate law (19). In the latter treatment the parabolic rate law constant was given by the expression

$$K = 2\gamma\nu a^2 e^{\left(\frac{\Delta S^\circ}{8/3} + \Delta S^*\right)/R} e^{-\left(\frac{\Delta H^\circ}{8/3} + \Delta H^*\right)/RT}$$

Here $\frac{\Delta S^\circ}{8/3}$ and $\frac{\Delta H^\circ}{8/3}$ are the entropy and heat of formation of the vacancies, while ΔS^* and ΔH^* are the entropy and heat of activation of diffusion, a is the interatomic distance between diffusion sites, ν is the frequency of vibration along the direction across the saddle configuration, R is the gas constant, T is the temperature, and γ a coefficient determined by the geometry of the atomic jumps. K has the units of $cm^2\ sec^{-1}$.

To evaluate ν and γ it was necessary to assume a particular oxide and a mechanism for diffusion. According to the recent work of Gulbransen and McMillan (3), Cr_2O_3 was the predominant oxide on alloys 12046 and 12246 while $MnO \cdot Cr_2O_3$ was found on alloy 13246. Since the parabolic rate law holds only above 650°C, the appearance of NiO at lower temperatures was not of concern.

Before assuming a mechanism of diffusion, consider the details of the Cr_2O_3 structure. Cr_2O_3 has the rhombohedral structure (20) with $a = 5.38$ Å and $\alpha = 54.83$. The oxygens are in approximately close-packed hexagonal array with Cr ions occupying two-thirds of available octahedral holes, i.e., sandwiched between planes of oxygens. The octahedral holes are situated in chains running vertically through the structure along [111], and along each chain is a succession Cr, Cr, hole, Cr, Cr, hole. In the horizontal metal atom planes, i.e., odd numbered (444) planes 1, 3, 5, etc., the metal atoms are slightly above or below the plane and the empty holes lie in these planes. Therefore, filled and unfilled holes form puckered sheets.

Each Cr has in its own puckered horizontal plane 3 Cr neighbors at 2.921 Å and 3 unfilled holes at 2.876 Å. Each Cr has either above or below it 1 Cr neighbor at 2.871 Å and either below or above it 1 unfilled hole at 1.982 Å. The easiest movement for a Cr is to the empty hole either above it or below it at only 1.982 Å. Movement horizontally to the three holes at 2.876 Å is more difficult because of the increased distance and because two barriers of oxygen triangles must be penetrated, while the vertical movement requires only the penetration of one set of oxygen triangles.

This structure makes it difficult to evaluate precisely the geometry of atomic movements during oxidation as well as the distance moved per jump. In the evaluation of ν and γ it was assumed that the ν's are equal for the various possible atomic jumps, that the distance between Cr atoms is equal, and that a random distribution of Cr atoms occurs in the structure. On this basis the average value for γ was calculated to be ¼.

The value of a was taken as 2.9 Å. This could be high if diffusion occurs largely at the short spacing between the Cr atoms and the unoccupied position adjacent to it in the C direction.

The value of ν was calculated from the characteristic Debye temperature, $\theta_D = h\nu_m/k$ (19). ν_m is the maximum allowed frequency, h is Planck's constant, and k is Boltzmann's constant. θ_D for Cr_2O_3 was 362. To estimate the frequency ν_{Cr} along the path of the reaction, two fundamental relationships were used:

$$\nu = \frac{1}{2\pi}\sqrt{\frac{f}{m}} \qquad \text{(I)}$$

$$\nu_{max} = \sqrt{\nu_{Cr} \cdot \nu_0} \qquad \text{(II)}$$

The first equation relates the frequency, the force constant f, and the mass of the atom, while

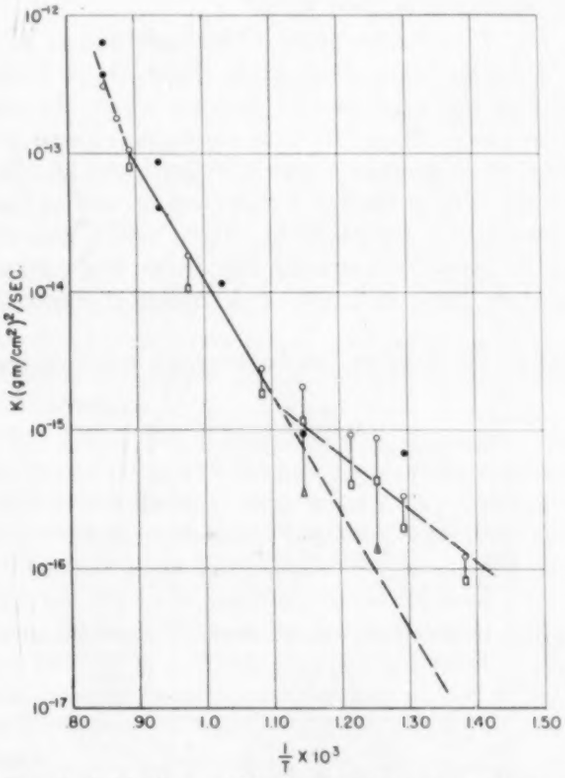

FIG. 7. Oxidation of 12046 Ni-Cr alloy, log plot K vs. $1/T \times 10^3$. ○ = 1–2 hr; □ = 3–6 hr; △ = 24–30 hr; ● = H_2 pretreated 30 min, 900°C, 1–2 hr; $\Delta H^* = 38{,}150$ cal/mole.

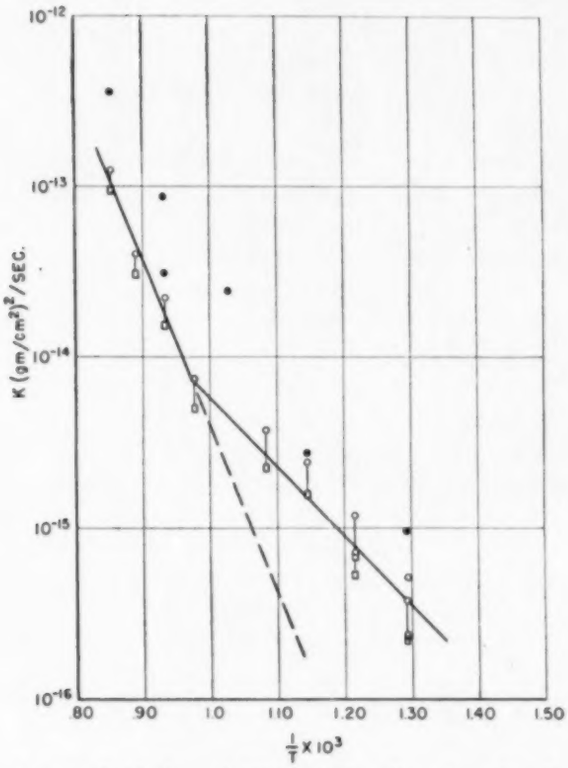

FIG. 8. Oxidation of 12246 Ni-Cr alloy, log plot K vs. $1/T \times 10^3$. ○ = 1–2 hr; □ = 3–6 hr; ● = H_2 pretreated 30 min, 900°C, 1–2 hr; $\Delta H^* = 44{,}400$ cal/mole.

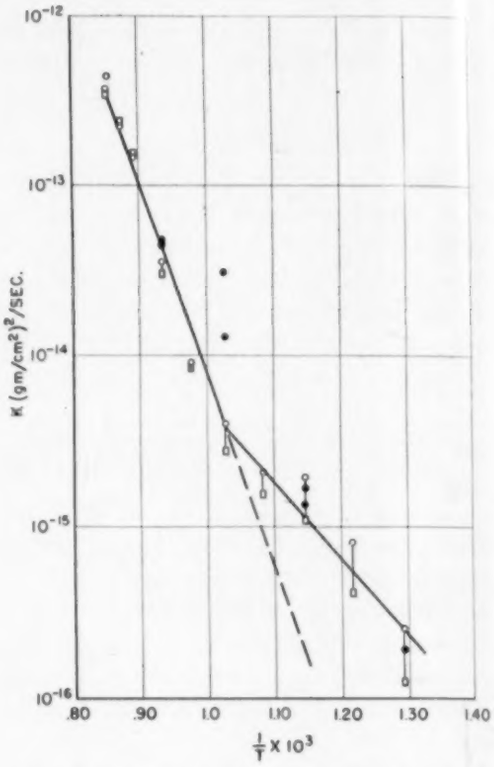

FIG. 9. Oxidation of 13246 Ni-Cr alloy, log plot K v $1/T \times 10^3$. ○ = 1–2 hr; □ = 3–6 hr; ● = H_2 pretreated min, 900°C, 1–2 hr; $\Delta H^* = 51{,}400$ cal/mole.

the second equation relates the maximum value of ν to the maximum values of ν for the atoms. ν_{Cr} was calculated to be 5.66×10^{12}.

Fig. 7 to 9 show plots of the logarithm of K vs. $1/T$ for the three alloys while Tables III to V show part of the experimental data on which the plots were made. Since the rate constants change with time, these constants were calculated and tabulated for the time periods of 1–2 hr, 3–6 hr, and at lower temperatures for 24–30 hr. Above 650°C the data can be fitted by a straight line; below this temperature the time variation of K makes it impossible to determine the slope. It may be noted that the values of K determined in the range of 24–30 h approach values given by the extrapolation of the straight line relationship. The deviation of data below 650°C from the parabolic rate law has been discussed in a previous section.

Table VI shows a summary of the experimental heats, entropies, and free energies of activation for the three alloys. In addition, the calculated value for entropy of activation of diffusion was tabulated. This is discussed in the next section. Using free energy of activation as a basis for comparison

TABLE III. *Parabolic rate law constants, entropies, heats, and free energies of activation for oxidation of 12046* Ni-Cr alloy

Temp, °C	K(1–2 hr) $(g/cm^2)^2/sec$	K(3–6 hr) $(g/cm^2)^2/sec$	K(avg) $(g/cm^2)^2/sec$	ΔS^* cal/mole/°C	ΔH^* cal/mole	$-T\Delta S^*$ cal/mole	ΔF^* cal/mole
650	2.78×10^{-15}	1.85×10^{-15}	2.315×10^{-15}	−15.7	38150	−14500	52650
750	1.832×10^{-14}	1.092×10^{-14}	1.462×10^{-14}	−16.2	38150	−16600	54750
850	1.082×10^{-13}	8.15×10^{-14}	9.485×10^{-14}	−15.8	38150	−17750	55900
875	1.805×10^{-13}	—	1.805×10^{-13}	−15.1	38150	−17300	55450

TABLE IV. *Parabolic rate law constants, entropies, heats, and free energies of activation for the oxidation of 12246* Ni-Cr alloy

Temp, °C	K(1–2 hr) $(g/cm^2)^2/sec$	K(3–6 hr) $(g/cm^2)^2/sec$	K(avg) $(g/cm^2)^2/sec$	ΔS^* cal/mole/°C	ΔH^* cal/mole	$-T\Delta S^*$ cal/mole	ΔF^* cal/mole
750	7.5×10^{-15}	4.90×10^{-15}	6.2×10^{-15}	−11.7	44400	−11980	56380
800	2.25×10^{-14}	1.573×10^{-14}	1.913×10^{-14}	−11.5	44400	−12300	56700
850	4.055×10^{-14}	3.14×10^{-14}	3.598×10^{-14}	−12.1	44400	−13600	58000
900	1.259×10^{-13}	9.43×10^{-14}	1.104×10^{-13}	−11.6	44400	−13600	58000

TABLE V. *Parabolic rate law constants, entropies, heats, and free energies of activation for the oxidation of 13246* Ni-Cr *alloy*

Temp. °C	K (1–2 hr) $(g/cm^2)^2/sec$	K (3–6 hr) $(g/cm^2)^2/sec$	K (avg) $(g/cm^2)^2/sec$	ΔS^* cal/mole/°C	ΔH^* cal/mole	$-T\Delta S^*$ cal/mole	ΔF^* cal/mole
700	4.0×10^{-15}	2.78×10^{-15}	3.39×10^{-15}	−3.5	51400	−3400	54800
750	9.16×10^{-15}	8.8×10^{-15}	8.98×10^{-15}	−4.26	51400	−4360	55760
800	3.52×10^{-14}	3.025×10^{-14}	3.273×10^{-14}	−4.04	51400	−4340	55740
850	1.185×10^{-13}	1.332×10^{-13}	1.259×10^{-13}	−3.46	51400	−3900	55300
850	1.46×10^{-13}	1.54×10^{-13}	1.50×10^{-13}	−2.92	51400	−3280	54680
875	1.805×10^{-13}	2.28×10^{-13}	2.043×10^{-13}	−3.37	51400	−3860	55260
875	2.22×10^{-13}	2.38×10^{-13}	2.30×10^{-13}	−3.14	51400	−3600	55000
900	2.565×10^{-13}	2.92×10^{-13}	2.743×10^{-13}	−3.80	51400	−4460	55860
900	3.70×10^{-13}	3.6×10^{-13}	3.65×10^{-13}	−3.22	51400	−3780	55180

TABLE VI. *Comparison of the parabolic rate law constants and heats, entropies, and free energies of activation at 850°C*

	12046	12246	13246
K cm²/sec	3.525×10^{-14}	1.339×10^{-14}	4.67×10^{-14}
ΔH^* cal/mole	38150	44400	51400
ΔS^* cal/mole/deg	−15.8	−12.1	−3.46
ΔF^* cal/mole	55900	58000	55300
ΔS_D^* cal/mole/deg	−8.4	−4.7	+3.9

alloys, it is seen that alloy 12246 shows a lower rate of reaction than the other alloys. Alloys 12046 and 13246 were approximately equal in their over-all performance although entropies and heats of activation differ appreciably.

Table VII shows a comparison of the heats, entropies, and free energies of activation for chromium, nickel, and alloy 13246. Chromium reacts 4.1 times and nickel 12.6 times as fast as alloy 13246.

Effect of Hydrogen Pretreatment

A number of the specimens were heated to 900°C and given a pretreatment in 2.4 cm of purified hydrogen for 30 min before reacting with oxygen at 7.6 cm of Hg of O_2 at the given temperatures. Parabolic rate law constants are plotted in Fig. 7 to 9. Results are in good agreement with results from abraded samples for alloy 12046 and, with some exceptions, agreement was good for alloy 13246. Somewhat higher rates of reaction were found for the hydrogen pretreated specimens for alloy 12246.

TABLE VII. *Comparison of the parabolic rate law constants and heats, entropies, and free energies of activation at 700°C*

	Cr	Ni	13246
K cm²/sec	2.38×10^{-14}	2.06×10^{-13}	1.261×10^{-15}
ΔH^* cal/mole	70,400	41,200	51,400
ΔS^* cal/mole/deg	22.0	−6.0	−3.50
ΔF^* cal/mole	49,000	47,040	54,800

THEORETICAL

The experimental entropy of activation is made up of two terms: (*a*) entropy of formation of vacancies, and (*b*) entropy of activation of diffusion. Theoretical and experimental studies by Zener have shown that the entropy of activation of diffusion should be positive. In a previous paper (19) calculations were made for the oxidation of nickel and these verified Zener's prediction. The essential problem was to evaluate the entropy of vacancy formation.

To make these calculations for the nickel-chromium alloys, assume that diffusion in Cr_2O_3 occurs through cation vacancies. These form by the reaction

$$\tfrac{1}{2}\,O_2 \rightleftarrows \tfrac{2}{3}\,\square_c + 2\oplus + O^{=}$$

Here $\square_c$ refers to the cation vacancy, $\oplus$ to the positive electron hole, and $O^{=}$ to the oxygen ion in the Cr_2O_3 structure.

Change in entropy can be calculated from the entropy of ½ mole of O_2 gas and 1 mole of $O^{=}$ in the Cr_2O_3 lattice and from the entropy change of distortion of the Cr_2O_3 structure due to the formation of positive holes and cation vacancies. Following the methods of a previous paper (19), we assume the entropy of the oxygen ions in Cr_2O_3 to be ⅕ of the molal entropy.

Since Cr_2O_3 has a rhombohedral structure, the authors have not attempted to calculate the entropy of distortion. Instead, they assume the distortion entropy changes associated with the NiO lattice. For NiO, an entropy of distortion of −1.34 cal/deg was calculated for each mole of cation vacancies and −0.47 cal/deg for each mole of positive holes. Since only ⅔ of a cation vacancy is formed in the reaction, total entropy of distortion is −1.8 cal/deg. Therefore, at 1000°K entropy change of condensation of ½ mole of O_2 and the formation of ⅔ mole of vacancies and 2 moles of positive holes at particular lattice sites in a large amount of Cr_2O_3 is $-(29.10 - 10.8 + 1.8) = -20.1$.

Since $2\frac{2}{3}$ defects are formed, entropy change per defect is -7.5 cal/mole/deg.

Since the entropy of activation term in the rate expression is made up of two terms, the entropy of formation of vacancies and the entropy of activation of diffusion, it is possible to evaluate the latter term. These values are tabulated in Table VI.

Alloy 13246 gave a positive entropy of activation for diffusion which agrees with theoretical predictions (18). However, alloy 12246 and 12046 gave negative values of -4.8 and -8.5 eu, respectively. Experimental errors in the determination of ΔH^* from the data may lead to errors in ΔS^* of diffusion of ± 2. In addition, until the details of the mechanism of diffusion can be given, the values of a, ν, and γ may be in error. In this interpretation, these errors would show up in the entropy term and may lead to errors of ΔS^* of diffusion of ± 2. The over-all error in ΔS^* was of the order of ± 4.

In addition to these errors in the picture of diffusion and in the evaluation of ΔH^*, several other factors are of importance. First, the mechanism of vacancy formation is influenced by alloying elements and impurities which leads to different values for the entropy of vacancy formation. Second, the oxide was not Cr_2O_3 alone but a segregated mixture with SiO_2, CaO, etc. Third, grain boundary diffusion phenomena may be of importance in this system. These effects would give in the correlation made here negative entropies of diffusion since all of the deviations from theory were thrown into the entropy term.

At present it is impossible to make a complete theoretical interpretation of the entropy term. It may be noted, however, that on an absolute basis the agreement of theory with the experimental rate is within a factor of ten for all of the alloys.

From a technical point of view, it is of interest to compare the results with the useful life test data. In this study alloy 12246 showed the lowest oxidation rate at constant temperature, while useful life tests showed alloy 12046 was superior. This has been discussed by Gulbransen and McMillan (3) in a recent paper. They conclude that performance in useful life tests was not a measure of normal oxidation processes alone but of resistance to cracking of the oxide from the alloy.

Any discussion of this paper will appear in a Discussion Section to be published in the December 1954 issue of the JOURNAL.

REFERENCES

1. J. W. HICKMAN AND E. A. GULBRANSEN, *Trans. Am. Inst. Mining Met. Engrs.*, **180**, 519 (1949).
2. B. LUSTMAN, *ibid.*, **188**, 995 (1950).
3. E. A. GULBRANSEN AND W. R. MCMILLAN, *Ind. Eng. Chem.*, **45**, 1734 (1953).
4. E. SCHEIL AND K. KIWIT, *Arch. Eisenhüttenw.*, **9**, 405 (1935–6).
5. F. E. BASH AND J. W. HARSCH, *Am. Soc. Testing Materials, Proc.*, **29**, Pt. II, 506 (1929).
6. W. HESSENBRUCH, "Metalle und Legierungen fur hohe Temperaturen," Julius Springer, Berlin (1940).
7. C. BUCKLE, P. JACQUET, AND J. POULIGNIER, Abstract of paper delivered to 1952 Autumn Meeting of the Societe Francaise de Metallurgie.
8. E. A. GULBRANSEN, *Trans. Electrochem. Soc.*, **81**, 187 (1942).
9. E. A. GULBRANSEN, *Rev. Sci. Instr.*, **15**, 201 (1944).
10. E. A. GULBRANSEN AND K. F. ANDREW, *Ind. Eng. Chem.*, **41**, 2762 (1949).
11. E. A. GULBRANSEN AND K. F. ANDREW, *This Journal*, **97**, 383 (1950).
12. E. A. GULBRANSEN AND K. F. ANDREW, *ibid.*, **98**, 241 (1951).
13. N. B. PILLING AND R. E. BEDWORTH, *J. Inst. Metals*, **29**, 529 (1923).
14. N. F. MOTT, *Trans. Faraday Soc.*, **36**, 472 (1940).
15. D. CAPLAN AND M. COHEN, *J. Metals*, **4**, 1057 (1952).
16. E. A. GULBRANSEN, Proceedings Gothenburg International Conference on Solid State Reactions, 1952, to be published.
17. E. A. GULBRANSEN, *Trans. Electrochem. Soc.*, **83**, 301 (1943).
18. C. ZENER, *J. Appl. Phys.*, **22**, 372 (1951).
19. E. A. GULBRANSEN AND K. F. ANDREW, *This Journal*, **101**, 128 (1954).
20. R. W. G. WYCKOFF, "Crystal Structures," Interscience Publishers, Inc., New York (1951).

Surface Reaction between Oxygen and Thorium[1]

A. F. Gerds and M. W. Mallett

Battelle Memorial Institute, Columbus, Ohio

ABSTRACT

The rate of reaction of oxygen with arc-melted and rolled iodide thorium has been found to obey the parabolic rate law in the temperature range of 850° to 1415°C at 1 atm pressure. The rate constant can be expressed as $k = 5.5 \times 10^7 e^{-62,800/RT}$ $(ml/cm^2)^2/sec$. The energy of activation, 62,800 cal/mole, has a probable error of 2400 cal/mole.

Introduction

Reactions between gases and metals generally have been found to obey a linear, parabolic, cubic, or logarithmic rate law. Factors controlling the various laws as well as their derivations have been adequately described in the literature (1–7) and are, therefore, not repeated here.

Levesque and Cubicciotti (8) studied the oxidation of thorium at 45 cm pressure in the temperature range of 250° to 700°C. They found the reaction to proceed in accordance with the parabolic rate law between 250° and 350°C and calculated the energy of activation to be 31,000 cal/mole. Between 350° and 450°C, the rates of oxidation were reported to be linear with time. An energy of activation of 22,000 cal/mole was found for this temperature range. Above 450°C, they reported that the temperature of the sample rose considerably above the temperature of the furnace, resulting in nonisothermal conditions.

The present investigation was made to study the reaction between oxygen and thorium for longer times and at higher temperatures and pressures than those studied by Levesque and Cubicciotti.

Materials

The thorium used in this investigation was iodide crystal bar produced by the de Boer process. The crystal bar was arc melted, forged into a 1-in. square rod, and cold finished to a $\frac{5}{16}$-in. cylindrical rod. Test specimens, each $1\frac{1}{2}$ in. long, were machined from this rod. Diameters of the specimens were reduced to slightly less than $\frac{5}{16}$ in. to remove surface contamination.

Thorium was analyzed by spectrographic, chemical, and vacuum-fusion methods. Principal impurities found were 300 ppm by weight each of carbon and oxygen and 100 ppm each of silicon and molybdenum. All other impurities were present in concentrations of less than 100 ppm.

Oxygen used in this study was prepared from degassed potassium permanganate by the method described by Hoge (9). Gas was dried by passing through a dry ice-acetone cold trap prior to its reaction with the thorium specimen.

Procedure

Experimental apparatus was similar to that described in an earlier paper (10) with a few modifications. Since the reaction being studied involved oxygen, it was necessary to use a zirconia tube to separate the thermocouple from the thorium specimen instead of a graphite tube liner. The dead volume of the reaction system was materially reduced by suspending a Vycor tube, sealed at both ends, from a hook in the cap of the reaction tube. A sketch of this arrangement is shown in Fig. 1.

A 4-kw tungsten-gap-type Lepel converter was used to heat the specimens. Temperature readings were made with a Pt-Pt + 10% Rh thermocouple calibrated against an optical pyrometer as in previous work (10).

A cylindrical thorium specimen to be used in a reaction rate study was abraded on 240-, 400-, and 600-grit kerosene-soaked silicon carbide papers. Kerosene minimized oxidation during abrasion and was removed by successively rinsing in naphtha, ether, and C. P. acetone. The specimen was then suspended in the reaction tube as noted above. The specimen was degassed by heating under a vacuum of less than 0.5 μ at 1200° to 1400°C for at least 15 min to remove hydrogen prior to adding the oxygen. Oxygen was added to the reaction tube to atmospheric pressure in measured amounts from a 50-ml glass buret. Progress of the surface reaction was followed by observing pressure changes in the closed system with an open-end mercury manometer. Further measured amounts of oxygen were added from time to time to maintain the pressure between about $\frac{3}{4}$ and 1 atm. The system was evacuated and the specimen was cooled to room

[1] Manuscript received August 20, 1953. This paper was prepared for delivery before the Wrightsville Beach Meeting, September 12 to 16, 1953. Work was done under Contract No. W-7405-eng-92 for the United States Atomic Energy Commission.

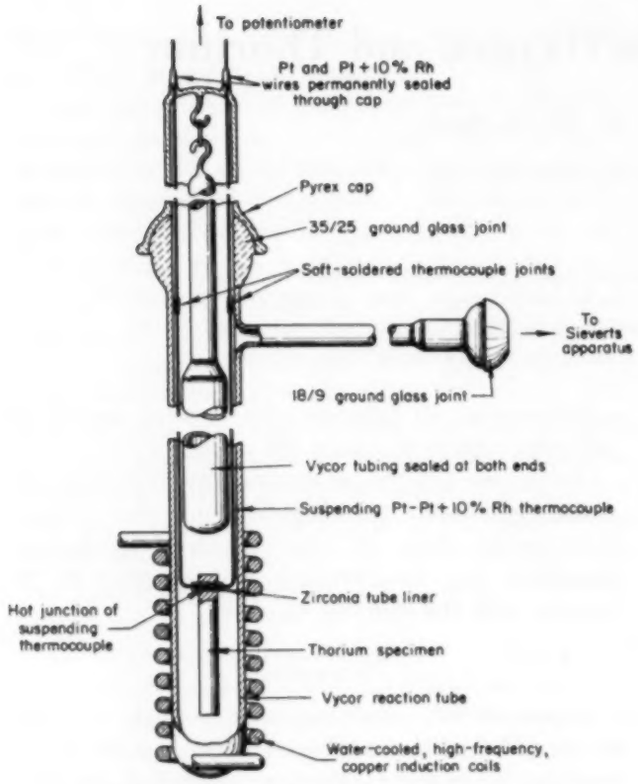

FIG. 1. Cutaway section of reaction tube assembly

temperature in vacuum after the reaction had been followed for the desired time.

The difference between the quantity of oxygen added to the reaction system and that remaining in the gas phase is a measure of the gas absorbed by the specimen at any time. Quantity of gas reacted per unit area was computed by using the original geometrical dimensions of the specimen.

RESULTS AND DISCUSSION

Solubility of Oxygen in Thorium

The solid solubility of oxygen in thorium is low even at elevated temperatures. Evidence of this can be obtained by observing the angular inclusions of oxide found in the microstructure of thorium. Magnesium-reduced thorium usually contains from 0.10 to 0.15 weight % oxygen and many oxide inclusions are evident. Arc-melted and rolled iodide thorium usually contains less than 0.05 weight % oxygen and, although fewer in number, discrete oxide inclusions can be noted in its microstructure. Even this lesser amount of oxygen in the arc-melted iodide thorium exceeds the solubility limit of oxygen in thorium at elevated temperatures. This was shown quite clearly by reacting a sample of this thorium with oxygen at 1415°C for 3 hr. The surface oxide layer was removed and the rest of the sample was analyzed for oxygen. A sample of the base material with no oxygen added was also analyzed. Both specimens analyzed 0.028 ± 0.003 weight % oxygen. These results indicate that no oxygen was diffused into the specimen as a result of the reaction at 1415°C, and that the thorium previously had been saturated with oxygen at a temperature higher than 1415°C, probably during reduction or arc melting. This low oxygen solubility made it impossible to obtain diffusion data.

Rates of Reaction

The rate of surface reaction of oxygen with thorium was studied in the temperature range of 850° to 1415°C at atmospheric pressure. These reactions produced a tightly adherent surface film of ThO_2 which was dark-gray to black for the higher temperatures and tended to be lighter-gray for the lower temperatures. Plots of the experimental data for several of the oxidation runs are shown in Fig. 2. For clarity, some of the curves for intermediate temperatures, and curves which crossed or fell close to other curves, were omitted.

It was observed that, as the oxygen first contacts the thorium, an exothermic reaction occurs, increasing the temperature of the specimen instantaneously by as much as several hundred degrees Celsius. A similar observation was made by Levesque and Cubicciotti (8) for temperatures above 450°C. With the use of induction heating and continuous control of power available, this effect could be counteracted by reducing rapidly the heat input

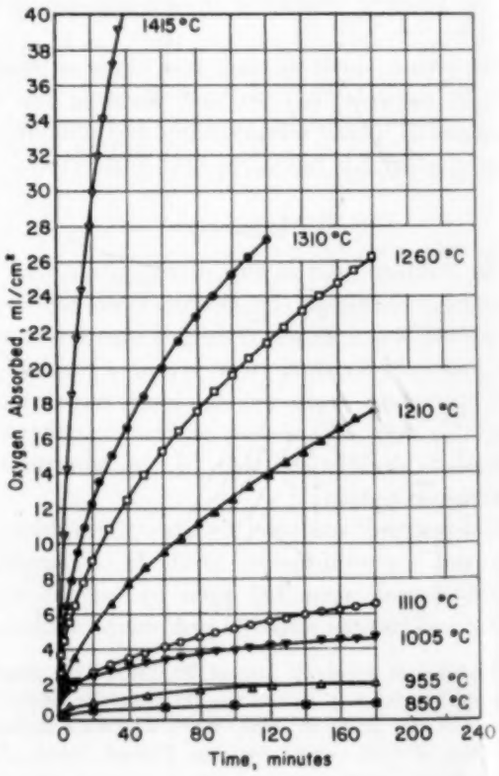

FIG. 2. Oxidation of thorium at 850° to 1415°C

from the converter. At higher temperatures, where the rate of reaction is quite rapid, the temperature could be effectively controlled by this technique. However, at lower temperatures, where the rate of reaction is normally quite slow, the amount of oxygen reacted during even a brief nonisothermal period is relatively large compared to the amount of gas reacted isothermally thereafter. This was especially significant at temperatures below about 1055°C where as much gas might be absorbed in the first fraction of a minute with the specimen at the elevated temperature as would be absorbed by the specimen at the desired temperature in several hours. It was obvious that in order to interpret the data, a correction for the non-isothermal period was required.

Moore (11) has described an equation for the parabolic law which provides for the discarding of initial deviations in reaction behavior. With the initial conditions, $y = y_o$ at $t = 0$, the integrated form of the equation is

$$y - y_o = \Delta y = k(t/\Delta y) - 2y_o , \qquad (I)$$

where: y = experimental value for the amount of oxygen reacted; y_o = amount of oxygen reacted nonisothermally; k = the parabolic rate constant; and t = time from origin at y_o.

Using equation (I), the rate constant, k, for each temperature was obtained from the slope of the straight line portion of a plot of y against $t/\Delta y$. Fig. 3 is an example of this type of plot.

Slopes obtained from log-log plots of the corrected data for the gas absorbed in milliliters per square centimeter vs. time for the 14 experimental runs in the temperature range of 850° to 1415°C are listed in

TABLE I. *Rate constants, k, determined at various temperatures*

Run No.	Temp, °C	Total time, t, of run, min	Total oxygen absorbed in time, t, ml/cm²	y_o, ml/cm²	$k \times 10^3$ (ml/cm²)²/sec	Slope of log-log plot*
1	850	180	0.99	0.36	0.040	0.55
2	900	180	2.13	0.82	0.181	0.53
3	955	180	2.12	0.66	0.259	0.58
4	1005	180	4.70	1.93	0.790	0.58
5	1055	180	6.52	1.09	2.70	0.51
6	1110	180	6.66	0	3.35	0.42
7	1110	180	5.46	0	2.18	0.42
8	1160	180	17.61	0	29.5	0.52
9	1210	180	17.69	0	33.9	0.52
10	1210	180	25.98	0	63.7	0.56
11	1260	180	26.33	0	62.3	0.50
12	1310	180	25.28	0	57.4	0.48
13	1310	120	27.32	0	95.2	0.44
14	1415	45	44.79	0	839.	0.55

* Slope of corrected experimental data. The origin of time, $t = o$, was set at amount of oxygen, y_o, reacted in first stage of oxidation. Slope of 0.50 indicates a parabolic rate law is being obeyed.

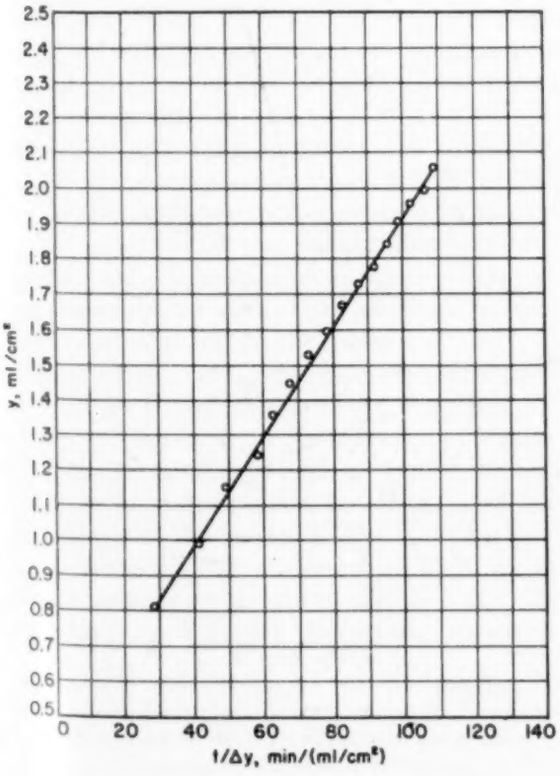

FIG. 3. Oxidation of thorium at 955°C

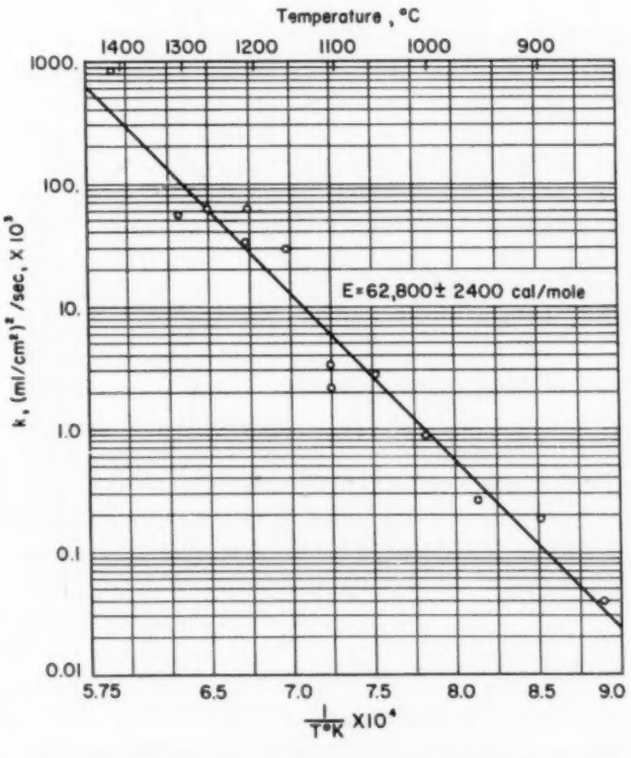

FIG. 4. Thorium-oxygen reactions; variation of rate constant, k, with temperature.

Table I. Slopes vary from 0.42 to 0.58, showing that corrected experimental data follow the parabolic rate law reasonably well. Values of the rate constants, k, calculated for the reactions are also listed in Table I. Fig. 4 shows a plot of these parabolic rate-law constants against $1/T$. The position of the best straight line through the experimental points was obtained by the method of least squares. Energy of activation of the reaction was calculated using the Arrhenius-type equation $k = Ae^{-Q/RT}$. The rate constant, k, in $(ml/cm^2)^2/sec$ can be expressed as:

$$k = 5.5 \times 10^7 e^{-62,800/RT} \qquad (II)$$

where 62,800 ± 2400 cal/mole is the energy of activation.

Levesque and Cubicciotti (8) reported an energy of activation of 31,000 cal/mole for the parabolic oxidation of thorium between 250° and 350°C. This value probably should not be compared with the value obtained in the present work because of the difference in level of temperature ranges involved. Another aspect of the oxidation of thorium at high temperatures is the relatively high activation energy for the reaction compared with those generally found for other metals. However, the reaction is not unique in this respect, since the activation energies for the parabolic oxidation of metals range from 18,000 to 62,000 cal/mole (12, 13).

Acknowledgments

It is a pleasure to acknowledge the assistance of Mr. B. G. Koehl, who performed the reaction rate experiments, and Mrs. Mary Penn and Mrs. Margaret Thomas, who made the many tedious calculations of the data. The counsel of Mr. W. M. Albrecht and Dr. Jack Belle in interpretation of the experimental data is also greatly appreciated.

Any discussion of this paper will appear in a Discussion Section to be published in the December 1954 issue of the JOURNAL.

REFERENCES

1. U. R. EVANS, *Trans. Electrochem. Soc.*, **91,** 547 (1947).
2. N. B. PILLING AND R. E. BEDWORTH, *J. Inst. Metals London*, **29,** 579 (1923).
3. N. F. MOTT, *Trans. Faraday Soc.*, **36,** 472 (1940).
4. C. WAGNER AND K. GRÜNEWALD, *Z. physik. Chem.*, **40B,** 455 (1938).
5. E. A. GULBRANSEN AND K. ANDREW, *Trans. Am. Inst. Mining Met. Engrs.*, **185,** 515 (1949).
6. A. DRAVNIEKS AND H. J. McDONALD, *Iron Age*, **164,** 78 (August 25, 1949); *ibid.*, **164,** 84 (September 1, 1949).
7. J. T. WABER, *Metal Prog.*, **62,** 76 (September, 1952).
8. P. LEVESQUE AND D. CUBICCIOTTI, *J. Am. Chem. Soc.*, **73,** 2028 (1951).
9. H. J. HOGE, *J. Research Natl. Bur. Standards*, **44,** 321 (1950).
10. M. W. MALLETT, J. BELLE, AND B. B. CLELAND, *This Journal*, **101,** 1 (1954).
11. W. J. MOORE, *ibid.*, **100,** 302 (1953).
12. A. DRAVNIEKS, *ibid.*, **100,** 95 (1953).
13. D. CUBICCIOTTI, *J. Am. Chem. Soc.*, **72,** 2084 (1950).

Reaction of Nitrogen with, and the Diffusion of Nitrogen in, Thorium[1]

A. F. Gerds and M. W. Mallett

Battelle Memorial Institute, Columbus, Ohio

ABSTRACT

Rates of reaction of nitrogen with thorium were determined for the temperature range of 670° to 1490°C at 1 atm pressure. The reaction follows a parabolic law and the parabolic rate constant in $(ml/cm^2)^2/sec$ is $k = 5.9\ e^{-24,300/RT}$. The activation energy of reaction has a probable error of 1300 cal/mole. Rates of diffusion of nitrogen in thorium were obtained over the temperature range of 845° to 1490°C at atmospheric pressure. The diffusion coefficient in cm^2/sec is $D = 2.1 \times 10^{-3}\ e^{-22,500/RT}$. The activation energy of diffusion has a probable error of 1300 cal/mole. Limiting solubilities of nitrogen were determined from the diffusion data. The heat of solution of atomic nitrogen (from ThN) in thorium is $\Delta H = 11{,}000$ cal/mole.

Introduction

Thorium is one of a number of metals that tarnish at room temperature rather rapidly when exposed to the atmosphere. The tarnish film formed is largely oxide resulting from a reaction of the thorium with oxygen and moisture from the air. At elevated temperatures both oxygen and nitrogen react with thorium. In its fabrication, such operations as melting, forging, rolling, swaging, and the like are commonly employed. It would be of interest to know the precautions that must be observed to prevent contamination of the metal during the various operations. A study of the reaction of thorium with oxygen at atmospheric pressure in the temperature range of 850° to 1415°C was recently completed at this laboratory (1). Levesque and Cubicciotti (2) have reported on the oxidation of thorium in the temperature range of 250° to 700°C in an oxygen atmosphere at a pressure of 45 cm. It was the objective of the present investigation to study the rate of reaction of nitrogen with massive thorium and also to obtain data on the diffusion and solubility of nitrogen in the metal.

Thorium metal has a face-centered-cubic structure with a lattice constant of 5.088 Å. Three nitrides of thorium are reported in the literature. Matignon and Delépine (3) produced a yellowish-maroon powder by heating thorium in nitrogen, to which they assigned the formula Th_3N_4. Chiotti (4) identified the crystal structure of ThN as face-centered cubic with a lattice constant of 5.18 Å. Zachariasen (5) reported the crystal structure of Th_2N_3 to be hexagonal, of the La_2O_3 type, with $a = 4.08 \pm 0.01$ Å and $c = 6.30 \pm 0.02$ Å.

No references have been found in the literature either to rates of reaction of nitrogen with thorium or to solubilities or rates of diffusion of nitrogen in thorium.

Materials

Iodide crystal-bar thorium, produced at Battelle Memorial Institute, was used in the investigation. The crystal bar was arc melted, forged to a 1-in.-square rod and cold finished to a $\frac{5}{16}$-in. cylindrical rod. Test specimens, each $1\frac{1}{2}$ in. long, were machined from this rod. Diameters of the specimens were reduced to slightly less than $\frac{5}{16}$ in. to remove surface contamination. Each specimen had a surface area of about 8 cm^2.

Impurities in the thorium were determined by spectrographic, chemical, and vacuum-fusion analyses. Principal impurities detected were carbon and oxygen, 300 ppm by weight each, and silicon and molybdenum, 100 ppm each. All other impurities were present in amounts less than 100 ppm by weight.

Nitrogen used in this study was prepared by passing prepurified tank nitrogen (The Matheson Company) over zirconium turnings heated at 850°C. The gas was then dried by passing through a dry ice-actone cold trap. Purified gas was analyzed by means of a mass spectrometer and found to contain 99.8 vol % nitrogen with 0.2 vol % argon as the only measurable impurity.

Procedure

The modified Sieverts apparatus used to measure rate of reaction of nitrogen with thorium is similar to that described in a previous report (6). In this

[1] Manuscript received August 20, 1953. This paper was prepared for delivery before the Wrightsville Beach Meeting, September 12 to 16, 1953. Work was done under Contract No. W-7405-eng-92 for the United States Atomic Energy Commission.

investigation, the thorium specimen, suspended by a platinum-platinum + 10% rhodium thermocouple threaded through a hole drilled near one end, was separated from the thermocouple by a small graphite tube liner. The thermocouple was calibrated against a standardized optical pyrometer (6).

A Vycor tube sealed at both ends was used to reduce the dead volume of the reaction system. Specimens were heated inductively. Power was supplied by a 4-kw tungsten-gap-type Lepel converter.

Cylindrical thorium specimens used in these reaction rate studies were prepared as has been described in a previous paper (1). Specimens were degassed by heating under a vacuum of less than 0.5 μ at 1150° to 1600°C for at least 10 min to remove hydrogen prior to adding the nitrogen.

Nitrogen was added to the reaction tube, containing the thorium specimen, to atmospheric pressure in measured amounts from a 50-ml glass buret. Progress of the reaction was followed by observing pressure changes in the closed system with an open-end mercury manometer. Further measured amounts of nitrogen were added from time to time to maintain the pressure between about ¾ and 1 atm. The system was evacuated and the specimen was cooled rapidly to room temperature in vacuum after the reaction had taken place for the desired period of time.

The difference between the quantity of nitrogen added to the reaction system and that remaining in the gas phase is a measure of the gas absorbed by the specimen at any time. The quantity of gas reacted per unit area was computed by using the original geometrical dimensions of the specimen.

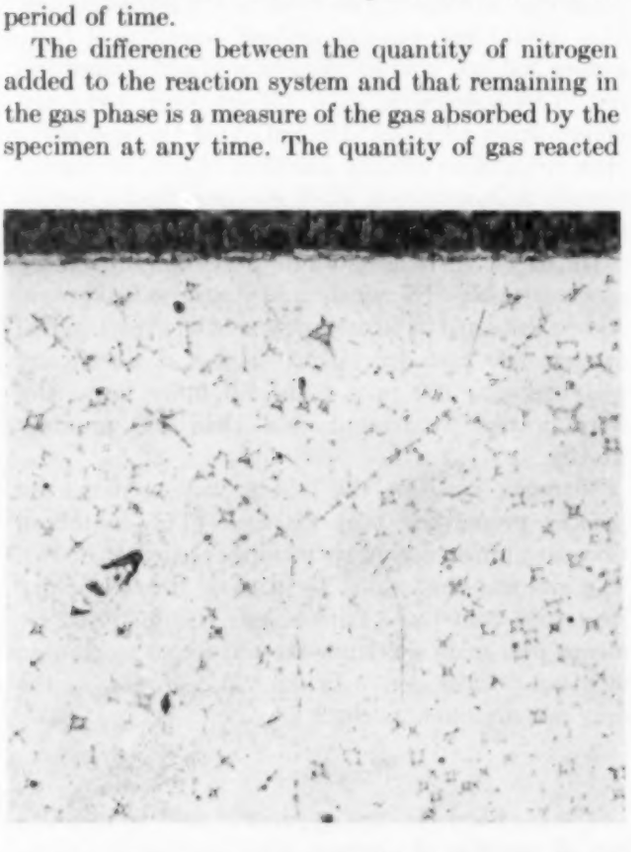

FIG. 1. Structure at surface of thorium reacted with nitrogen at 1370°C. 250×.

Specimens reacted with nitrogen in order to study the rates of reaction at various temperatures were also used to obtain diffusion data. Lengths equal to the radius were cut from the bottom end of the specimens and also from the lower edge of the hole that had been drilled near the top to suspend the specimens. The remainder was machined radially into layers of equal weight which were then analyzed for nitrogen by a modified Kjeldahl method. Diffusion coefficients and the energy of activation of diffusion were determined using the average nitrogen concentration of each layer, the average radius of the layers, the original radius of the specimen, and the time of diffusion.

RESULTS AND DISCUSSION

Surface Reaction

The rate of surface reaction of nitrogen with thorium was studied in the temperature range of 670° to 1490°C. The nitride film formed on the surface of the specimen is characterized by a golden-yellow color when the reaction takes place below 750°C. At higher temperatures, the surface film is a dark-gray color which seemed in some cases to be composed of discrete grains. However, the golden-yellow film, noted when the reaction took place at lower temperatures, was visible if the gray outer film was cracked away. Fig. 1 shows the microstructure at the surface of a sample of thorium reacted with nitrogen at 1370°C. At a magnification of 250×, the relatively thick dark-gray outer layer of Th_2N_3 can be distinguished easily from the inner, thin, golden-yellow layer. This golden-yellow material was reported to be ThN by Chiotti (4). The discrete and somewhat dendritic-shaped inclusions, which are present abundantly, have the characteristic color of the mononitride. These can easily be distinguished from the few very dark-etching oxide inclusions which are also shown in Fig. 1. Both surface films appear to react at room temperature with moisture from the atmosphere to form the powdery gray oxide, ThO_2.

The reaction between nitrogen and thorium was found to follow a parabolic law in the temperature range of 670° to 1490°C at atmospheric pressure. Experimental data for several representative runs are plotted in Fig. 2. At temperatures below 1255°C, some slight initial deviations were found in a few cases. Between 1370° and 1605°C, reactions were parabolic initially, and, after a short time, became linear (see Fig. 3). At 1370° and 1490°C, the initial period of parabolic reaction was 20 to 30 min. At 1605°C, the parabolic rate law was obeyed for only the first 5 min of reaction. Reaction then be-

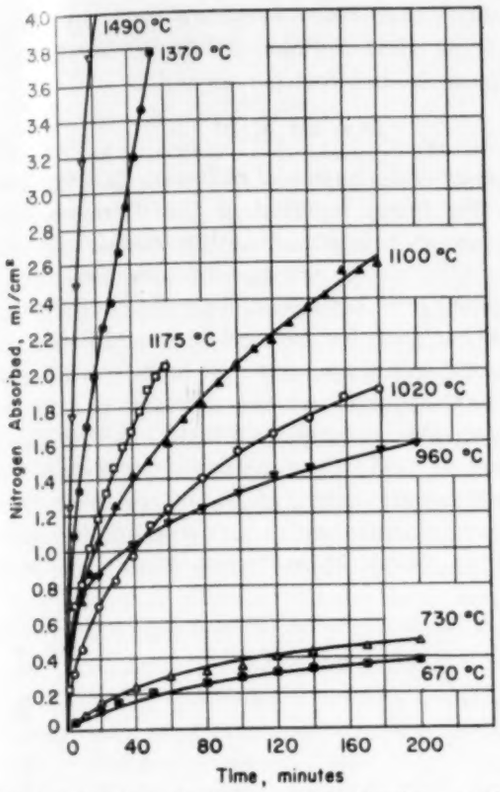

FIG. 2. Reaction of nitrogen with thorium at 670° to 1490°C.

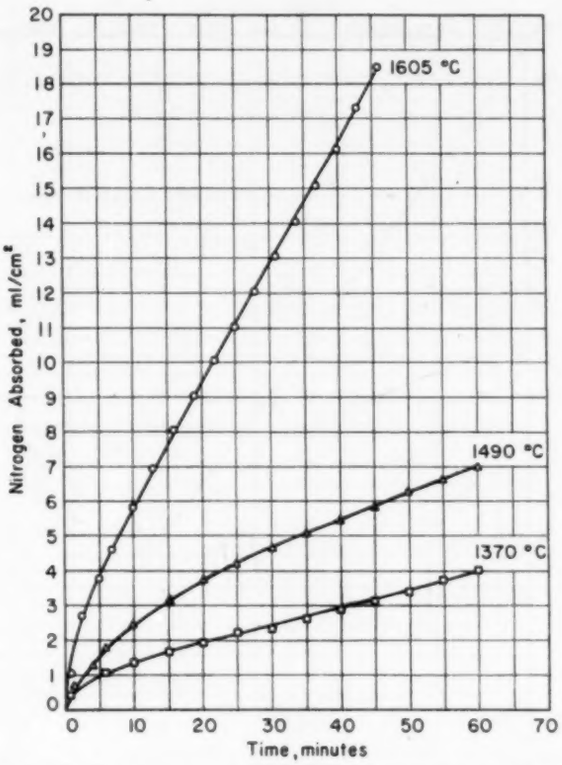

FIG. 3. Reaction of nitrogen with thorium at 1370° to 1605°C.

came linear with time for at least 40 min longer. It is also rather interesting to note that the reactions at 1490° and 1605°C changed from parabolic to linear when about 6 mg of nitrogen per square centimeter of surface area had been reacted.

Cubicciotti noted a similar change in type of rate in the oxidation of uranium (7) at about 200°C and also in the oxidation of cerium (8) between 160° and 190°C. Gulbransen and Andrew (9) studied the reaction between nitrogen and beryllium and found a similar effect for the reaction at 925°C. In the three instances cited above, reactions proceeded parabolically with time initially and then increased to a rate faster than parabolic, becoming linear with time in two cases. Cubicciotti (7) explained this phenomenon by reasoning that, since the volume of the compound formed on the surface is larger than that of the metal reacted, the surface film must be under stress. When the film reaches a certain thickness, the stress becomes large enough that the film begins to crack or flake. At this point, the film is no longer protective and the reaction then is linear or faster than linear with time. As the temperature of the reaction is increased, cracking can occur sooner since the rate of reaction is more rapid. At some temperature, the entire reaction might appear to be linear. This hypothesis seems also to fit well data obtained in this study of the reaction between nitrogen and thorium.

TABLE I. *Experimental rate constants, k, for the thorium-nitrogen reaction*

Sample	Temp, °C	$k \times 10^4$, $(ml/cm^2)^2/sec$
1	670	0.13
2	730	0.28
3	900	2.94
4	900	4.00
5	960	1.97
6	1020	3.55
7	1100	6.00
8	1175	11.9
9	1200	6.62
10	1200	9.83
11	1255	22.3
12	1370	36.0
13	1490	130

The parabolic-rate constant, k, was calculated by determining the slope of the straight line resulting when the square of the amount of gas absorbed per unit area was plotted against time. Values of k determined in individual experiments at temperatures in the range of 670° to 1490°C are shown in Table I. A plot of log k vs. $1/T$ of these experimental points is shown in Fig. 4. The position of the best straight line through these points was determined by the method of least squares. The activation energy, obtained using the Arrhenius-type equation, $k = Ae^{-Q/RT}$, is 24,300 ± 1300 cal/mole. The correspond-

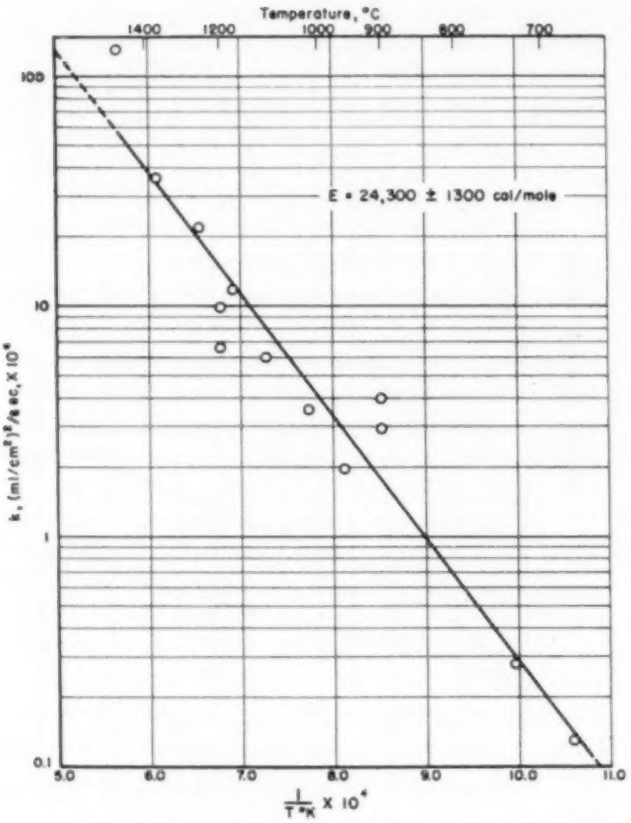

FIG. 4. Thorium-nitrogen reactions; variation of parabolic reaction rate constant, k, with temperature.

ing rate constant for the reaction in $(ml/cm^2)^2/sec$ is

$$k = 5.9\ e^{-24,300/RT} \qquad (I)$$

where the frequency factor is 5.9.

The energy of activation of 24,300 cal/mole is much lower than the value obtained for the oxidation of thorium, namely, 62,800 cal/mole. Energies of activation for the reaction between various metals and nitrogen reported in the literature vary from 31,400 cal/mole for the reaction of vanadium with nitrogen (10) to 75,000 cal/mole for the reaction of beryllium with nitrogen (9). All of these activation energies are higher than that found in the present investigation.

Diffusion

Diffusion data for nitrogen in thorium were computed by the graphical method described by Mallett and coworkers (11). Values of the diffusion coefficient, D, obtained from the experimental data in the temperature range of 845° to 1490°C, are listed in Table II.

A plot of the logarithms of the diffusion coefficients vs. reciprocal temperature is shown in Fig. 5. The equation of the best straight line through the experimental points was determined by the method of least squares. The energy of activation of diffusion, obtained from the Arrhenius-type equation, is 22,500 ± 1300 cal/mole. Diffusion coefficient, D, in square centimeters per second is

$$D = 2.1 \times 10^{-3}\ e^{-22,500/RT} \qquad (II)$$

Energy of activation of diffusion, 22,500 cal/mole, is in the range reported in the literature for the diffusion of nitrogen in other metals. Wert and Zener (12), using internal friction measurements, calculated an activation energy of diffusion of 17,700 cal/mole for nitrogen in iron. Kê (13), using the same technique, obtained an activation energy of 44,000 cal/mole for the diffusion of nitrogen in tantalum. Mallett and coworkers (11), with the same method as used in the present investigation, report an activation energy of 33,600 cal/mole for the diffusion of nitrogen in a zirconium-2 weight % hafnium alloy. More recent work by Mallett,

TABLE II. *Experimental diffusion coefficients for nitrogen in thorium*

Sample	Time, hr	Temp, °C	c_o, wt % nitrogen	$D \times 10^7$ cm²/sec
1	6¼	845	0.048	0.530
2	3	900	0.079	1.09
3	6	960	0.097	2.19
4	3	1020	0.117	3.08
5	3	1100	0.159	6.61
6	1	1175	0.185	14.6
7	2	1200	0.177	8.65
8	1	1255	0.216	16.4
9	1	1370	0.276	17.0
10	1	1490	0.335	34.6

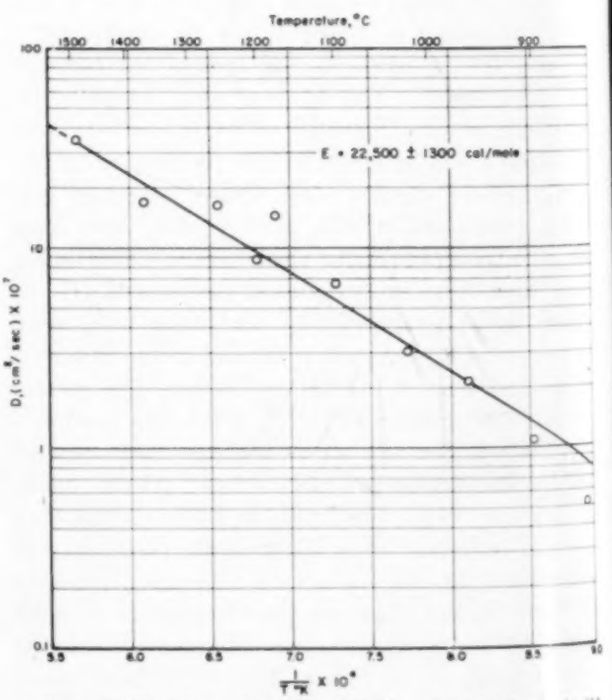

FIG. 5. Thorium-nitrogen diffusion; variation of diffusion coefficient, D, with temperature.

Belle, and Cleland (6), with low-hafnium zirconium, yielded a value of 30,700 cal/mole.

Solubility

The limiting solubility (11), c_o, of atomic nitrogen is the concentration of nitrogen just inside the interface between the ThN surface film and the thorium metal. This concentration may also be considered as the solubility of nitrogen at a partial pressure equal to the dissociation pressure of ThN. Since the surface layer is quite thin, no serious error is introduced in obtaining maximum solubility by extrapolating data to the outer surface of the specimen rather than the interface between the surface film and the specimen.

Values of c_o at the various temperatures are listed in Table II. A plot of these values against temperature is shown in Fig. 6. The line described in this plot is a boundary between a single- and two-phase region on the thorium-nitrogen phase diagram. The course of the line below about 0.05 weight % nitrogen is not known, but it appears likely that the line may approach zero concentration asymptotically with decreasing temperature.

A plot of the values of c_o, listed in Table II, on a logarithmic scale vs. reciprocal temperature is shown in Fig. 7. The slope of the best straight line through the experimental points was determined by the method of least squares. The solubility in weight per cent nitrogen in thorium over the temperature range involved, 845° to 1490°C, can be expressed as

$$\log_{10} c_o = -2405/T + 0.9115 \qquad \text{(III)}$$

where T is the temperature in degrees Kelvin. From this equation, the heat of solution per mole of atomic nitrogen (from ThN) dissolved in thorium is $\Delta H = 11{,}000 \pm 400$ cal.

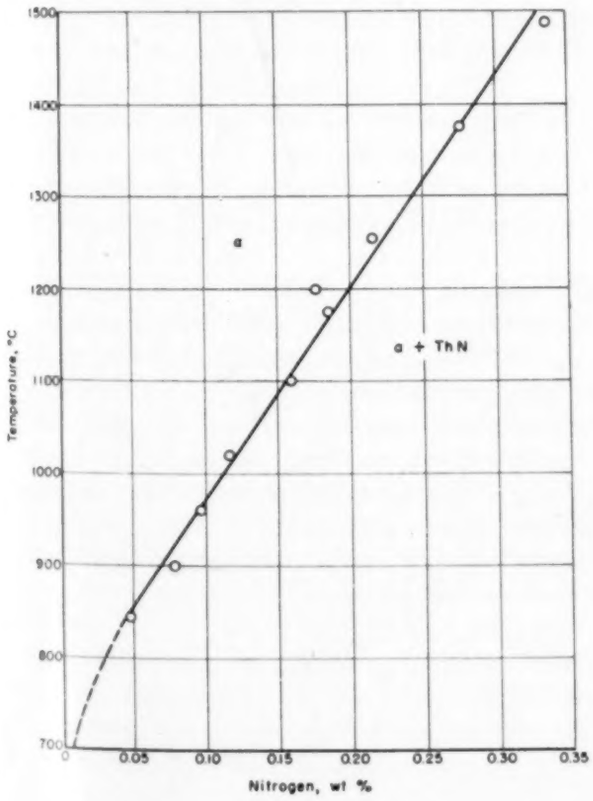

Fig. 6. Solubility limits of nitrogen in thorium

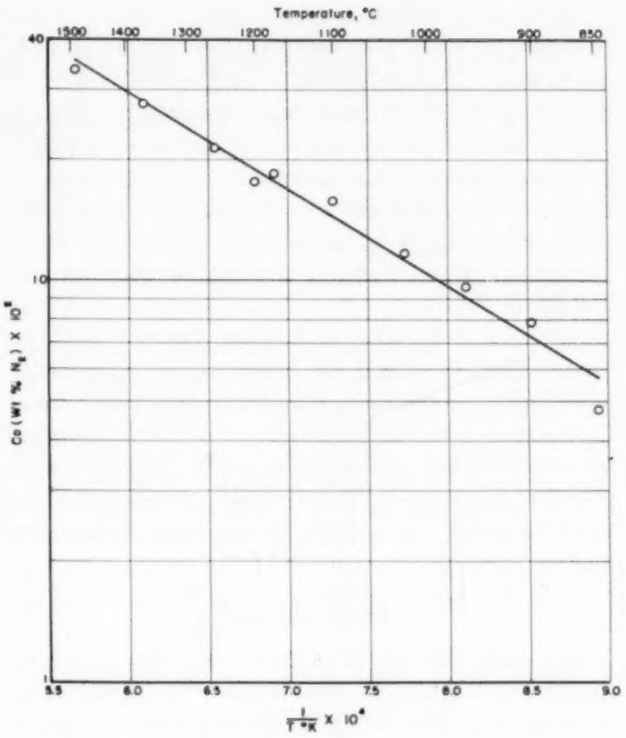

Fig. 7. Variation of solubility of nitrogen in thorium with temperature.

Conclusions

Reactions of thorium with nitrogen were studied, using a modified Sieverts apparatus, over the temperature range of 670° to 1605°C. Below about 750°C, a golden-yellow nitride film of ThN formed on the surface of the specimens. At higher temperatures, the surface film was the dark-gray Th_2N_3. Beneath this and adjacent to the thorium, the golden-yellow nitride was found. Both products reacted slowly at room temperature with oxygen and moisture from the air to form ThO_2.

Reaction-rate data were found to obey the parabolic rate law between 670° and 1490°C. At 1370° and 1490°C, reactions were parabolic the first 30 min and then became linear. The reaction at 1605°C became linear after only about 5 min of parabolic reaction. An activation energy of reaction of 24,300 ± 1300 cal/mole was calculated for the parabolic reaction between 670° and 1490°C. This value is lower than activation energies reported in the literature for the reaction of nitrogen with other metals.

The rate of diffusion of nitrogen in thorium was determined over the temperature range of 845° to 1490°C. An activation energy of diffusion of 22,500 ± 1300 cal/mole was calculated, which is in the range reported for the diffusion of nitrogen in other metals. Limiting solubilities of nitrogen in thorium were obtained from the diffusion data. From these solubility data, a heat of solution, ΔH = 11,000 ± 400 cal/mole for nitrogen in thorium, was calculated.

In the hot working of thorium below 850°C, no great difficulty would be expected by diffusion or solution of nitrogen into the metal. Even if such hot fabrication were carried out in a 100% nitrogen atmosphere, the principal contamination would be the formation of a thin surface nitride film. In working in air, the surface film is oxide rather than nitride.

Acknowledgments

The authors wish to acknowledge the assistance of Mr. B. G. Koehl who performed the reaction-rate experiments, Mrs. Mary Penn and Mrs. Margaret Thomas who made the many calculations required to interpret the data, and Miss Betty Hannahs who prepared the specimens for metallographic study. The counsel of Dr. Jack Belle in interpretation of the experimental data is also greatly appreciated.

Any discussion of this paper will appear in a Discussion Section to be published in the December 1954 issue of the JOURNAL.

REFERENCES

1. A. F. Gerds and M. W. Mallett, *This Journal*, **101**, 171 (1954).
2. P. Levesque and D. Cubicciotti, *J. Am. Chem. Soc.*, **73**, 2028 (1951).
3. C. A. Matignon and M. Delépine, *Ann. chim. et phys.*, **8**, 10, 130 (1907).
4. P. Chiotti, Atomic Energy Commission Declassified Report, AECD-3072, 48 (June 5, 1950).
5. W. H. Zachariasen, *Acta Cryst.*, **2**, 388 (1949).
6. M. W. Mallett, J. Belle, and B. B. Cleland, *This Journal*, **101**, 1 (1954).
7. D. Cubicciotti, *J. Am. Chem. Soc.*, **74**, 1079 (1952).
8. D. Cubicciotti, *ibid.*, **74**, 1200 (1952).
9. E. A. Gulbransen and K. F. Andrew, *This Journal*, **97**, 383 (1950).
10. E. A. Gulbransen and K. F. Andrew, *ibid.*, **97**, 387 (1950).
11. M. W. Mallett, E. M. Baroody, H. R. Nelson, and C. A. Papp, *ibid.*, **100**, 103 (1953).
12. C. Wert and C. Zener, *Phys. Rev.*, **76**, 1169 (1949).
13. T. S. Kê, *ibid.*, **74**, 917 (1948).

The Cathodic Reduction of Anions and the Anodic Oxidation of Cations[1]

CARL WAGNER

Department of Metallurgy, Massachusetts Institute of Technology, Cambridge, Massachusetts

ABSTRACT

Anions approach a cathode by diffusion and convection rather than by electrolytic migration in view of the adverse potential gradient. The rate of transport of anions of valence z_j toward a cathode is decreased appreciably if the potential difference across the diffusion boundary layer is of the order of, or greater than, $kT/|z_j|e = 0.025/|z_j|$ volt. This effect may account for the prevention of the reduction of hypochlorite at a cathode covered by a diaphragm of chromium oxide. Similarly, the rate of transport of cations toward an anode is decreased appreciably if the potential difference across the diffusion boundary layer is of the order of, or greater than $kT/z_je = 0.025/z_j$ volt.

INTRODUCTION

When a negatively charged ion X^- is reduced cathodically, it has to approach the cathode by diffusion and convection against an adverse potential gradient. If no other cathodic process takes place and the solution contains a large excess of other ions providing a high electrical conductivity, the adverse potential gradient is small and the transport rate of anions X^- is affected only slightly. If, however, in addition to the reduction of anions X^-, a second electrochemical reaction takes place and the total current density is sufficiently high, the adverse potential gradient may become significant and, thereby, the transport rate and the reduction rate of anions X^- may be decreased considerably.

If positively charged ions are oxidized anodically, e.g., $Fe^{2+} = Fe^{3+} + e^-$, they also have to approach the electrode against an adverse potential gradient. Thus one has a situation analogous to the reduction of anions at a cathode.

In the following, calculations are presented for idealized conditions. Since these ideal conditions are not easy to realize, theoretical conclusions have not been verified. The following analysis, however, is based only on well-established electrochemical principles which do not require verification. A comparison between experimental results and theoretical conclusions would, therefore, show only whether actual experimental conditions were sufficiently close to ideal conditions underlying the theoretical analysis.

Most important are certain qualitative results which are independent of idealizing assumptions. In particular, it is shown that the cathodic reduction of anions, e.g., hypochlorite in solutions with excess sodium hydroxide, may virtually be prevented at high current densities.

REDUCTION PROCESSES IN A SOLUTION WITH EXCESS SODIUM HYDROXIDE

When a solution of sodium hydroxide is electrolyzed, hydrogen is evolved at the cathode,

$$H_2O + e^- = OH^- + \tfrac{1}{2} H_2. \qquad (I)$$

The cathodic formation of hydroxyl ions leads to an enrichment of hydroxyl ions at the cathode. For the sake of simplification, we assume a stagnant boundary layer of thickness δ beyond which concentration differences are negligible, owing to vigorous stirring and turbulent mixing. In an ideal experiment, such a type of boundary layer may be realized by means of a diaphragm whose pores are so large that specific effects due to adsorption and the electrical double layer can be disregarded.

The transport rate of ions of type i per unit time per unit area in the direction of the x coordinate in a dilute aqueous solution at rest can be expressed as

$$\frac{1}{A}\frac{dn_i}{dt} = -D_i\frac{\partial c_i}{\partial x} - \frac{D_i}{kT}c_i z_i e\frac{\partial \phi}{\partial x} = -c_i D_i\left(\frac{\partial \ln c_i}{\partial x} + \frac{z_i e}{kT}\frac{\partial \phi}{\partial x}\right) \qquad (II)$$

where dn_i/dt is the number of moles of ions, i, passing cross section A per unit time, D_i the diffusion coefficient of ions of type i, c_i their concentration, z_i their valence (positive for cations and negative for anions), e the electronic charge, ϕ the electrical potential, k the Boltzmann constant, and T absolute temperature. The first term on the right-hand side of equation (II) accounts for transport due to the concentration gradient, whereas the second term accounts for electrolytic migration.

[1] Manuscript received August 3, 1953.

The "mobility" of ions i does not appear explicitly, since it is expressed in terms of the diffusion coefficient by using the Nernst-Einstein relation, D_i = mobility $\times$ kT.

Under steady-state conditions, the concentration c of sodium hydroxide in a stagnant boundary layer is a linear function of the distance x from the surface of the electrode as follows by applying equation (II) to cations and anions, respectively, for an anion transport rate corresponding to the cathodic process formulated in equation (I), eliminating the potential gradient, and calculating the concentration c as a function of distance x from the cathode. Thus,

$$c = c_o[\gamma - (\gamma - 1)x/\delta] \qquad \text{(III)}$$

where c_o is the bulk concentration of sodium hydroxide and $\gamma = c_K/c_o$ is the ratio of the sodium hydroxide concentration c_K at the electrode to the bulk concentration c_o outside the boundary layer ($x > \delta$).

Upon substituting equation (III) in equation (II) for sodium ions whose transport rate is zero, it follows that

$$\frac{\partial \phi}{\partial x} = \frac{kT}{e} \frac{\gamma - 1}{\gamma\delta - (\gamma - 1)x} \qquad \text{at } 0 \leqq x \leqq \delta. \quad \text{(IV)}$$

Now we assume that in addition to sodium hydroxide the solution contains a small amount of ions of type j which are readily reduced at the cathode so that their concentration vanishes at $x = 0$. Applying equation (II) to ions j, we may show that the transport rate of ions j will be affected appreciably by the potential gradient only if the potential difference across the diffusion boundary layer is of the order of, or greater than, $kT/|z_i|e = 0.025/|z_i|$ volt. If the concentration of ions j is much less than the concentration of sodium hydroxide, equations (III) and (IV) remain approximately valid. The reduction rate, v_j, of ions j in moles per unit area per unit time is equal to the negative value of the transport rate in the direction of the x coordinate. Upon substituting equation (IV) in equation (II) for $i = j$, it follows that

$$v_j = D_j \frac{\partial c_j}{\partial x} + \frac{D_j z_j c_j(\gamma - 1)}{\gamma\delta - (\gamma - 1)x} \qquad \text{(V)}$$

where c_j, but not v_j, depends on x. Integrating equation (V) with respect to x and putting $c_j = c_{j(0)}$ for $x = \delta$ as the bulk concentration of ions j outside the boundary layer, we obtain

$$c_j = \frac{v_j\delta}{(z_j - 1)D_j(\gamma - 1)}\left[\gamma - (\gamma - 1)\frac{x}{\delta}\right] + \left[c_{j(0)} - \frac{v_j\delta}{(z_j - 1)D_j(\gamma - 1)}\right] \times \left[\gamma - (\gamma - 1)\frac{x}{\delta}\right]^{z_j} \quad \text{if } z_j \gtrless 1 \qquad \text{(VIa)}$$

$$c_j = \left\{c_{j(0)} - \frac{v_j\delta}{D_j(\gamma - 1)} \ln\left[\gamma - (\gamma - 1)\frac{x}{\delta}\right]\right\} \times \left[\gamma - (\gamma - 1)\frac{x}{\delta}\right] \quad \text{if } z_j = 1. \qquad \text{(VIb)}$$

As mentioned above, we assume that ions of type j are readily reduced at the cathode if hydrogen is developed. Thus, letting $c_j = 0$ for $x = 0$ in equations (VIa) and (VIb), we find the reduction rate v_j to be

$$v_j = \frac{(z_j - 1)D_j(\gamma - 1)c_{j(0)}}{\delta} \frac{\gamma^{z_j}}{\gamma^{z_j} - \gamma} \quad \text{if } z_j \gtrless 1 \qquad \text{(VIIa)}$$

$$v_j = \frac{D_j(\gamma - 1)c_{j(0)}}{\delta \ln \gamma} \quad \text{if } z_j = 1. \qquad \text{(VIIb)}$$

If the sodium hydroxide concentration at the surface of the cathode differs only slightly from the bulk concentration, i.e., if $\gamma \cong 1$, it follows from equations (VIIa) and (VIIb), with the aid of series expansions, that the reduction rate is

$$v_j^{(0)} \equiv v_j(\gamma \to 1) = D_j c_{j(0)}/\delta. \qquad \text{(VIII)}$$

Under these conditions, the reduction rate of ions j is independent of the simultaneous evolution of hydrogen, since the total potential difference across the boundary layer is small as compared to $kT/e = 0.025$ volt. This relation is well-known in polarography.

If the concentration of sodium hydroxide at the cathode is much greater than the bulk concentration, i.e., if $\gamma \gg 1$, we have the following three cases.

1. For reducible cations with a valence z_j equal to or greater than 2, it follows from equations (VIIa) and (VIII) that

$$v_j/v_j^{(0)} \cong (z_j - 1)(\gamma - 1) \text{ if } \gamma \gg 1 \text{ and } z_j \geqq 2. \qquad \text{(IXa)}$$

2. For univalent reducible cations it follows from equations (VIIb) and (VIII) that

$$v_j/v_j^{(0)} = (\gamma - 1)/\ln \gamma \text{ if } z_j = 1. \qquad \text{(IXb)}$$

3. For reducible anions ($z_j < 0$) it follows from equations (VIIa) and (VIII) that

$$v_j/v_j^{(0)} = -(|z_j| + 1)(\gamma - 1)\gamma^{-|z_j|}/(\gamma^{-|z_j|} - \gamma) \cong (1 + |z_j|)/\gamma^{|z_j|} \text{ if } \gamma \gg 1 \text{ and } z_j < 0. \qquad \text{(IXc)}$$

The value of γ is related to the current density, J, used for the evolution of hydrogen. According to Faraday's law and equation (I), $J/\mathbf{F}$ must be equal to the transport rate of hydroxyl ions per unit area. Substituting $J/\mathbf{F} = (dn_{OH^-}/dt)/A$ in equation (II) for hydroxyl ions and combining with equation (II) for sodium ions with zero transport rate, we obtain

$$J/\mathbf{F} = (c_K - c_o)(D_{Na^+} + D_{OH^-})/\delta \qquad \text{(X)}$$

whence

$$\gamma = c_K/c_o = 1 + J\delta/[c_o(D_{Na^+} + D_{OH^-})\mathbf{F}]. \qquad \text{(XI)}$$

At high current densities, the value of γ is, therefore, virtually proportional to the current density. From equations (IXa), (IXb), and (XI), it follows that at high current densities ($\gamma \gg 1$) the transport or reduction rate of positively charged ions j is essentially proportional to the current density, i.e., the electrical field in the boundary layer supports the diffusion of these ions toward the cathode.

On the other hand, it follows from equations (IXc) and (XI), that at high current densities ($\gamma \gg 1$) the transport or reduction rate of anions is essentially inversely proportional to the $|z_j|^{\text{th}}$ power of the current density. In this case, the adverse potential gradient in the boundary layer has a strong retarding effect on the reduction of ions j.

To satisfy the condition $\gamma \gg 1$, the potential difference across the boundary layer must be greater than $kT/e = 0.025$ volt. Since the effective thickness δ of the boundary layer is in general less than 0.05 cm, this condition is satisfied only if the potential gradient in the bulk electrolyte is much greater than 0.5 volt/cm. In most cases, such conditions are avoided, and, therefore, diffusion of anions toward the anode is hindered only to a small extent. However, locally high current densities and, thus, potential differences exceeding 0.025 volt across the boundary layer may occur at a cathode with a diaphragm as is discussed below.

Oxidation Processes in a Solution with Excess Acid

Analogous relations hold for the anodic oxidation of an oxidizable substance dissolved in acid when oxygen is evolved at the anode. Since the potential gradient has the opposite sign, z_j has to be replaced by $-z_j$ in equations (V) to (VIIb). Thus the oxidation rate of cations becomes inversely proportional to the $(z_j)^{\text{th}}$ power of the current density used for the evolution of oxygen, if $\gamma \gg 1$.

Reduction Processes in a Solution with Excess Acid

Next, we assume conditions under which at the cathode a depletion of electrolyte occurs. As an example, we consider the reduction of ions j in a solution of excess hydrochloric acid when hydrogen is evolved. In this case, the acid concentration c_K at the surface of the cathode is less than the bulk concentration c_o and, thus, $c_K/c_o = \gamma < 1$. Equation (III) is, therefore, rewritten as

$$c = c_o[\gamma + (1 - \gamma)x/\delta] \qquad \text{(XII)}$$

where c is the acid concentration at distance x from the cathode. Upon substituting equation (XII) in equation (II) for Cl^- ions with $z_i = -1$ and zero transport rate, it follows that

$$\frac{\partial \phi}{\partial x} = \frac{kT}{e} \frac{1 - \gamma}{\gamma\delta + (1 - \gamma)x} \text{ at } 0 \leqq x \leqq \delta. \qquad \text{(XIII)}$$

Upon introduction of equation (XIII) into equation (II) for $i = j$, the reduction rate of a reducible substance j at a sufficiently small concentration, equal to the negative value of the transport rate in the direction of the x coordinate, is found to be

$$v_j = D_j \frac{\partial c_j}{\partial x} + \frac{D_j z_j (1 - \gamma)}{\gamma\delta + (1 - \gamma)x}. \qquad \text{(XIV)}$$

Integration with $c_j = c_{j(0)}$ for $x = \delta$ as the bulk concentration of ions j gives

$$c_j = \frac{v_j \delta}{(z_j + 1)D_j(1 - \gamma)} \left[\gamma + (1 - \gamma)\frac{x}{\delta}\right] + \left[c_{j(0)} - \frac{v_j \delta}{(z_j + 1)D_j(1 - \gamma)}\right] \times \left[\gamma + (1 - \gamma)\frac{x}{\delta}\right]^{-z_j} \quad \text{if } z_j \gtrless -1 \qquad \text{(XVa)}$$

$$c_j = \left\{c_{j(0)} + \frac{v_j \delta}{D_j(1 - \gamma)} \ln\left[\gamma + (1 - \gamma)\frac{x}{\delta}\right]\right\} \times \left[\gamma + (1 - \gamma)\frac{x}{\delta}\right] \quad \text{if } z_j = -1. \qquad \text{(XVb)}$$

Assuming that ions j are readily reduced at the cathode and, therefore, putting $c_j = 0$ for $x = 0$, we obtain the reduction rate v_j from equations (XVa) and (XVb) as

$$v_j = \frac{(z_j + 1)D_j(1 - \gamma)c_{j(0)}}{\delta(1 - \gamma^{z_j+1})} \quad \text{if } z_j \gtrless -1 \qquad \text{(XVIa)}$$

$$v_j = \frac{D_j(1 - \gamma)c_{j(0)}}{\delta \ln \gamma^{-1}} \quad \text{if } z_j = -1. \qquad \text{(XVIb)}$$

If the acid concentration at the surface of the cathode differs only slightly from the bulk concentration, i.e., if $\gamma \cong 1$, equations (XVIa) and (XVIb) transform to equation (VIII), i.e., the reduction rate is proportional to the concentration $c_{j(0)}$ and independent of the current density.

If the current density is close to the limiting value of the current density due to concentration polarization with respect to hydrogen ions and thus $\gamma = c_K/c_o \ll 1$, we have the following three cases.

1. For positively charged ions j it follows from equations (XVIa) and (VIII) that

$$v_j/v_j^{(0)} \cong z_j + 1 \text{ if } \gamma \ll 1 \text{ and } z_j > 0. \qquad \text{(XVIIa)}$$

2. For univalent anions it follows from equations (XVIb) and (VIII) that

$$v_j/v_j^{(0)} \cong 1/\ln \gamma^{-1} \text{ if } \gamma \ll 1 \text{ and } z_j = -1. \qquad \text{(XVIIb)}$$

3. For anions with a valence greater than unity it follows from equations (XVIa) and (VIII) that

$$v_j/v_j^{(0)} \cong (|z_j| - 1)\gamma^{|z_j|-1} \text{ if } \gamma \ll 1 \text{ and } z_j \leqq -2. \qquad \text{(XVIIc)}$$

According to equation (XVIIc) the reduction rate v_j of divalent or trivalent anions is greatly diminished by applying a high cell voltage which results in a current density close to the limiting value due to concentration polarization with respect to hydrogen ions and, thus, gives a value of γ much less than unity. In general, such conditions are not likely to occur. This case is, therefore, only of academic interest.

Oxidation Processes in a Solution with Excess Sodium Hydroxide

Relations analogous to equations (XII) to (XVIIb) can be derived for the anodic oxidation of oxidizable substances in a sodium hydroxide solution when oxygen is evolved at the anode. Since the potential gradient has the opposite sign, z_j has to be replaced by $-z_j$ in equations (XIV) to (XVIb). Thus, the oxidation rate of cations with a valence greater than unity becomes proportional to the $(z_j - 1)^{th}$ power of the concentration ratio $\gamma = c_R/c_o$ of sodium hydroxide if $\gamma \ll 1$.

Prevention of the Cathodic Reduction of Hypochlorite

When hypochlorite is produced by the electrolysis of a sodium chloride solution for industrial purposes, reduction of hypochlorite at the cathode must be minimized. This can be accomplished by a thin diaphragm at the surface of the cathode. According to Foerster and Bischoff (1) and others (2), a small amount of calcium or magnesium chloride is added to the electrolyte so that, at the cathode, a precipitate of calcium or magnesium hydroxide is formed. According to Müller (3), a small amount of chromate is added, which is reduced at the cathode and yields a very thin but effective diaphragm of chromium oxide.

If the current density in the pores of such a diaphragm is sufficiently high, cathodic reduction of hypochlorite will be minimized by the adverse potential gradient in the pores in view of conclusions drawn from equation (IXc).

It seems significant that the reduction of chromate takes place as long as the current density is relatively low, but will practically cease after a sufficient portion of the surface of the cathode has been covered by chromium oxide and, thus, a sufficient current density has been reached, for chromate ions are also rejected by an adverse potential gradient. This mechanism automatically gives a diaphragm which is effective, but does not cause an excessive IR drop or polarization potential.

According to this interpretation, no specific repulsing forces are needed in order to prevent the approach of hypochlorite toward the cathode, or its reduction. Specific adsorption in the pores of the diaphragm seems of minor importance because of the small thickness of the electrical double layer at high electrolyte concentrations.

Frumkin and Florianovich (4) have pointed out that reduction of anions at a cathode may also be prevented if the electrical double layer next to the cathode contains virtually no anions, as is characteristic of a cathode kept at a sufficiently negative potential with respect to a standard hydrogen electrode if the total electrolyte concentration is low. This effect, however, becomes insignificant at high electrolyte concentrations used for the electrolytic production of hypochlorite.

To summarize, the adverse potential gradient in pores of a diaphragm seems to be sufficient in order to account for the prevention of the reduction of hypochlorite ions.

Any discussion of this paper will appear in a Discussion Section to be published in the December 1954 issue of the Journal.

REFERENCES

1. H. Bischoff and F. Foerster, *Z. Elektrochem.*, **4**, 464 (1898).
2. F. Oettel, *ibid.*, **5**, 1 (1898); E. Müller and M. Buchner, *ibid.*, **16**, 93 (1910); P. Prausnitz, *ibid.*, **18**, 1025 (1912).
3. E. Müller, *ibid.*, **5**, 469 (1899); **7**, 398 (1900); **8**, 909 (1902).
4. A. N. Frumkin and G. M. Florianovich, *Doklady Akad. Nauk. S. S. S. R.*, **80**, 907 (1951).

Stability of 2,6-Di-Tertiary-Butyl-Para-Cresol Inhibited Transformer Oil in an Arc[1,2]

R. Nichols Hazelwood, Kazumi Oura,[3] and Raymond M. Frey

Line Material Company, Milwaukee, Wisconsin (A McGraw Electric Company Division)

ABSTRACT

Behavior in an arc of transformer oil inhibited with 0.3% by weight 2,6-di-tertiary-butyl-para-cresol was studied. It is shown that there is no essential difference between decomposition of inhibited and uninhibited transformer oil. By quantitative determinations and paper chromatography, it was found that there is no preferential destruction of the inhibitor itself by arcing. The path of arcing breakdown of transformer oil was studied, and it was found that the process was similar to thermal cracking of petroleum.

Introduction

Three years ago the electrical industry initiated use of inhibitors to prevent oxidation in transformer oil. This step had been advocated by Von Fuchs (1) who had shown that inhibitors increased the life of transformer oil in laboratory tests. Requirements of a satisfactory inhibitor are: (*A*) oxidation products of the inhibitor must be oil soluble. (*B*) The inhibitor should be relatively nonpolar, insoluble in water, and should not react directly with molecular oxygen. (*C*) The inhibitor should not be removed by oil reclamation procedures and should not be incompatible with regular grades of transformer oil.

Compounds known as "hindered phenols" were found to be excellent oxidation inhibitors for petroleum products (2). Many persons felt that earlier oxidation inhibitors of the phenylene diamine or aminophenol types were not as satisfactory because of their susceptibility to air oxidation and their high water solubility (3). The hindered phenols are characterized by tertiary butyl groups on the 2 and 6 positions of the aromatic ring and an *n*-alkyl group on the 4 position. Effectiveness of the inhibitor increases with increasing length of this alkyl group and decreases with decreased branching of groups on the 2 and 6 positions (4).

Commonest of hindered phenols in commercial practice is 2,6-di-tertiary-butyl-para-cresol, known as DBPC. DBPC is a clear white crystalline solid melting at 70°C and boiling at 265°C. Specific gravity at 20°C is 1.048. It is soluble in common organic solvents and insoluble in water and aqueous solutions (5). It does not react with alkalies or undergo any of the usual reactions of a phenol due to the shielding effect of the large tertiary butyl groups (6).

The primary function of an oxidation inhibitor in mineral oil is to react with hydroperoxides formed by oxidation (3).

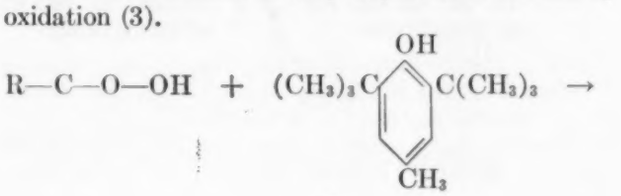

a

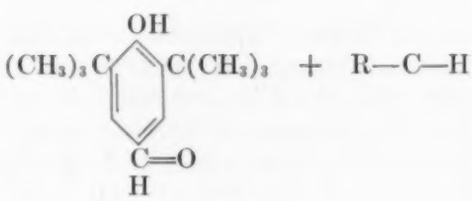

b

The aldehyde (*b*) has some anti-oxidant properties itself, although not to the extent that DBPC (*a*) has (4).

The function of an inhibitor is to interrupt a chain reaction. It is now thought that the reaction chain in hydrocarbons follows the sequence of: hydrocarbon → hydroperoxide → aldehyde → acid. This chain is interrupted at the stage of formation of hydroperoxide. The inhibitor is oxidized to the aldehyde (*b*). This aldehyde can be produced by chromic acid oxidation of DBPC (4), or by oxidation with bromine in alcohol solution (7). It has been isolated by chromatographic methods from oxidized inhibited oil samples (4).

Zwelling (8) has shown that DBPC-inhibited transformer oil decreases formation of sludge and maintains the transformer in better condition. Because of this and previous work,[4] most of the electrical industry adopted inhibited oil for use in distribution transformers. Use of inhibited oil in switchgear and circuit interrupting devices was started in January 1951. Recent studies on small distribution oil circuit reclosers (9) and on large

[1] Manuscript received July 24, 1953. This paper was prepared for delivery before the New York Meeting, April 12 to 16, 1953.

[2] Second in a series of studies on inhibited transformer oil. For first paper see Reference (9).

[3] Deceased (August 10, 1953).

[4] Previous work done by Shell Oil Company.

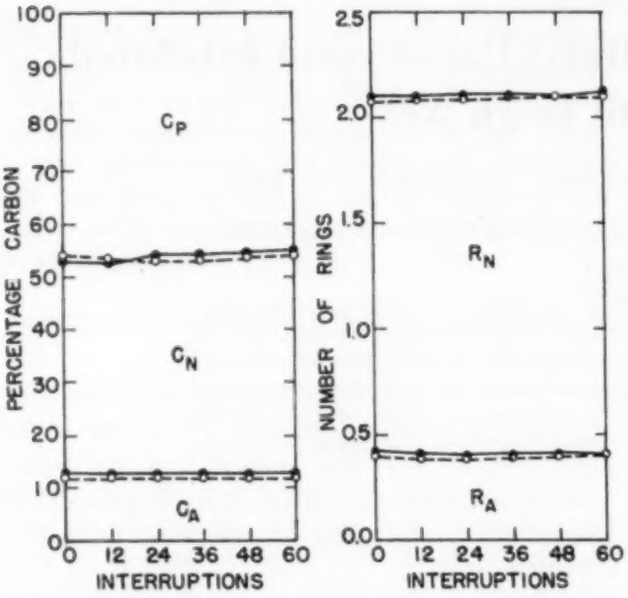

FIG. 1. Carbon distribution and ring content for series 1. 60 interruptions at 7.2 kv, 490 amp, 30% power factor. C_A = aromatic carbon, C_N = naphthenic carbon, C_P = alkyl carbon, R_A = aromatic rings, and R_N = naphthenic rings. ——●—— = inhibited oil, — —○— — = uninhibited oil.

circuit breakers (10) have shown that there is no essential difference in behavior and size of carbon particles formed in inhibited and uninhibited oils, and that presence of inhibitor causes no apparent anomalies in performance of these devices.

EXPERIMENTAL

Oil samples to be arced were placed in standard production Model KYLE Type H oil circuit reclosers. These reclosers had coil ratings of 5, 25, or 50 amp. Varying conditions of voltage, current, and power factor of the short circuit faults were then applied. Conditions chosen simulate extreme heavy duty field operation.

In each series of experiments, one recloser was filled with uninhibited transformer oil drawn from a newly received tank car. The other recloser was filled with oil inhibited in the laboratory with crystalline DBPC. The same base stock oil was used for all samples. Concentration of DBPC was 0.3% by weight (common concentration in commercial practice).

Viscosity of oil samples was measured using calibrated Ostwald-Fenske viscosity pipettes in constant temperature baths controlled at 37.8°C (100°F) and at 98.9°C (210°F). Densities were measured with a Leach pycnometer at 20°C. The pycnometer was calibrated at 20°C with distilled H_2O and then corrected to absolute density (20/4°C). Refractive index and refractive dispersion were measured with an Abbe refractometer at 20°C. The weight per cent of DBPC was determined colorimetrically by reduction of phosphomolydbic acid to molybdenum blue (11). Molecular weights were measured by the cyroscopic method in benzene or by viscosity-density correlations (12). Data for various sample series were analyzed for carbon distribution and ring content by the *n-d-M* method (13). These data, combined with viscosity index and specific dispersion data, give a picture of reactions which take place in the arc.

RESULTS AND DISCUSSION

Fig. 1 is a plot of a series of 60 interruptions at 7200 volts, 490 amp, and 30% power factor. The recloser had a coil rating of 25 amp. In this and all subsequent cases, arcing time was approximately ½ to 1 cycle/interruption.

Results of this series of arcings show that there is a small but continuing decrease in aromatic content and an increase in naphthenic content. The alkyl carbon shows a decrease. These changes are seen in both carbon distribution and ring content. It is also notable that the method is sensitive enough to show the presence of the aromatic inhibitor (DBPC) in the inhibited oil.

Fig. 2 is a plot of a series of 64 arcings at 7200 volts, 700 amp, and 30% power factor in a recloser with a coil rated at 50 amp. In inhibited oil, the trend is similar to results shown in Fig. 1, that is, increased naphthenes and decreased aromatics and paraffins. However, the uninhibited oil appears to show just the opposite behavior. Fig. 3 shows specific dispersion which is another measure of aromatic content, for the series in Fig. 2. Here, the decrease for both samples indicates that the aromatic content is decreasing in each case.

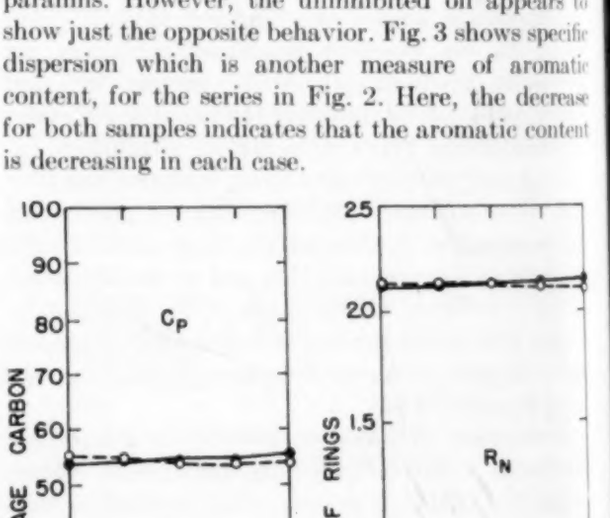

FIG. 2. Carbon distribution and ring content for series 2. 64 interruptions at 7.2 kv, 700 amp, 30% power factor. ——●—— = inhibited oil, — — —○— — — = uninhibited oil.

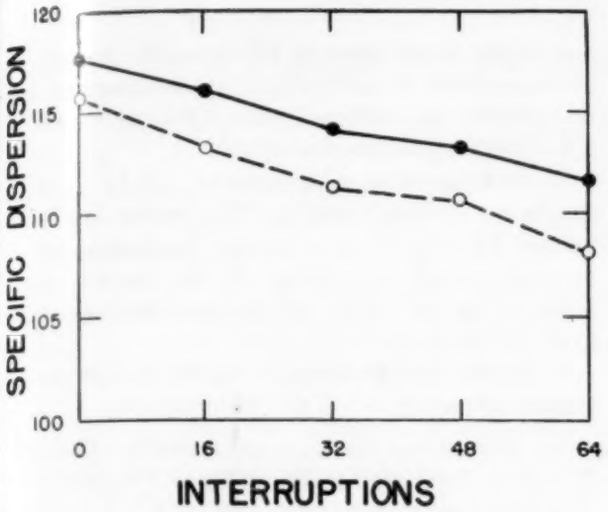

FIG. 3. Specific dispersion for series 2. Specific dispersion, $\delta_i = n_F - n_C/d_4^{20} \times 10^4$.

A series of four reclosers having 5-amp coils was prepared for studies of oxidation stability of oil. Two of these had inhibited oil and two had uninhibited oil. A total of 20 interruptions at 13,200 volts, 100 amp, and 30% power factor was performed.

Table I shows the results of these conditions on carbon distribution and ring content.

The only statistically significant changes are in decreased aromatic content and increased naphthenic content of the inhibited oil, and decrease in paraffinic carbon of both oils. Decrease in aromatic content of the inhibited oil might be interpreted as inhibitor destruction. However, this was not found to be the case.

A 50-amp coil recloser was filled with an inhibited oil and arced 40 times at 7200 volts, 705 amp, and 30% power factor. Samples were drawn at 0, 20, and 40 operations. Table II presents results of this series.

Inspection of data presented indicates that the following changes occur when transformer oil is arced in a circuit recloser: aromatic content is decreased, alkyl chains are broken, and viscosity, molecular weight, and viscosity index are decreased.

These changes are in addition to formation of carbon, hydrogen, and hydrocarbon gases from complete breakdown of the oil. Cracking of oil to gaseous hydrocarbons, hydrogen, carbon, and acetylene polymers has been described by Salzer (14).

These changes are consistent with what would be expected in a thermal cracking process. In thermal cracking, side chains are cleaved, aromatics are reduced to cycloalkanes, and cycloalkyl rings may be broken. As the temperature of the thermal cracking process is raised, another phenomenon occurs. Aromatics are produced at the expense of saturated

TABLE I

No. of interruptions	Oil sample	% C_A	% C_N	% C_P	R_A	R_N
0	Inhibited	12.6	40.0	47.4	0.42	1.71
20	Inhibited	11.3	43.0	45.7	0.37	1.79
0	Uninhibited	11.2	42.1	46.7	0.37	1.81
20	Uninhibited	11.6	42.7	45.7	0.38	1.78

% C_A = % aromatic carbon; % C_N = % naphthenic carbon; % C_P = % paraffinic carbon; R_A = number of aromatic rings; R_N = number of naphthenic rings.

TABLE II

No. of interruptions	% C_A	% C_N	% C_P	VI*	η†	d_4^{20}	M‡	$\frac{cc}{g}$ DBPC§
0	12.3	42.8	44.9	73	9.09	0.8869	267	0.30
20	12.0	43.7	44.3	67	8.93	0.8873	264	0.31
40	11.5	44.7	43.8	45	8.89	0.8884	260	0.32

* Viscosity index.
† Centistokes at 37.8°C (100°F).
‡ Cryoscopic.
§ All ±10%. Differences here not significant.

molecules. The same thing happens in catalytic cracking, although the process is more selective and operates at a lower temperature.

From these considerations and from data presented above, a series of equations may be written to describe a portion of what happens to transformer oil in an arc. These equations make use of a so-called "average molecule" which merely represents approximate composition of the transformer oil.

Current theories of the composition of petroleum indicate that above the gasoline range, ring compounds are present primarily as 6-membered fused ring systems, with aliphatic side chains (13). In transformer oil, wax-free crudes are used, so there are no free paraffins present. Aromatics are thought to be part of a fused ring system along with naphthenic rings, rather than free (15). With these factors in mind, the following equations can be written:

$$C_9H_{19} \rightarrow C + (C_2H_2)_x + H_2 + CH_4 + C_2H_2 + C_2H_4, \text{etc.} \quad \text{(I)}$$

$$\rightarrow R + H_2 + C, \text{etc.} \quad \text{(II)}$$
$$R < C_9H_{19}$$

$$C_9H_{19} \rightarrow$$

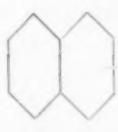

$$C_9H_{19} \quad \text{(III)}$$

$$\rightarrow R + H_2 + C, \text{etc.} \quad \text{(IV)}$$
$$R < C_9H_{19}$$

Orientation and number of alkyl side chains is not specified, but, probably the chains are present in one long unbranched alkyl group. This is indicated from viscosity index and viscosity data. If there were more than one chain or branched chains, a lower viscosity index would be expected (13).

These equations lead to certain expected results. If equations (II) and (IV) are true, the molecules would become more spherical in shape. This would result in an increase in density and a decrease in molecular weight, viscosity, and viscosity index. All these have been shown experimentally.

Analysis indicates that there is no specific decomposition of DBPC in the arcing process. The phosphomolybdate method for determination of DBPC (11) is not specific but is characteristic of all cresols. However, it was found that alkyl cyclohexanols did not react in the phosphomolybdate spot test (6). To check further the possibility that some side chains might be cleaved from DBPC by the arc, thus destroying much of the antioxidant character (4), paper chromatograms were run on arced oil samples. With Whatman No. 1 paper, butanol saturated with ammonia served as a developing solvent for ascending or descending chromatograms. In this system, the R_f value of phenol is 0.78; of *p*-cresol, 0.31; of 2-tert-butyl-*p*-cresol, 0.2; and of DBPC, 0.00. No compound other than DBPC was found in the developed chromatograms, using a 1% phosphomolybdic acid solution in methanol as a spray reagent, followed by exposure to ammonia vapor for five minutes. It is, therefore, reasonable to conclude that, within the limits of detection, DBPC is not preferentially destroyed by arcing.

Further studies are in progress to determine more specific information about the effects of arc energy on cracking of transformer oil in an arc, on the effect of repeated arcing for a prolonged period, and on fractionation of arced oil.

Conclusions

1. There is no essential difference in the path of decomposition of uninhibited transformer oil and transformer oil inhibited with 0.3% by weight of 2,6-di-tertiary-butyl-para-cresol.

2. Decomposition of transformer oil by arcing is similar to thermal cracking. The process is characterized by side chain cleavage, hydrogenation of aromatics, and formation of the decomposition products carbon, acetylene polymers, hydrogen, and hydrocarbon gases.

3. There is no preferential destruction of the inhibitor by arcing.

Any discussion of this paper will appear in a Discussion Section to be published in the December 1954 issue of the JOURNAL.

REFERENCES

1. G. H. Von Fuchs, *ASTM Symposium on Insulating Oils* (3rd series), **1949**, 28.
2. D. R. Stevens and W. A. Gruse, U. S. Pat. 2,265,582 (1941).
3. M. C. K. Jones, A. R. Jones, and B. R. Strickland, *Ind. Eng. Chem.*, **44**, 2721 (1952).
4. J. I. Wasson and W. M. Smith, *ibid.*, **45**, 197 (1953).
5. W. A. Pardee and W. Weinrich, *ibid.*, **36**, 595 (1944).
6. G. H. Stillson, D. W. Sawyer, and C. K. Hunt, *J. Am. Chem. Soc.*, **67**, 303 (1945).
7. G. M. Coppinger and T. W. Campbell, *ibid.*, **75**, 734 (1953).
8. M. I. Zwelling, *Elec. World*, **134** [7] 73 (1950).
9. K. Oura, R. N. Hazelwood, and R. M. Frey, *Trans. AIEE*, **72**, Part III, 297 (1953).
10. W. M. Leeds and R. F. Seubert, *ibid.*, **72**, Part III, 718 (1953).
11. Koppers Co. Method # C-520, Koppers Company, Chemical Division, Pittsburgh.
12. A. E. Hirschler, *J. Inst. Petroleum*, **32**, 133 (1946).
13. K. Van Nes and H. A. Van Westen, "Aspects of the Constitution of Mineral Oils," Elsevier Publishing Co., New York (1951).
14. E. Salzer, "Fundamentals of AC Circuit Interruption," p. 36, Allis-Chalmers Mfg. Co., Milwaukee, Wis. (1950).
15. K. Van Nes, H. I. Waterman, H. A. Van Westen, and H. Van Kranen, *J. Inst. Petroleum*, **38**, 998 (1952)

New Manganese-Activated Fluoride Phosphors[1]

ARTHUR L. SMITH

Tube Department, Radio Corporation of America, Lancaster, Pennsylvania

ABSTRACT

The following manganese-activated fluorides were found to exhibit efficient cathodoluminescence: $NaZnF_3$, $KZnF_3$, K_2ZnF_4, $NaMgF_3$, $KMgF_3$, K_2MgF_4, CaF_2, $KCaF_3$, $KCdF_3$, and the solid solutions formed between CaF_2 and AlF_3. With MgF_2 and ZnF_2, AlF_3 was found to be only a diluent; with CaF_2, however, three compounds, $2CaF_2 \cdot AlF_3$, $CaF_2 \cdot AlF_3$, and $CaF_2 \cdot 2AlF_3$, were discovered, the first having a peak emission at 5380 Å and the latter two at 5250 Å. Emission of Mg and Zn compounds containing K or Na was almost identical with that of the original MgF_2 and ZnF_2. Although CaF_2:Mn has an efficient green and CdF_2:Mn a weak green emission, their K-perovskites show strong yellow-orange emission. From the above results, a hypothesis is advanced relating a coordination number of six for the divalent cation in fluorides to orange emission, and a coordination number of eight to green emission.

INTRODUCTION

Manganese-activated fluorides of zinc, magnesium, and zinc-magnesium have been investigated previously from both practical and theoretical viewpoints. Because these fluorides have predominantly exponential decay, they have been used in cathode ray tubes designed for applications such as radar and loran requiring long-persistence phosphors (1, 2). They have also been used by Williams and coworkers in the formulation of basic concepts of the luminescence process (3–6).

Other manganese-activated fluorides have received scant attention. Calcium fluoride is a possible exception, although even it has not been studied in any systematic fashion. The only positive statement found in available literature was that CaF_2:Mn has a green cathodoluminescence (7). Therefore, a program was begun to determine whether fluorides other than zinc and magnesium could be effectively activated by manganese.

Fluorides of the alkali metals are poor phosphors, probably because of ion charge differences. There is a lack of suitable sites at which the manganese ions can function as activators. Manganese activation also failed to produce luminescence in the fluorides of strontium and barium. It produced only an inefficient luminescence in cadmium fluoride, probably because the ions in these structures are too large to be replaced effectively by manganese. Perovskite-type fluorides of the class $M^{I}M^{II}F_3$, on the other hand, were found to be excellent base matrices. Spectral energy emission characteristics of this class of fluorides led to the formulation of a new hypothesis concerning the role of manganese as an activator (8).

Compounds and solid solutions of aluminum fluoride and alkali or alkaline earth fluorides were also investigated. The combination of aluminum fluoride and calcium fluoride was the only combination which gave efficient phosphors. An x-ray investigation of this system led to the discovery of hitherto unreported compounds of AlF_3—CaF_2.

PREPARATION OF PHOSPHORS

All the simple fluorides were prepared in platinum vessels by reaction between excess C.P. H_2F_2 or $(NH_4)_2F_2$ and purified carbonates or oxides of the requisite cation. The slurry was carefully evaporated to dryness and then baked at 500° C to decompose any remaining acid or ammonium fluorides. Manganese fluoride was added to the simple fluorides (or, in cases where complexes were to be formed, to the suitable combination of the simple fluorides) in the amount of 1 mole %/mole of base matrix. Mixtures were then dry ground in a mortar and fired in either carbon crucibles or platinum crucibles surrounded by carbon to prevent oxidation. Firing temperature depended on the melting point of the final compound. For compounds melting above 1000°C that temperature was used; for compounds melting below 1000°C, the firing temperature was 50° below the melting point. All mixtures except those containing CaF_2—AlF_3 were fired for two half-hour periods and were ground between firings. CaF_2—AlF_3 mixtures were fired for three half-hour periods.

TESTING OF PHOSPORS

X-ray diffraction analyses were made with nickel-filtered radiation from a copper-target tube

[1] Manuscript received October 1, 1953. This paper was prepared for delivery before the New York Meeting, April 12 to 16, 1953.

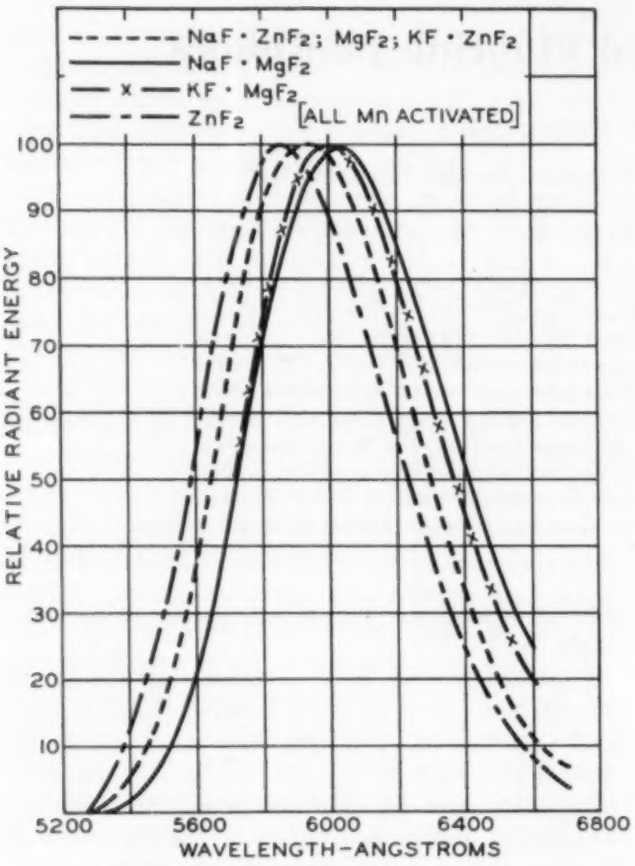

FIG. 1. Spectral energy distribution curves of manganese-activated zinc fluoride, magnesium fluoride, and their alkali fluoride perovskites.

operated at 40 kv and 15 ma. Phosphor samples were rotated within a circular camera 14.32 cm in diameter.

Cathodoluminescence efficiencies and emission spectra were determined with a defocused electron beam having a current density of 1.5 μa/cm^2 and an accelerating potential of 8000 volts. Peak efficiencies and spectral distribution of energy were measured by the spectroradiometer and method described by Hardy (9).

Simple Fluorides

The cathodoluminescence of the manganese-activated alkali fluorides and aluminum fluoride was of such low order that accurate readings were not possible. Because of differences in ion size and charge between these cations and manganese, the manganese probably cannot be built into the lattice in the proper manner to form active centers. Ion-size differences alone probably prevent the effectivent activation of fluorides of beryllium, strontium, and barium by manganese. No accurate data could be obtained for any of these mixtures.

Manganese-activated zinc, magnesium, and zinc-magnesium fluorides have been thoroughly described (1–6). Their spectral-energy peak is approximately 5900 Å, as shown in Fig. 1.

Calcium and cadmium fluorides are not as well known as the zinc and magnesium fluorides. Concurrently with the work described in this article, Ginther (10) was investigating properties of calcium fluoride activated by cerium and manganese. Results given here concerning the peak and shape of the spectral energy emission curves are in substantial agreement with his results. The peak value of 4950 Å for calcium fluoride activated with 1 mole % manganese checks reasonably well with Ginther's value of 4900 Å for this concentration. CaF_2:0.01 Mn is a moderately efficient phosphor having 30% of the efficiency of ZnF_2:Mn. The spectral energy emission curve for this mixture is shown in Fig. 4. Its persistence is the shortest of all the fluorides, although exact data are not yet available. CdF_2:0.01 Mn is a very poor phosphor; its efficiency is only 1% of that of zinc fluoride. It has essentially the same spectral energy emission characteristic and peak emission as calcium fluoride.

Fluoride Perovskites

Structural Considerations

The perovskite structure is one in which large cations together with either $O^=$ or F^- form a close-packed arrangement with smaller cations in the interstices of sixfold coordination. A definite relationship must exist between the ionic radii of the ions in order that this structure be formed. For fluorides, this relationship is expressed by the equation

$$r\mathrm{M^I} + r\mathrm{F^-} = t\sqrt{2}\,(r\mathrm{M^{II}} + r\mathrm{F^-})$$

where t can have a value between 0.8 and 1.0 (11*a*). The large ions M^I and F^- form a close-packed arrangement with the smaller M^{II} ions in the interstices. The M^{II} ions are surrounded by six F^- in octahedral configuration. Substitution of the values of the ionic radii of Li, Na, K, Mg, Zn, Mn, Cd, and Ca in their proper places in the above equation indicates that Li should form no complexes at all, Na should form a complex with Mg, Zn, or Mn, but not with Ca or Cd, and K should form complexes with Mg, Zn, Mn, Ca, or Cd. All theoretically possible structures have been prepared in the laboratory except those of manganese, which were not tried. No compound formation occurred where theory indicated it was impossible. Potassium perovskites of Mg, Zn, and Ca have been reported previously and their x-ray diffraction pattern published (12). The compound $NaF \cdot MgF_2$ has also been investigated and was found to have a melting point of 1030°C (13). Although $NaF \cdot ZnF_2$ and $KF \cdot CdF_2$ are predicted by the above equation,

they have not been reported previously. These compounds were made, and were found to have x-ray diffraction patterns typical of the group.

Another complex fluoride, K_2MgF_4, has also been reported (14). Although the diffraction pattern of this fluoride is available (12), its exact crystal structure has not yet been determined. The previously unreported zinc analogue, K_2ZnF_4, was also prepared, and was found to have an x-ray diffraction pattern very similar to that of the magnesium compound. Calcium, however, did not form this type of structure; x-ray diffraction patterns of a fired mixture containing 2 moles of KF per mole of CaF_2 showed only the lines of KF and $KCaF_3$.

Spectral-Energy Emission Characteristics

The perfect and near-perfect coincidence of cathodoluminescent spectral-energy emission characteristic of these perovskites, illustrated in Fig. 1, 2, and 3, and Table I, is of major interest. The spectral energy emission curves of $NaF \cdot ZnF_2$, $KF \cdot ZnF_2$, and MgF_2 are identical within experimental error; each mixture in the pairs $NaF \cdot MgF_2$—$KF \cdot MgF_2$, $KF \cdot CaF_2$—$KF \cdot CdF_2$, and $2KF \cdot ZnF_2$—$2KF \cdot MgF_2$ differs from the other mixture in the pair by less than 50 Å. Within the group of compounds formed in the system NaF—KF—ZnF_2—MgF_2, the maximum difference in peak of emission is only

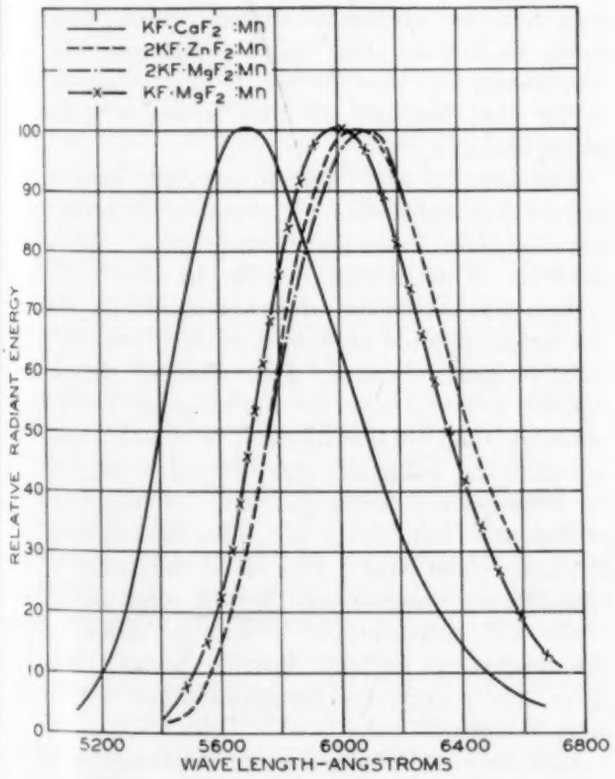

FIG. 2. Potassium-magnesium-fluoride:Mn spectral energy distribution compared with those of potassium-calcium-fluoride:Mn $2KF \cdot ZnF_2$:Mn and $2KF \cdot MgF_2$:Mn.

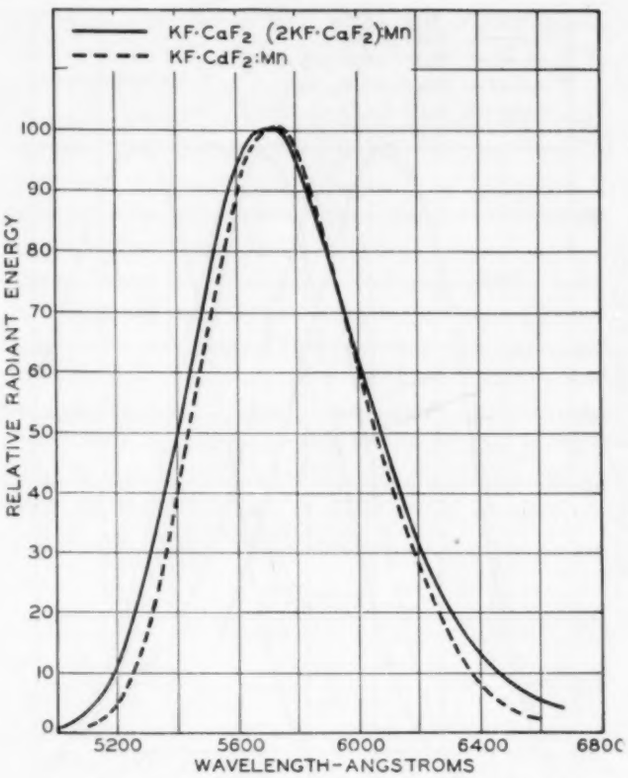

FIG. 3. Spectral energy distribution curves for the manganese-activated potassium-fluoperovskites of calcium and cadmium showing the almost coincident spectra.

TABLE I. *Wave lengths (Å) of peak spectral emission of phosphors formed from compounds shown in left vertical column in combination with compounds shown in top horizontal line*

		NaF	KF	2KF	AlF_3
MgF_2	5920	6080	6000	6100	5920
ZnF_2	5870	5920	5920	6070	5870
CaF_2	4950	5020	5710	5710	5250
CdF_2	4950	—	5720	5720	—

230 Å, with zinc fluoride at one extreme at 5870 Å and $2KF \cdot MgF_2$ at the other extreme at 6100 Å.[2]

The difference of 750 Å in the spectral energy peak between CaF_2 or CdF_2 (4950 Å) and $KF \cdot CaF_2$ or $KF \cdot CdF_2$ (5710 Å) is also important. It is in sharp contrast to the much smaller shifts in the perovskite complexes of ZnF_2 and MgF_2. The shift caused by the addition of sodium fluoride to calcium fluoride is less than 100 Å, as shown in Fig. 4. This

[2] One of the reviewers has called attention to the work of J. T. Randall, [*Proc. Roy. Soc. London*, **170A**, 272 (1939)] on the low temperature cathodoluminescent spectra of manganese halides. At 90°K, the peak emission occurred at 6285Å for the fluoride, 6360Å for the chloride, and 6330Å for the bromide. Randall concluded that the red fluorescence is a property of all the manganese ions in the crystal, with the transitions of the forbidden type ($^2E \rightarrow {}^4F$) characteristic of the divalent manganese ion. In all cases manganese occurs in sixfold coordination.

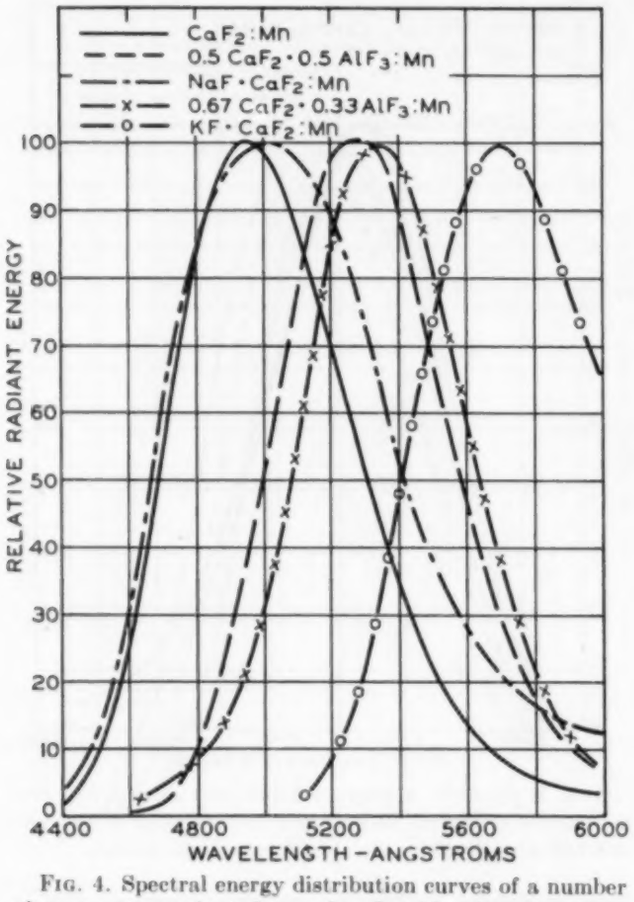

FIG. 4. Spectral energy distribution curves of a number of manganese-activated complex fluoride phosphors containing calcium compared with that of calcium fluoride:Mn itself.

relatively small shift confirms the observation that sodium fluoride forms no definite perovskite structure such as that formed with potassium fluoride. As shown in Fig. 3, the spectral energy emission characteristics of $KF \cdot CaF_2$ and $KF \cdot CdF_2$ do not differ by more than 25 Å. This small change indicates that precisely the same mechanism caused the shift for both the calcium and cadmium compounds.

Efficiencies

Table II gives the relative peak efficiencies of the various fluorides. The peak efficiency of zinc fluoride, the highest of all the fluoride efficiencies, has been used as the standard to which all the others are related. Most of the phosphors containing alkali fluorides are less efficient than those free from alkali fluoride, with two exceptions. The compound $KF \cdot ZnF_2$ is as efficient as ZnF_2 itself, and $KF \cdot CdF_2$ shows a considerable improvement in efficiency over CdF_2. The probable reason for the difference in these two mixtures is treated later.

TABLE II. *Relative peak spectral emission efficiencies (%) of phosphors formed*

		NaF	KF	2KF	AlF_3
MgF_2	54	24	41	20	40
ZnF_2	100	61	100	53	20
CaF_2	30	3	20	4	50
CdF_2	1	0	45	6	1

TABLE III. *Emission color and relative peak efficiencies of inefficient phosphors containing alkali fluorides*

Compound	Color	Relative peak efficiency (ZnF_2 = 100)
$LiF \cdot AlF_3$	Orange-yellow	1
$3LiF \cdot AlF_3$	Yellow-green	1
$NaF \cdot AlF_3$	Blue-green	1
$3NaF \cdot AlF_3$	Blue-green	2
$NaF \cdot 2AlF_3$	Yellow-orange	1
$5NaF \cdot 3AlF_3$	Yellow-green	5
$KF \cdot 2AlF_3$	Orange-red	1
$LiF \cdot CaF_2$	Green	2
$LiF \cdot CdF_2$	Blue-green	1

Fluoride Phosphors Containing Aluminum

There is a considerable number of compounds which contain alkali metals, aluminum, and fluorine, as shown in Table III. None of these produced efficient phosphors when manganese was used as an activator. The disparity in size and charge between manganese ions and alkali or aluminum ions is probably the reason why manganese could not effectively substitute in these structures. There was, however, enough weak but definite luminescence to indicate that some manganese was incorporated, and that the nature and concentration of the alkali ion were the main factors in the color of the emission.

Fluorides of zinc and magnesium form only limited solid solutions with aluminum fluoride, but form definite compounds with alkali fluorides. Addition of aluminum fluoride to zinc or magnesium fluorides merely decreases the efficiencies of the simple fluoride phosphors without causing any shift of peak emission. The effect of aluminum fluoride is less drastic on the magnesium fluoride phosphor than on zinc fluoride. In a 50-50 mole % mixture, the reduction of efficiency is only 20% for magnesium fluoride, but 80% for zinc fluoride, as shown in Table II. X-ray diffraction analyses of $ZnF_2 \cdot AlF_3$ and $MgF_2 \cdot AlF_3$ show the presence of both original components. There is some distortion of the AlF_3 structure, but little or no distortion of the magnesium or zinc fluoride lattice. Results differ only slightly for variations about the 50-50 mole % composition.

Addition of aluminum fluoride to calcium fluoride produces different results, as shown in Table IV and Fig. 4. Within this system at least three compounds, or phases, are found, as well as solid solu-

TABLE IV. *Emission color and relative peak efficiencies of a series of calcium-aluminum-fluorides*

Molar composition	Peak emission (approx) (Å)	Relative peak efficiency (ZnF_2 = 100)
CaF_2	4950	30
0.9 CaF_2—0.1 AlF_3	4950 and 5250 (two bands)	30/30
0.8 CaF_2—0.2 AlF_3	4950 and 5380 (two bands)	15/32
0.7 CaF_2—0.3 AlF_3	5380	35
0.6 CaF_2—0.4 AlF_3	5380	45
0.5 CaF_2—0.5 AlF_3	5250	50
0.3 CaF_2—0.7 AlF_3	5250	35
0.2 CaF_2—0.8 AlF_3	5250	20

tions. It is not yet possible to assign unambiguous stoichiometric ratios to the various phases, but a reasonable approximation can be made. Correlation of the spectral distribution data with x-ray diffraction data indicates that three compounds are present in the system, having the following spectral distribution characteristics and identifying lattice spacings:

Compound	Peak emission (Å)	Lattice spacing (d values in Å)
$2CaF_2 \cdot AlF_3$	5380	(3.5), 2.90, 2.75, 1.87, 1.83, 1.74, 1.76
$CaF_2 \cdot AlF_3$	5250	(3.5), 3.25, 2.80, 2.00, 1.82
$CaF_2 \cdot 2AlF_3$	5250	(3.5), 3.20, 2.80, 1.98, 1.81

Interpretation of these data is difficult because of the probability that some lines are common to more than one phase, and because one line at 3.5 is common to all phases as well as to AlF_3 itself. There is no doubt, however, that the phase which emits at 5380 Å can be distinguished by the unique lines at d values of 2.90, 1.87, and 1.83, and that the 5250 Å emission is associated with a phase uniquely determined by d values of 3.25, 2.80, and 2.00. The third phase has lines very similar to those of the previous phase (d = 3.20, 2.80, 1.98) and also emits at 5250 Å. It is possible, therefore, that this compound is not a unique phase but a solid solution of $CaF_2 \cdot AlF_3$ with AlF_3. However, the lack of graduation of this slight, but very definite, shift, and the existence of the shift even in very large discernible excesses of AlF_3 make it probable that a definite phase does exist having a crystal configuration very similar to the $CaF_2 \cdot AlF_3$ compound.

The freezing point diagram of CaF_2—AlF_3—NaF (15) is in rough agreement with these findings. A eutectic was reported at 62.5 CaF_2—37.5 AlF_3. Here, a compound formation was hypothesized at 66.7 CaF_2—33.3 AlF_3 ($2CaF_2 \cdot AlF_3$). Between this eutectic point and the composition 42.5 CaF_2—57.5 AlF_3, the curve for CaF_2—AlF_3—NaF shows two very minor peaks at 52.5 CaF_2—47.5 AlF_3 and 47.5 AlF_3 and 47.5 CaF_2—52.2 AlF_3.

In this region, a new "phase" called $CaF_2 \cdot AlF_3$ was found. Fedotieff and Iljinsky (15) did not investigate concentrations beyond 57.5 mole % AlF_3; they said such concentrations were in an "unrealizable" or "indeterminate" region. At a concentration of 80 mole % CaF_2 and 20% AlF_3, they were also unable to determine a freezing point. Laboratory analysis of this concentration indicated that there were two phases coexistent—CaF_2 and the "$2CaF_2 \cdot AlF_3$" phase. It is hoped that a careful study may be made in the future of the melting point, x-ray diffraction pattern, and spectral energy emission characteristics of this binary so that the system may be positively defined.

Discussion

The crystal structure of all simple fluorides has been determined previously and may be found summarized in various publications (11*b*, 16). Both calcium fluoride and cadmium fluoride are of the fluorite (CaF_2) structure, in which each cation is surrounded by six fluoride ions. The fluorides of zinc, magnesium, and manganese are classed in the rutile (TiO_2) structure, in which each cation is surrounded by six fluoride ions. Aluminum fluoride crystallizes with a symmetry close to that of the rutile type, each aluminum ion occupying octahedral holes formed by close-packed fluoride ions. The perovskite-type structure has been described previously; the divalent cation in this type is surrounded by six fluoride ions.

The coordination number of the divalent cations may explain the almost negligible influence of the alkali ions on the spectral energy emission characteristics of zinc and magnesium fluorides and the pronounced shift of emission characteristics produced with calcium and cadmium fluorides. Zinc and magnesium are in sixfold coordination in both their simple fluorides and in perovskite complexes. Calcium and cadmium, on the other hand, are in eightfold coordination in their simple fluorides, but in sixfold coordination in their potassium perovskite complexes. It appears that in fluoride structures, therefore, substitution of manganese into a sixfold coordination structure produces a spectral energy emission in the orange region, and substitution in an eightfold coordinated structure produces emission in the green region. This hypothesis is analogous to that of Linwood and Weyl (17) for oxygen-dominated structures, in which green emission is attributed to fourfold coordination and red emission to sixfold or higher coordination. All the spectral energy emissions in the orange region of fluorides

occur in sixfold coordinated structures, while the two in the green region are in eightfold coordinated structures. When the coordination structure of calcium is changed from eightfold to sixfold, the emission shifts 750 Å toward the orange region. Cadmium shows a similar shift, and also produces an efficient perovskite phosphor, although its simple fluoride is poorly efficient. Reduction in size of the holes in which manganese can substitute probably permits a more efficient energy transfer.

Addition of sodium fluoride to calcium fluoride does not produce new compounds, but only solid solutions. The spectral energy emission curve is broadened and the peak shifted slightly by about 100 Å. Efficiency is decreased by 90%.

Little can be said about the CaF_2—AlF_3 compounds, because nothing is known about their crystal structure. From conclusions reached on a hole-size-and-coordination theory (8), it can be hypothesized, however, that in these new compounds calcium remains in eightfold coordination, but its ionic radius is decreased.

Acknowledgments

The assistance of the following associates is gratefully acknowledged: L. E. Whitmer for the preparation of samples, A. E. Hardy and staff for optical measurements, and A. D. Power and S. B. Deal for x-ray diffraction measurements.

Any discussion of this paper will appear in a Discussion Section to be published in the December 1954 issue of the JOURNAL.

REFERENCES

1. H. W. Leverenz, "Research and Development Leading to New and Improved Radar Indicators," NDRC Publication, PB25481.
2. H. W. Leverenz, "An Introduction to Luminescence of Solids," J. Wiley & Sons, Inc., New York (1950).
3. F. E. Williams, *J. Opt. Soc. Amer.*, **37**, 302 (1947).
4. J. H. Crawford, Jr., and F. E. Williams, *J. Chem. Phys.*, **18**, 775 (1950).
5. W. W. Parkinson, Jr., and F. E. Williams, *ibid.*, **18**, 534 (1950).
6. P. D. Johnson and F. E. Williams, *ibid.*, **18**, 323 (1950).
7. F. Wick, *J. Opt. Soc. Amer.*, **27**, 275 (1937).
8. A. L. Smith, Electrochem. Society 103rd Meeting, April 1953, Abstract #20.
9. A. E. Hardy, *Trans. Electrochem. Soc.*, **91**, 127 (1947).
10. R. J. Ginther, *This Journal*, to be published.
11*a*. A. F. Wells, "Structural Inorganic Chemistry," p. 330, Oxford University Press, London (1945).
11*b*. *Ibid.*, p. 275.
12. "Alphabetical and Grouped Numerical Index of X-Ray Diffraction Data," Special Technical Publication 48-B, American Society for Testing Materials, Philadelphia (1950).
13. A. G. Bergman and E. P. Dergunov, *C. A.*, **37**, 829 (1943); Compt. rend. Acad. U.R.S.S., **31**, 7534 (1941).
14. H. Remy and W. Seemann, *Rec. Trav. Chem.*, **59**, 516 (1940).
15. P. P. Fedotieff and W. P. Iljinsky, *Z. anorg. u. allgem. Chem.*, **129**, 93 (1923).
16. R. W. G. Wyckoff, "Crystal Structures," Vol. I, Interscience Publishers, Inc., New York (1951).
17. S. H. Linwood and W. A. Weyl, *J. Opt. Soc. Amer.*, **32**, 443 (1942).

Effect of Chain Branching on Electrochemical Carbon-Halogen Bond Fission. Possible Mechanism for the Process[1,2]

PHILIP J. ELVING AND JOSEPH M. MARKOWITZ

University of Michigan, Ann Arbor, Michigan

AND

ISADORE ROSENTHAL[3]

The Pennsylvania State College, State College, Pennsylvania

ABSTRACT

As part of a continuing study of the electrochemical reduction of carbon-halogen bonds, a group of branched-chain α-bromoalkanoic acids with several of their ethyl esters and straight-chain isomers were investigated polarographically. The relation between half-wave potential, $E_{1/2}$, and *p*H for the acids follows an S-shaped pattern having *p*H-invariant regions in the alkaline and acidic ranges, $E_{1/2}$ in the latter region being considerably more negative. The $E_{1/2}$ values for the esters are *p*H-independent, being slightly more positive than those of the corresponding acids in the acidic region. Polarographic waves all involve a diffusion-controlled two-electron reduction. In the acidic region, the branched-chain acids are more easily reducible than their straight-chain isomers by 0.20 to 0.13 volt, the larger differences being observed for the lower molecular weight acids. In the alkaline region the situation is more complicated; all acids in the series having ethyl groups or larger in the α-position have their $E_{1/2}$ shifted to more negative values.

The trend of the variation of $E_{1/2}$ with chain length is treated as the operation of three effects: (*a*) electrostatic effects which are important in the lower acids and esters; (*b*) steric effects related to ring-formation, which become important in the higher acids and make reduction more difficult; (*c*) bulk effects which are responsible for the over-all trend of reducibility in the higher acids. Variation of $E_{1/2}$ with *p*H is discussed briefly. Two hypothetical mechanisms, ionic and free-radical, are compared on the basis of the structural influences developed by the data.

INTRODUCTION

Previous polarographic work on electrochemical carbon-halogen bond fission in α-halogenated alkanoic acids is reviewed in a study (1) of the straight chain acids. At all *p*H values, as chain length increases, observed $E_{1/2}$ decreases, there being one exception, bromobutanoic, in the alkaline region. The bond fission involves a two-electron reduction with conversion to the corresponding saturated acid. The effect of ethanol on $E_{1/2}$ and diffusion current, i_d, is also discussed, as are the influences of structure and inductive effect on the ease of reduction.

For several reasons, it seemed logical to inquire next into the effect of branching of the carbon chain and of chain lengths on the ease of reduction. In the first place, one objective of the systematic study of electrochemical carbon-halogen bond fission is the possibility of defining a correlation between organic chemical reactivity of such bonds and polarographic half-wave potentials. Since both the chemical and electrochemical processes are usually irreversible, analogy between chemical reactivity and half-wave potential would be expected if both processes involved the same essential reaction pattern. Obviously, in any attempt to ascertain whether the electrochemical process is a displacement reaction or a free radical process, the structural factor of branching is important.

The behavior of 2-bromobutanoic acid in the previous study (1) was considered anomalous. The authors felt, however, that an attempt should be made to determine whether this anomaly was more general, and if so, whether some pattern underlay its occurrence. This represents a further reason for extending the study to the branched acids.

Another matter which required further investigation is the consistently observed and repeatedly verified result (1–8) that, for α-haloalkanoic acids, $E_{1/2}$ varies with *p*H in an S-shaped pattern. This behavior has never been satisfactorily explained on a quantitative basis, although related phenomena

[1] Manuscript received June 18, 1953. This paper was prepared for delivery before the New York Meeting, April 12 to 16, 1953.

[2] No. XVI in a series on the polarographic behavior of organic compounds.

[3] Present address: Rohm and Haas Company, Research Laboratories, Philadelphia, Pennsylvania.

TABLE I. *Polarographic data for straight and branched chain 2-bromoalkanoic acids,* C_2 *to* C_5

Temp, 0°C; mercury head, 50 cm. Diffusion coefficients were calculated from the Stokes-Einstein equation. n-Value from Ilkovic equation is 2 in all cases. Concentration of bromoacid ran from 0.1 to 0.7 mM; lower values were used to eliminate maxima.

Acid	MM		ME		EE		BE		HH		HM		HE	
$D \times 10^6$	2.02		1.97		1.92				2.15		2.08		2.02	
*p*H	$-E_{\frac{1}{2}}$	I	$-E_{\frac{1}{2}}$	I	$-E_{\frac{1}{2}}$	I	$-E_{\frac{1}{2}}$	I	$-E_{\frac{1}{2}}$	I	$-E_{\frac{1}{2}}$	I	$-E_{\frac{1}{2}}$	I
1.1	0.29	2.1	0.25	2.3	0.22	1.6	0.14	1.7	0.67*	2.3	0.52*	2.1	0.47*	1.8
1.4							0.16	1.9						
1.8	0.28	2.1	0.26	2.1	0.22	1.8	0.16	1.9	0.67*	2.2	0.56*	2.0	0.50*	1.9
4.0	0.47	1.5	0.40	1.4	0.39	1.2								
4.8	0.58	1.7	0.49	1.6	0.48	1.2								
5.6	0.80	1.8	0.69	1.5	0.71	1.4	0.45	1.3						
7.8	1.06	1.9	1.03	1.6	1.10	1.5								
8.2							0.82	1.2	1.24	2.2	1.20	2.2	1.22	1.8
8.6							0.78	1.3						
8.9	1.06	1.7	1.03	1.7	1.07	1.4			1.23	2.2	1.20	2.0	1.22	1.8
9.0							0.79	1.4						

* 0.01% gelatine was used in this solution to eliminate maxima.

in other groups of compounds, e.g., the double wave in pyruvic acid, have been more or less successfully treated (9, 10). It is not clear at present whether the S-shaped curve requires merely a modification of some of these treatments or whether entirely new concepts are required. An attempt by Saito (11) to use a modification of Brdicka and Wiesner's (9) approach to the problem is quite unsatisfactory. No completely satisfactory treatment of this matter can be formulated at present. Accordingly, the phenomenon of the S-shaped curve is given only brief attention in the present paper.

Consequently, the polarographic behavior of bromoethanoic (HH), 2-bromopropanoic (MH), 2-bromobutanoic (EH), 2-bromo-2-methylpropanoic (MM), 2-bromo-2-methylbutanoic (ME), 2-bromo-2-ethylbutanoic (EE), and 2-bromo-2-ethyl hexanoic (BE) acids was investigated, the first three for comparison with the previous study (1).[4] In order to complete the work, the ethyl esters of five of these acids were also investigated.

Experimental

Experimental conditions differ somewhat from those of previous work (1–3). The following buffer systems, adjusted to an ionic strength of 0.5M, were used: HCl—KCl (*p*H 1 to 2), $HC_2H_3O_2$—$NaC_2H_3O_2$ (*p*H 4 to 6), and NH_3—NH_4Cl (*p*H 8 to 9). The operating temperature was 0° ± 0.1°C; the test solution contained 9.5% ethanol by volume; the mercury head was 50 cm. To determine the nature of the current-controlling processes, temperature coefficients for i_d were found by making supplementary measurements at 25°C. Likewise, supplementary measurements at 75 cm mercury head allowed computation of current ratios for different values of drop-time. The capillary (Corning marine barometer tubing) had a drop-time of 5.94 sec and an m-value of 1.071 mg/sec at open circuit in distilled water (50 cm, 0°C). A Sargent Model XXI Polarograph was used in connection with a Leeds and Northrup student-type potentiometer. All potentials given are corrected for IR drops and are referred to the S.C.E. Beckman Model G and H *p*H meters were used to measure *p*H. In view of the 9.5% ethanol content of the test solutions, strict interpretation of the *p*H values is unwarranted; accordingly, *p*H values are given to only one decimal place in the summary table (Table I) even though measured to ±0.02 *p*H units and so reported in the primary data tables which are available from the authors.

MM, EE, EtBe, EtEE, and EtMM were obtained from Sapon Laboratories. EtEH, EtMH, HH, MH, and EH were Eastman Kodak white label grade chemicals. ME and BE were synthesized. No special attempt was made to purify these compounds, except for ME and BE which were purified in the course of their synthesis. The former distilled at 104°–107°C/8 mm; the latter at 100°–101°C/2 mm. All compounds were found to be polarographically pure.

Test solutions were prepared by diluting a 5-ml portion of stock solution, containing a known concentration of the compound in 95% ethanol, to 50 ml with buffer solution. All stock solutions were

[4] For brevity and clarity, the various acids will be subsequently referred to through the use of the abbreviations indicated. These consist of the initial letters of the substituents, other than bromine, on the *alpha* carbon atom, i.e., H is hydrogen, M is methyl, E is ethyl, etc.; in the case of the ethyl esters, Et will be prefixed, e.g., EtMH is ethyl-2-bromopropionate.

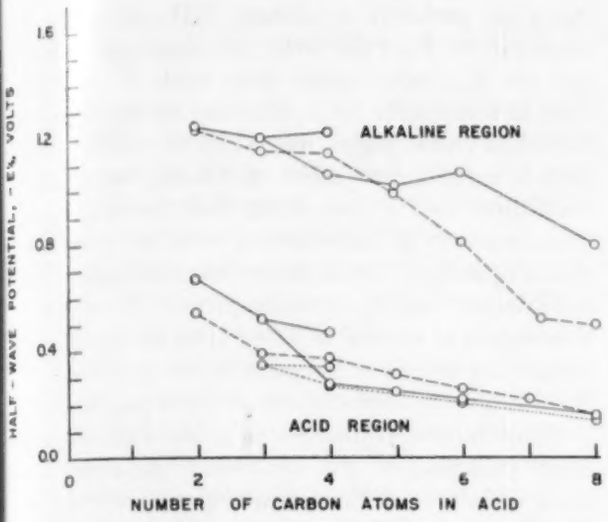

FIG. 1. Relation of $E_{1/2}$ to chain length of the acid for *alpha* bromo acids and their ethyl esters. Solid lines: acids; dotted lines: esters; dashed lines: data for acids in Reference (1).

prepared at 0°; stock and buffer solutions were stored at 0°. Concentration and *p*H values subsequently given are those of the final test solutions. Solutions were deoxygenated with nitrogen, purified as described (2). Base solution (obtained by mixing 95% ethanol with buffer) curves were used in every case to correct the test solution curves.

Choice of operating conditions was governed by the following factors: poor solubility of some of the compounds in water indicated the necessity for a mixed solvent; use of ethanol and the proportion of 9.5% by volume were somewhat arbitrary, being selected on the basis of solubility improvement and minimum $E_{1/2}$ effect. At 25°C, the rapid hydrolysis of some compounds, particularly in alkaline media, even during the relatively short period of deoxygenation and electrolysis, resulted in curves worthless for calculation; this difficulty was effectively eliminated at 0°.

TABLE II. *Effect of structure on half-wave potential for acids and esters*

Acid	Structure	$-E_{\frac{1}{2}}$		Ester	Structure	$-E_{\frac{1}{2}}$
		Acidic region	Alkaline region			
HH	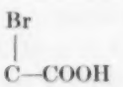	0.67	1.24			
MH	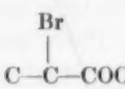	0.54	1.20	EtMH	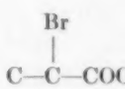	0.35
EH	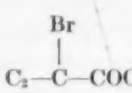	0.48	1.22	EtEH	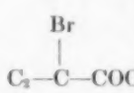	0.34
MM	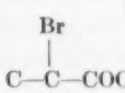	0.28	1.06	EtMM	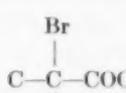	0.25
ME	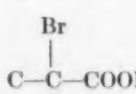	0.26	1.03			
EE	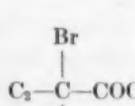	0.22	1.08	EtEE	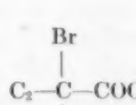	0.21
BE	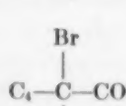	0.15	0.80	EtBE	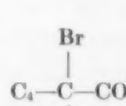	0.14

TABLE III. *Polarographic data for the esters of the 2-bromo acids*

(Temp: 0°C; mercury height: 50 cm)

Ester	pH	Ester conc	$-E_{\frac{1}{2}}$	I
		mM	v	
EtMH	1.07	0.108	0.348	1.82
	1.41	0.169	0.353	1.85
	8.60	0.169	0.368	1.70
EtEH	1.07	0.112	0.336	1.83
	1.41	0.156	0.335	1.63
	8.60	0.156	0.340	1.85
EtMM	1.41	0.546	0.243	1.34
	9.00	0.109	0.268	1.46*
	9.00	0.109	0.269	1.39*
	9.00	0.109	0.268	1.43*
EtEE	1.41	0.509	0.212	1.48
	1.41	0.102	0.205	2.05†
EtBE	1.41	0.116	0.143	1.48

* Maxima present even at this low concentration. Distortion of wave makes these data less accurate.

† The current values here are inexplicably high.

Observed Behavior

All the acids exhibited a sigmoidal variation of $E_{1/2}$ with pH, the curve having flat portions in the acid region below pH 2 and in the alkaline region above pH 8; values of $E_{1/2}$ in these invariant regions are given in Table II and are plotted in Fig. 1 against the number of carbon atoms. Complete data for the acids are available from the authors and are summarized in Table I. Fig. 1 includes a similar plot for the straight chain 2-bromoalkanoic acids (1). Since the latter data were obtained under somewhat different experimental conditions (temperature difference and alcohol absence), the curve is displaced along the ordinate. However, the similarity in the trends of those acids covered by both sets of data (HH, HM, and EH) is such that a qualitative extrapolation may be made for purposes of comparison. This plot and its interpretation constitute the basis of much of the subsequent discussion.

In the acid region, the acids exhibit a continuous decrease in (negative) $E_{1/2}$ with chain length, i.e., they become more easily reducible. However, the difference in $E_{1/2}$ between MH and EH is very much less than that between other neighboring pairs of acids. There is a sharp break between straight chain acids and their branched chain isomers, the latter being more easily reducible. Following this break, the trend is almost the same for both series.

In the alkaline region, the situation is more complicated. In general, $E_{1/2}$ again decreases continuously with increasing molecular weight in both series of acids. The pattern of the decrease is not, however, perfectly consistent. EH, ME, and EE seem out of line; the latter, in particular, actually has an $E_{1/2}$ value larger than both its neighbors. This is responsible for a crossover in the curves for branched and straight-chain acids (even when allowance is made for the effect of differing experimental conditions used in assembling data for each curve). This crossover is not expected to be reversed, since the complexity of these curves has a straightforward explanation, which is subsequently discussed; in this regard, it should be noted that the onset of the complexity occurs at the point in the series at which there is an ethyl substituent in the α position.

Temperature coefficients of i_d and current ratios upon variation of the drop-time (mercury head) agree closely with theoretical values consequent to diffusion-controlled current-producing processes. Values of α [the empirical constant in the equation for $E_{1/2}$ (12)] vary from 0.6 or 0.7 in the acidic region to 0.3 or 0.4 in the alkaline region. Diffusion current constants, I, are lower in the alkaline region than in the acidic region, passing through a minimum in the intermediate region.

The $E_{1/2}$ values for the esters (Table III) are invariant with pH. Such slight variations as do occur can be attributed to the specific effect of the buffer systems used. Variation of ester $E_{1/2}$ with number of carbon atoms in the parent acid is shown in Fig. 1. The ester $E_{1/2}$ is in each case very close to $E_{1/2}$ of the corresponding acid in the acidic region, being slightly less negative. These results agree with previous observation (4, 5). The activating influence of the carbonyl group on the carbon-halogen bond fission is emphasized by the fact that the β-bromoalkanoic acids and esters do not show reduction within the observable potential range. It is interesting that the slight difference between EtMH and EtEH appears to reflect the situation for the corresponding acids.

Discussion

Variations of $E_{1/2}$ with pH and with chain length indicate that at least three effects are operative, i.e., data obtained can be explained only by the action of all three and, in that sense, are evidence for them. These effects are: (*a*) short range, electrostatic effects; (*b*) steric effects involving those molecules which have an α ethyl or larger substituent; and (*c*) bulk effects (adsorption, orientation). In addition, there exists the important question of mechanism.

Dependency of $E_{1/2}$ on pH

Although a detailed analysis of the sigmoid relation between $E_{1/2}$ and pH cannot now be presented,

certain aspects of the phenomena involved will be discussed.

The appearance of only one diffusion-controlled polarographic wave in the fission of the carbon-halogen bond in α-halo acids and esters indicates that the kinetic process of acid-anion equilibration is not directly rate-controlling. Consequently, one or another of the following processes probably prevails. (*A*) Only one of the equilibrium forms is reducible over the potential span used; its $E_{1/2}$ is *p*H-dependent. (*B*) Both forms are reducible, and the form reducible at the less negative potential is reduced preferentially over the whole *p*H range; its $E_{1/2}$ is *p*H-dependent. (*C*) Both forms are reducible and one or both of the forms have $E_{1/2}$ *p*H-dependent; the separate curves of $E_{1/2}$ vs. *p*H cross, i.e., one form is preferentially reduced over one end of the *p*H range, and the other form over the other end. (*D*) Both forms are reducible with *p*H-independent $E_{1/2}$; the rising portion of the curve is due to some as yet undetermined feature of the electrode process kinetics.

It is highly probable that the more readily reducible form is the undissociated acid. Brdicka and Wiesner (9) made this assumption in the case of pyruvic acid; their mathematical treatment produced calculated results in good agreement with the data. Secondly, the ethyl esters of the haloacids, which are more closely related to the undissociated acid form than to the anion of the parent acid, have *p*H-invariant $E_{1/2}$ values very close to those of the acids in the acid region [Fig. 1, Table III (4, 5)]. It is important in this connection to emphasize that the data on the esters indicate the fundamental phenomenon of carbon-halogen bond fission to be itself *p*H-independent; thus, the *p*H-dependence of $E_{1/2}$ for the acids must be ascribed to other phenomena.

Electrostatic Effects

Without entering into mechanism at this point, it appears that the initial decrease in $E_{1/2}$ in going from HH to MH and the sharp drop in going to MM (and similarly with the esters) are best explained by the electron drift from the alkyl substituents, i.e., by a permanent polarization effect. Such an hypothesis requires a tapering off of this effect after one or two carbon atoms (13); this expectation is contradicted by the data. Consequently, other effects must enter into the situation when the α alkyl substituent is ethyl or larger.

Using the data reported in this paper for the α-bromoalkanoic acids (with the exception of BE) at *p*H 1.1, Taft (14) has been able to correlate $E_{1/2}$ values with polar substituent σ-values similar to those developed by Hammett (15). The calculated ρ-value for this correlation is 0.397 ± 0.012. However, BE does not fit this correlation. Furthermore, the straight chain acids (1) do not correlate at all beyond the first three members, the deviations of the higher members being of such a trend as to indicate that $E_{1/2}$ is becoming positive at too great a rate as the chain length increases. This and other attempts at similar correlation indicate that, if Taft's parameters are indeed reflections of the polar character of the substituents, a polar effect cannot be used to explain the continuing trend of $E_{1/2}$ as the substituent size increases above that of ethyl.

Branching has a very pronounced effect on $E_{1/2}$ (Fig. 1). In the acidic region, the difference in reducibility between corresponding isomers in the straight and branched series varies from 0.20 to 0.13 volt in going from the C_4 to C_8 isomers. The difference appears to converge gently, indicating that higher branched acids would be more difficult to reduce; this is in accord with steric effects discussed in the following section. In the alkaline region, the effect of branching is not so clearly delineated, although the effect is evidently present.

The pronounced effect of branching in the acidic region is explicable on the basis of permanent polarization. The combined effects of two alkyl substituents on the same carbon atom will be much greater than the effect of one substituent alone. There is ample evidence to support this in the known lability of tertiary carbon atoms as compared with the secondary or primary carbon atoms. Elving and Westover (16) found the polarographic behavior of the butyl bromides to be in accord with the effects observed here, although the differences were not so striking. They find $E_{1/2}$ values of −2.47, −2.44, and −2.35 volts for *n*-butylbromide, *iso*-butylbromide, and *sec*-butylbromide, respectively.

Steric Effects

It is proposed that the complexity of behavior encountered in the alkaline region has its source in the tendency toward stable ring formation found in compounds having chains of at least six members with terminal atoms differing in electronegativity. In each of the acids having α substituents at least as large as ethyl, there is a possibility of forming at least one ring of the form:

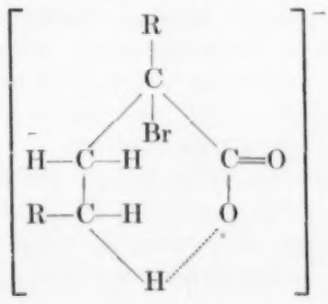

Such rings, if closed by a loose, nonbonding interaction, would possess an augmented steric resistance to reaction; thus, the carbon-bromine bond would gain an increased stability toward fission.

The trend of data supports this hypothesis. It is very obvious (Fig. 1) that EH, for example, possesses an augmented stability. Further, if one compares the $E_{1/2}$ values for MH and PH, it is seen that the difference is much less than that between PH and BH. Thus, the extra stability of EH must also be possessed by larger acids, or else all points after EH should have a more positive $E_{1/2}$ value. It can therefore be concluded from the data that all acids having ethyl substituents or larger have their $E_{1/2}$ shifted to larger negative values.

The concept of *6-number*, devised by Newman (17) in elucidating rules for predicting the rates of certain acid-catalyzed esterifications, fits in well with this behavior. The *6-number* is the number of atoms in the six-position on the acid chain if counting is begun at the carbonyl oxygen. Newman's prediction, that the larger the *6-number*, the larger the steric hindrance to reaction, is borne out by present data. In the straight chain series, the largest *6-number* possible is 3, and the lowest molecular weight acid to possess it is EH. Consequently, it should be expected that EH, PH, BH, and higher acids would be relatively more stable than HH and MH; this is precisely the conclusion reached in the preceding paragraph. In the branched series, the *6-number* values are: MM, 0; ME, 3; EE and BE, 6. Actually, ME is only slightly less stable than MM (Fig. 1), while EE, for which the *6-number* doubles, has a greater (negative) $E_{1/2}$.

Smith (18, 19), Berliner (20, 21), Dippy (22), and Evans (23, 24) have described similar behavior. Dippy's work is of particular interest because of the close association of the compounds studied with those of the present work; he presents ionization constant values for saturated straight chain aliphatic acids out to octanoic, and for certain of their branched chain isomers. There is a consistent decrease in K_i among the straight chain acids except for the striking anomaly of *n*-butanoic acid, whose K_i is greatly in excess of the values for its neighbors in the series. The *n*-butanoic and the succeeding acids lie on a curve which is shifted to higher values of K_i than expected, based on the first two acids of the series. In the branched series, diethylacetic and ethylmethylacetic show a similar shift. These are the parent acids of the very compounds found to show anomalies in the present work.

To explain these phenomena, the authors cited have suggested formation of a cyclic six-member structure whose angles conform more closely than any other ring structure to the normal tetrahedral bond angle for carbon. Stabilization of this structure is supposed to be effected by a loose chemical connection which is discussed in terms of hydrogen bonding (Dippy), hyperconjugation (Berliner), and resonance (Evans). Hunter (25), in a review on hydrogen bonding, states that C—H—O bonds are very weak, and are probably manifested only under some directing influence; such bonds are very difficult to detect. Nevertheless, even such a weak influence might exert sufficient stabilization on the structure to produce the effects observed. Thus, in the data on the straight-chain acids (1), the increment of potential associated with the $E_{1/2}$ shift cited (EH) is, as a guess, about 0.1 volt, corresponding to an energy increment for a two-electron process of about 5 kcal/mole; this is of the commonly accepted magnitude for many hydrogen bonds. EE, as can be demonstrated with models, can so dispose itself that the two possibilities for C—H—O bonds can be simultaneously realized, thus accounting for its increased stability.

Thus far, only the alkaline region has been discussed. The reason that EE, for example, does not show as marked an interaction in the acidic region as in the alkaline region is that in the anion carboxylate group there are two oxygen atoms possessing a negative charge; this is not so for the acid carboxyl group, where only one uncharged oxygen is available for closure. In general, the deviation from Newman's rule of six in the acid region must be due to a near "saturation" of this one carboxyl oxygen.

A final proof of this interpretation of the shift of $E_{1/2}$ to more negative values would be the fulfillment of the prediction in the case of the C_8 acids, that di-*n*-*P* (α-bromodi-*n*-propylacetic acid; *6-number* = 6, where 4 of the *6-atoms* are hydrogens) would have an $E_{1/2}$ less than, but close to, that of BE (*6-number* = 6, where 5 of the *6-atoms* are hydrogens). Certainly the $E_{1/2}$ would be greater than that of 2-bromo-octanoic acid. Furthermore, di-*iso-P* (*6-number* = 12) should have a value of $E_{1/2}$ more negative than that of BE, with *iso-P*-*n*-*P* somewhere in between.

In concluding the discussion of steric effects, it must be noted that B-strain (26, 27) may contribute to the effect of branching on $E_{1/2}$, which has been discussed in a previous paragraph in terms of electrostatic effects.

Bulk Effects

It has been shown how electrostatic effects can cause an initial decline in $E_{1/2}$ with chain length, and how the ring formation effect shifts the whole $E_{1/2}$ vs. chain length relation to more negative values. To explain the further decline of $E_{1/2}$ when the chain length has reached a point beyond which

electrostatic factors can cause no significant variation, it is necessary to recognize other factors.

In discussing the straight chain acids, Rosenthal, Albright, and Elving (1) indicate that the apparent conflict with the concept of permanent polarization is due to the operation of such factors as ease of approach to, orientation to, and adsorption on the electrode surface. In particular, they consider that adsorption may be the principal factor in causing the steady decrease in $E_{1/2}$ with chain length. Adsorption on mercury of the normal primary alcohols from the vapor phase shows a regular increase in free energy as chain length increases (28). Further confirmation is found in the fact that the ease of adsorption of long chain acids, esters, and alcohols from hydrocarbon solution onto metals increases with chain length (29). If a similar situation exists in the case of adsorption of the acids on mercury from aqueous solution, and if the adsorption is fast enough so that it is not the rate-determining step, the electrode reaction could take place within the adsorbed film, and still reveal itself as diffusion-controlled. Thus, differences in the energy of adsorption would contribute to the potential, as well as differences in bond strength, in the acids; the factors may be related. It must be emphasized, in this connection, that data are consistent in indicating diffusion control.

Mechanism

Elucidation of reaction mechanism in a polarographic process is extremely difficult. To be perfectly satisfactory, it must assign, unambiguously, a potential-determining step and a rate-controlling step to the proper chemical processes; these steps are generally masked by the current-limiting process, e.g., diffusion, as in the present case. The nature of the polarographic process makes rate studies impossible. It is often a matter of great difficulty even to determine the nature of the products with certitude. One can only assign steps according to various hypotheses and compare consequences with the data. The authors present the following discussion in full awareness of the limitations of this method; the basis for and value of such treatment has been discussed (8).

Three hypothetical reaction schemes can be described:

[1] S_N1:

$$R_2\overset{Br}{C}COOH \xrightarrow[\text{interphase}]{\text{electrode}} R_2\overset{\oplus}{C}COOH + Br^- \quad \text{(i)}$$

$$R_2\overset{\oplus}{C}COOH + 2e \rightarrow R_2\overset{\ominus}{C}COOH \quad \text{(ii)}$$

$$R_2\overset{\ominus}{C}COOH + H_2O \rightarrow R_2\overset{H}{C}COOH + OH^- \quad \text{(iii)}$$

[2] S_N2:

$$R_2\overset{Br}{C}COOH \overset{2e}{\longleftrightarrow} \left[\begin{array}{c} Br \\ \vdots \\ R_2C\text{—}COOH \\ \vdots \\ \text{electrode} \\ \text{complex} \end{array}\right] \longrightarrow$$

$$R_2\overset{\ominus}{C}COOH + Br^- \quad \text{(i)}$$

$$R_2\overset{\ominus}{C}COOH + H_2O \rightarrow R_2CHCOOH + OH^- \quad \text{(ii)}$$

[3] Free radical:

$$R_2\overset{Br}{C}COOH + e \rightarrow R_2\dot{C}COOH + Br^- \quad \text{(i)}$$

$$R_2\dot{C}COOH \overset{e}{\rightarrow} R_2\overset{\ominus}{C}COOH \xrightarrow{H_2O} R_2CHCOOH + OH^- \quad \text{(ii}a\text{)}$$

or

$$H^+ + e \rightarrow \dot{H} \quad \text{(ii}b\text{)}$$

$$R_2\dot{C}COOH + \dot{H} \rightarrow R_2CHCOOH$$

There is actually little difference between the S_N1 and S_N2 mechanisms in this case, as the following considerations will show. In the description given of the S_N1 reaction, the electron-transfer step (ii) ought to be potential-determining, leaving aside for a moment the possibility of a contribution from adsorption energy. But if this were the case, it would be hard to justify, for example, the effect of branching; entry of reduction electrons would be made more difficult in the branched compound by the augmented electron drift to the carbon center. To restore agreement with the data, it seems necessary to assume that (i) is potential-controlling, which is unreasonable unless the electrons enter simultaneously. But such a situation is exactly the transition state described for the S_N2 mechanism. Thus, it is justifiable to speak of "the" ionic mechanism.

The ionic mechanism accommodates the data in the following respects. The slow step involves attack by electrons, so that it is potential-determining; moreover, there is simultaneous dissociation of the bromide entity, so that the carbon-bromine bond strength must be involved in the potential required for reaction. According to the electron-releasing properties of alkyl groups, bond strengths in the acids ought to decrease in the order HH > MH > EH > MM > ME; this is the order shown by the data, after allowance is made for the magnitude of the *6-effect*. For the longer range decrease of $E_{1/2}$ with chain length, it is necessary to include the concept of a contribution from adsorption energy, discussed in a previous paragraph. The *6-effect* itself is clarified by this mechanism with its pronounced susceptibility to steric influences.

The free radical hypothesis is even more satisfactory, and is considerably more popular (30, 31).

The isolation of dimer products (30, 32–35) is powerful evidence for this mechanism. The potential-determining step in this mechanism may be assigned to the introduction of the first electron, i.e., to step (i). This is reasonable because this step involves bond fission, and, as has been shown, the $E_{1/2}$ values reflect the influence of carbon-bromine bond strengths. Further confirmation can be found in the work of Gardner (36) who studied the reduction of benzophenone. Two diffusion-controlled waves appear in the acid region, each involving a one-electron reduction; the first wave is *p*H-dependent and the second is *p*H-independent, so that the waves merge as the *p*H increases. Gardner postulates a two-step free-radical mechanism for carbonyl group reduction, a radical being produced at the potential of the first wave and reduced at the potential of the second wave. This is completely analogous to the present case, except that the possibility for resonance stabilization in Gardner's postulated intermediate, diphenylhydroxymethyl, is of a much higher order than in the case of the dialkylcarboxymethyl. Consequently, radical destruction in Gardner's case occurs in the acid region at a higher potential than radical formation. In the present case, step (ii*a*) occurs immediately after step (i), the radical having poor stability at potentials requisite for its formation; consequently, there is only one wave. To explain the continuing decline of $E_{1/2}$ at longer chain lengths, the same adsorption phenomenon must be postulated as for the ionic mechanism.

Acknowledgment

The authors wish to thank the Atomic Energy Commission, the Office of Naval Research, and the Research Corporation for grants-in-aid which supported the work described.

Any discussion of this paper will appear in a Discussion Section to be published in the December 1954 issue of the JOURNAL.

REFERENCES

1. I. Rosenthal, C. H. Albright, and P. J. Elving, *This Journal*, **99**, 227 (1952).
2. P. J. Elving, I. Rosenthal, and M. K. Kramer, *J. Am. Chem. Soc.*, **73**, 1717 (1951).
3. I. Rosenthal and P. J. Elving, *ibid.*, **73**, 1880 (1951).
4. P. J. Elving and C.-S. Tang, *ibid.*, **74**, 6109 (1952).
5. I. Rosenthal, C.-S. Tang, and P. J. Elving, *ibid.*, **74**, 6112 (1952).
6. P. J. Elving, J. C. Komyathy, R. E. Van Atta, C.-S. Tang, and I. Rosenthal, *Anal. Chem.*, **23**, 1218 (1951).
7. E. Gergely and T. Iredale, *J. Chem. Soc.*, 1951, 3502.
8. P. J. Elving, *Record Chem. Progr.*, **14**, 99 (1953).
9. R. Brdicka and K. Wiesner, *Collection Czechoslov. Chem. Communs.*, **12**, 138 (1947).
10. J. Loutecky and R. Brdicka, *ibid.*, **12**, 337 (1947).
11. E. Saito, *Bull. soc. chim. France*, **1951**, 957.
12. I. M. Kolthoff and J. J. Lingane, "Polarography," 2nd ed., Vol. I, Interscience Publishers, New York (1952).
13. E. R. Alexander, "Principles of Ionic Organic Reactions," John Wiley & Sons, Inc., New York (1950).
14. R. W. Taft, Jr., *J. Am. Chem. Soc.*, **75**, 4231 (1953).
15. L. P. Hammett, "Physical Organic Chemistry," McGraw-Hill Book Co., New York (1940).
16. P. J. Elving and L. C. Westover, unpublished work.
17. M. S. Newman, *J. Am. Chem. Soc.*, **72**, 4783 (1950).
18. H. J. Smith, *ibid.*, **61**, 254 (1939).
19. H. J. Smith and J. P. McReynolds, *ibid.*, **61**, 1963 (1939).
20. E. Berliner and F. Berliner, *ibid.*, **71**, 1195 (1949).
21. E. Berliner and F. Berliner, *ibid.*, **72**, 222 (1950).
22. J. Dippy, *Chem. Revs.*, **25**, 189 (1939).
23. D. Evans, *J. Chem. Soc.*, **1936**, 785.
24. D. Evans and J. Gordon, *ibid.*, **1938**, 1434.
25. L. Hunter, *Ann. Repts. on Progress Chem. (Chem. Soc. London)*, **43**, 141 (1946).
26. H. C. Brown, H. Bartholomay, and M. D. Taylor, *J. Am. Chem. Soc.*, **66**, 435 (1944).
27. H. C. Brown and R. S. Fletcher, *ibid.*, **71**, 1845 (1949).
28. C. Kemball, *Proc. Roy. Soc. London*, **A190**, 117 (1947).
29. S. G. Daniel, *Trans. Faraday Soc.*, **47**, 1345 (1951).
30. C. L. Wilson, *Record Chem. Progr.*, **10**, 25 (1949).
31. W. A. Waters, "The Chemistry of Free Radicals," Oxford University Press, New York (1946).
32. C. J. Haggerty, *Trans. Am. Electrochem. Soc.*, **56**, 421 (1929).
33. G. W. Wheland, "Advanced Organic Chemistry," 2nd ed., John Wiley & Sons, Inc., New York (1949).
34. P. J. Elving and C. E. Bennett, unpublished work.
35. P. J. Elving and J. T. Leone, unpublished work.
36. H. J. Gardner, *Chemistry & Industry*, **1951**, 819.

Cation Exchange Process for the Preparation of Potassium Cyanide[1]

C. H. Lemke

Research Division, Electrochemicals Department, E. I. du Pont de Nemours & Co., Inc., Niagara Falls, New York

ABSTRACT

Equilibrium data are presented for the reactions of Na + KCN, KCl + NaCN, and KOH + NaCN in the fused state. The latter two reactions were effected by a new "alloy bridge" technique which does not require direct contact of reactant salts. In this manner, potassium cyanide was obtained substantially free of anions other than CN^-. Reaction rate data are presented for reaction of KCl + NaCN by the "alloy bridge" method, and other possible applications of the method are suggested.

Introduction

Chemical equilibria between fused alkali metals and their salts have been extensively studied by Rinck (1) who established equilibria for the systems:

$$KCl + Na \rightleftarrows K + NaCl \qquad (I)$$

$$KOH + Na \rightleftarrows K + NaOH \qquad (II)$$

Reactions (I) and (II) have been used for production of sodium-potassium alloys and metallic potassium.

In such systems, fused metals form layers which float on top of fused salts. It is thus possible to have an alloy layer simultaneously in contact with two separate salt melts. For example, a vessel divided into two compartments by a vertical partition may be used as a reactor to produce KCN from KCl and NaCN. Fused KCl is charged to one compartment, and fused NaCN to the other. Fused sodium metal, which floats on the fused salts, is added until it rises to a level above the top of the partition to form a "bridge" between the two fused salts (Fig. 1). On the chloride side of the reactor, potassium metal is extracted from KCl and replaced by equivalent sodium. Potassium rapidly diffuses through the metallic layer to the cyanide side, where it displaces equivalent Na from NaCN to form KCN. This process of exchanging K and Na between the two salt fusions continues until chemical equilibrium is reached. The resulting melt of KCN—NaCN may in like manner be reacted with a fresh batch of KCl in a second stage of the process, and a further exchange of K and Na will occur with resultant increase in KCN content of the cyanide melt. Similarly, chloride melt from the first stage may be reacted with fresh NaCN to achieve a greater utilization of KCl.

This may be regarded as a double countercurrent extraction in which the fused alloy replaces K with Na on the chloride side and simultaneously replaces Na with K on the cyanide side. Compositions of the alloy bridges in the several stages remain unchanged after the system has been brought to steady operation, and no metallic Na or K is consumed by the process except for mechanical losses. Composition of the cyanide melt and chloride melt at their respective discharge ends can be controlled by varying the number of stages or the ratio of KCl to NaCN fed to the apparatus.

It is evident that this technique is not limited to the application described, but could be used for exchange of alkali cations between hydroxides, bromides, iodides, chlorides, cyanides, or other suitable salts (2). Only salts which melt below the boiling points of the alkali metals and anions which are not readily reduced by alkali metals can be used.

Discussion

Equilibrium Studies

Having Rinck's data for the equilibria represented by reactions (I) and (II) above, it was only necessary to determine the equilibrium in the fused state for reaction (III) to be able to calculate the equilibria for reactions (IV) and (V).

$$NaCN + K \rightleftarrows KCN + Na \qquad (III)$$

$$NaCN + KCl \rightleftarrows KCN + NaCl, \Delta H_{298} = 0.51 \text{ kcal} \qquad (IV)$$

$$NaCN + KOH \rightleftarrows KCN + NaOH, \Delta H_{298} = -5.65 \text{ kcal} \qquad (V)$$

Assuming the law of mass action to hold, Rinck's values for the equilibrium constants for reactions (I) and (II) may be expressed as:

$$\frac{(NaCl)(K)}{(KCl)(Na)} = 0.087 \text{ at } 900°C \qquad (VI)$$

[1] Manuscript received May 5, 1953. This paper was prepared for delivery before the New York Meeting, April 12 to 16, 1953.

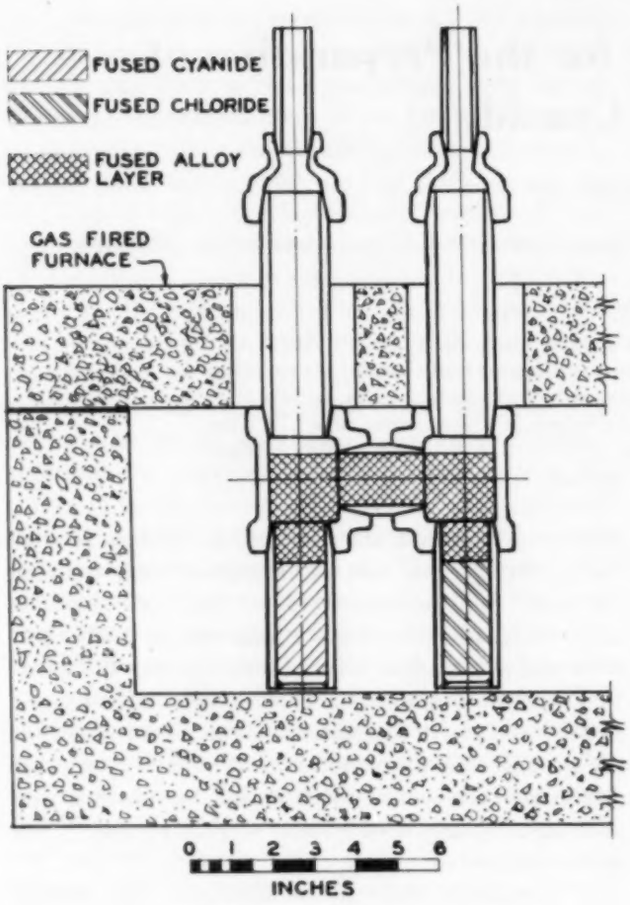

FIG. 1. Apparatus

and

$$\frac{(NaOH)(K)}{(KOH)(Na)} = 2 \text{ at } 700°C \qquad (VII)$$

where the quantities in parentheses represent mole percentages of the respective salts in the salt phase and respective metals in the metal phase.

Experimental value for the equilibrium constant for reaction (III) (Table I and Fig. 2) is:

$$\frac{(Na)(KCN)}{(K)(NaCN)} = 8.7^{2} \text{ at ca. } 680°C. \qquad (VIII)$$

This value was obtained statistically, and the 90% confidence interval for the average constant for reaction (III) is 6.0–11.7. From this result and the values given by Rinck, constants for reactions (IV) and (V) may be calculated as follows:

$$\frac{(Na)}{(K)} = 8.7\,\frac{(NaCN)}{(KCN)} \qquad (IX)$$

$$\frac{(Na)}{(K)} = \frac{1}{0.087}\,\frac{(NaCl)}{(KCl)} \qquad (X)$$

[2] A logarithmic transformation of individually calculated values of the constant for reaction (III) gives an approximately normal distribution of "log C" values. The antilog of the average "log C" value then gives a measure of "C" which is least affected by extreme determinations.

Equating (IX) and (X):

$$\frac{(NaCl)(KCN)}{(KCl)(NaCN)} = 8.7 \times 0.087 = 0.76 \qquad (XI)$$

Thus, the calculated constant for reaction (IV) is approximately 0.76. A similar calculation gives a constant for reaction (V) of 17.4.

These calculated constants indicate that reactions (IV) and (V) are favorable for the production of KCN, using NaCN and either KCl or KOH, respectively, as raw materials.

The equilibrium constant for reaction (IV) was checked experimentally and found to be 1.4 as compared with the calculated value of 0.76. Equilibrium was approached in all cases from the NaCN + KCl side. Experimental data are presented in Table II. These data were analyzed statistically, and the 90% confidence interval for the true value of the equilibrium constant is 0.9–2.0.

Fig. 3 shows a plot of experimental data and the spread covered by the 90% confidence interval.

The equilibrium constant for reaction (V) was checked at three points, starting in all cases from the NaCN + KOH side. Reactions of K and KOH

TABLE I. *Experimentally determined equilibrium for the reaction* K + NaCN ⇄ KCN + Na

Mole % K in alloy	Mole % KCN in cyanide	°C	Calculated log C*
Part 1: Points determined by analysis of alloy and stoichiometric calculation of cyanide composition.			
24.2	74.0	650–690	0.949
15.7	81.0	650	1.360
17.0	61.5	580–620	0.892
10.8	83.5	650–700	1.621
42.0	85.0	680–690	0.892
41.0	38.0	650–670	−0.046
10.8	56.2	520	1.025
Part 2: Points determined by analysis of both phases.			
2.0	39.8	600	1.511
17.2	73.3	680	1.121
7.8	60.9	660–675	1.265
46.0	90.6	640–660	1.053
52.3	90.5	650–680	0.940
3.5	23.2	740–770	0.919
12.5	57.0	760–780	0.969
3.6	29.4	780–820	1.045
16.4	48.5	730–820	0.681
35.1	69.5	740–760	0.623
4.4	21.9	620–640	0.785
21.8	40.2	550–650	0.380
80.2	96.3	620–660	0.806
Average			0.940
C			8.7

* $C = \frac{(Na)(KCN)}{(K)(NaCN)}$.

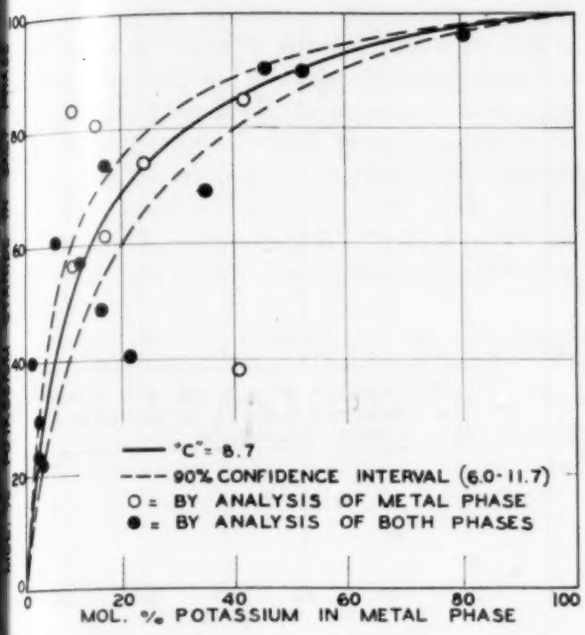

FIG. 2. Equilibrium data; K + NaCN ⇌ KCN + Na

such as 2K + KOH ⇄ K_2O + KH are known to occur, but such side reactions were neglected in this study. The experimental value of the constant, 7.5, compares with the calculated value of 17.4. Experimental data are given in Table III and are plotted in Fig. 4, which also shows reaction curves corresponding to the equilibrium constants 7.5 and 17.4. It has been estimated that the difference in the two curves corresponds to about one stage in a countercurrent process for KCN from KOH and NaCN.

Effect of Temperature on Equilibria

Heats of reaction for (IV) and (V) are small. From the van't Hoff equation (3) it may be expected that the effect of temperature on the equilibrium constant will be small, and no attempt was made to determine this effect. Equilibrium studies were all made at temperatures which would be required for operation of a commercial process.

TABLE II. *Experimentally determined equilibrium for the reaction* KCl + NaCN ⇄ KCN + NaCl

Mole % KCN in cyanides	Mole % KCl in chlorides	°C	Calculated log C†
39.8	46.4	800	−0.097
23.2	9.8	740–770	0.447
29.4	22.5	780–820	0.146
48.5	23.6	730–740	0.477
69.5	74.4	750–770	−0.097
61.6	57.2*	710–760	0.079
63.6	72.3*	740	−0.155
85.5	73.5	680–720	0.322
Average			0.140
C			1.4

* 3-5% cyanide was found in the chloride melts from these runs; all others were cyanide free.

† $C = \frac{(NaCl)(KCN)}{(KCl)(NaCN)}$.

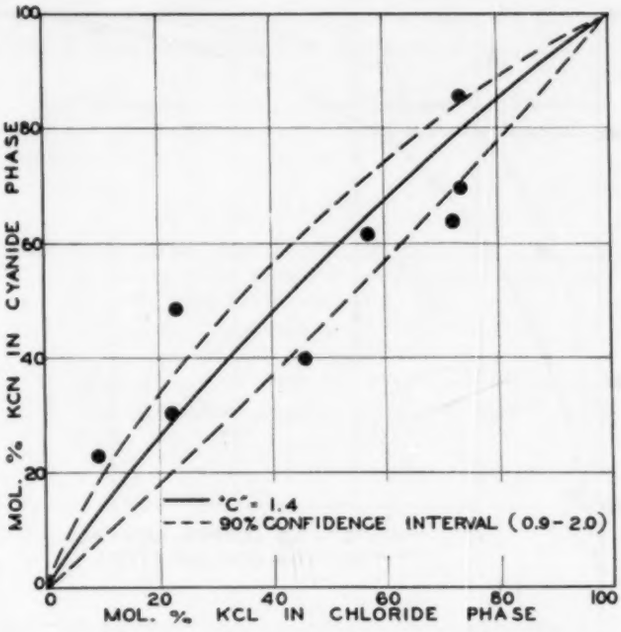

FIG. 3. Equilibrium data; KCl + NaCN ⇌ KCN + NaCl.

Reaction Rate

A limited amount of work was done to obtain order-of-magnitude rate data for the reaction: KCl + NaCN ⇄ KCN + NaCl when carried out by the alloy bridge method.

The mechanism of this reaction is complex. Two reactions are involved:

$$KCl + Na \rightleftarrows NaCl + K$$

$$NaCN + K \rightleftarrows KCN + Na$$

These are linked to each other by the layer of fused K—Na alloy in contact on one end with the fused KCl—NaCl melt, and on the other end with the

TABLE III. *Experimentally determined equilibrium for the reaction* KOH + NaCN ⇄ KCN + NaOH

Mole % KCN in cyanides	Mole % KOH in hydroxides	°C	Calculated log C*
61.5	9.7	580–620	1.173
21.9	5.0	620–660	0.724
96.3	83.0	620–660	0.724
Average			0.874
C			7.5

* $C = \frac{(NaOH)(KCN)}{(KOH)(NaCN)}$.

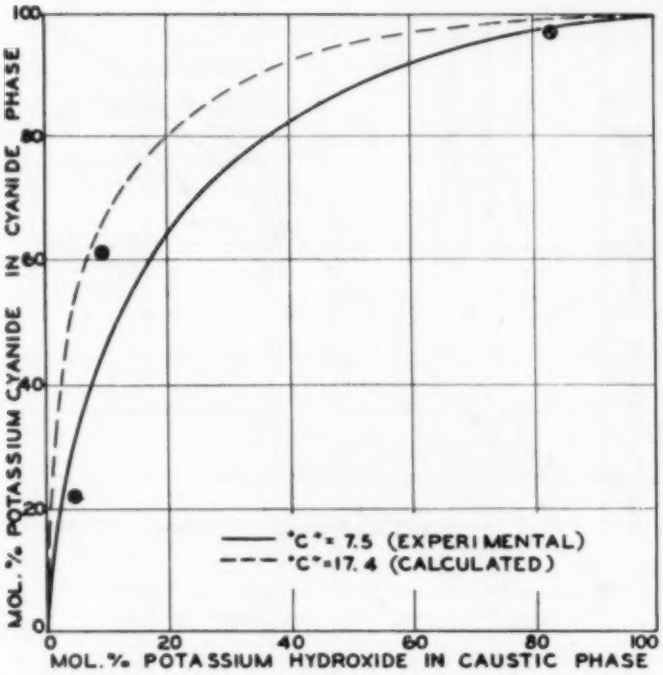

FIG. 4. Equilibrium data; KOH + NaCN ⇌ KCN + NaOH.

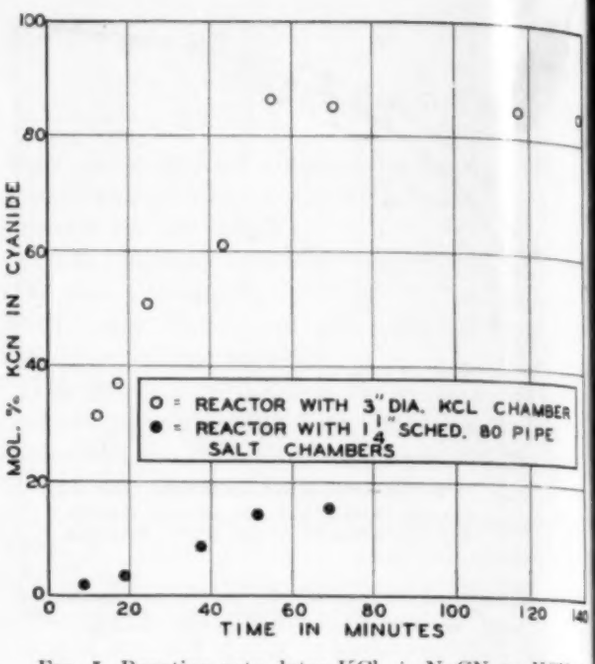

FIG. 5. Reaction rate data; KCl + NaCN ⇌ KCN + NaCl.

fused KCN—NaCN melt. The rate of reaction may be limited for any given set of conditions by rate of either of the above reactions or rate of transport of K and Na to opposite ends of the bridge.

No effort has been made to measure these quantities independently. It was not practical in the laboratory to operate a continuous countercurrent system. Therefore, all measurements were made on a batch basis. Based on earlier studies involving the above reactions, it was probable that the rate of reaction would not be the limiting factor. This supposition is substantiated by data which show that the over-all reaction does not slow down as equilibrium is approached.

Results of the rate experiments are summarized in Table IV and plotted in Fig. 5. Rates of the order of 0.2 kg KCN/hr/dm² (4 lb/hr/ft²) were obtained, based on total contact area.

TABLE IV. *Results of the rate experiments for the reaction* KCl + NaCN ⇌ KCN + NaCl

	Both salt chambers of 3.25 cm ID	KCl chamber 7.62 cm ID, NaCN chamber 3.25 cm ID
Kg KCN made/hr/dm², based on:		
Cyanide—alloy contact area	0.23	0.88
Chloride—alloy contact area	0.23	0.16
Combined contact area	0.11	0.14
Average temperature, °C	725	730

EXPERIMENTAL

Apparatus

Steel pipes 1.9 cm ID and 25 cm long were used to study the reaction K + NaCN ⇌ KCN + Na. These pipes were closed by welding a plate in the bottom, and a rapid stream of purified nitrogen was fed to the open upper end to prevent oxidation. The pipes were heated by immersion to a depth of about 15 cm in a fused NaCl-$CaCl_2$ bath.

The apparatus used for the bridge reaction studies was an H-tube as shown in Fig. 1. This was made of steel pipe approximately 3.25 cm ID (A.S.A. Standards B-36, 10-1939 1¼ in. schedule 80 steel pipe) connected with pipe fittings. Bottom ends of the legs were closed with steel plate welded in place. Top ends were threaded and fitted with connections for purified nitrogen, thermocouple wells, and openings for removal of samples.

A special apparatus was constructed for part of the rate study. This was essentially an H-tube as shown in Fig. 1, except that one leg was made of 7.62-cm (3-in.) ID tubing. The H-tubes were heated in a gas-fired furnace controllable to ±50°C.

Procedure

Weighed quantities of the dry salts, KCl, KOH, NaCN, etc., as desired, were charged to the salt compartments and melted. The apparatus was blanketed with nitrogen, and weighed amounts of sodium and/or potassium were charged to the reactor.

Obtaining clean, representative samples presented many difficulties. Ultimately, samples of the fused

salts and alloys were taken by steel pipettes at temperatures of 650°–800°C. Salt samples were cast on a slab of cold iron, and alloy samples were quenched in cold white mineral oil. In nearly all cases there were small globules of alkali metal present in the salt samples. So far as possible, these were removed by hand sorting. Oil quenching of alloy samples did not entirely prevent oxidation. Under such circumstances it is known that potassium is selectively oxidized.

Potassium was determined by the perchlorate method. Potassium content of alloy samples was checked by freezing point determination (4). Sodium components were calculated by difference. Results were not corrected for the small amounts of iron which were determined in some samples.

Any discussion of this paper will appear in a Discussion Section to be published in the December 1954 issue of the JOURNAL.

REFERENCES

1. E. RINCK, *Ann. chim.* (*Paris*), **18,** 395 (1932).
2. C. H. LEMKE (to E. I. du Pont de Nemours & Co., Inc.) U. S. Pat. 2,533,593, December 12, 1950.
3. S. GLASSTONE, "Textbook of Physical Chemistry," 2nd ed., p. 828, D. Van Nostrand Co., Inc., New York (1946).
4. G. VAN BLEISWIJK, *Z. anorg. u. allgem. Chem.*, **74,** 152 (1912).

Technical Note

Semiconductors as Solid Electrolytes in Electrochemical Systems[1]

KURT LEHOVEC[2] AND JACOB BRODER

Signal Corps Engineering Laboratories, Fort Monmouth, New Jersey

INTRODUCTION

There are many applications of batteries where weight and space are of concern. Considerable progress in the miniaturization of batteries would be achieved if the liquid electrolyte, conventionally used in present batteries, could be replaced by a solid ionic conductor.

At the end of 1951, the authors started the development of "solid state batteries," which was directed toward two types of batteries: (*a*) a high current density "single-shot" battery; (*b*) a low current density long-life battery for use in connection with the transistor device. This note describes the initial phase of the program until the summer of 1952, when one of the authors (K. L.) left this laboratory.

THEORY

Consider a compound, AB, sandwiched between two phases A and B, to which electrodes are applied. If at least one of the phases A or B can migrate through the reaction product, AB, the reaction $A + B = AB$ can proceed. Under favorable conditions, to be discussed later, the free energy of the reaction gives rise to an emf between the phases A and B. Such a system is the prototype of a solid state battery.

In ionic compounds AB, the migration of A or B takes place in the form of ions. Usually only one of the components is mobile, say A^+. If the ions A^+ were the only charges to move from A to B, then phase B would aquire a positive charge and the reaction would stop soon because of repulsion of further ions A^+, approaching B. However, a continuous reaction is possible if migration of ions A to B is accompanied by a transfer of electrons from A to B. Transfer of electrons from A to B can occur in a twofold manner: (*a*) externally through a metal connection between A and B (external load), or (*b*) internally by means of partial electronic conduction[3] of AB. In the absence of an external connection, the partial electronic conduction of AB, even if very small as compared to the ionic conduction, becomes rate-determining for the progress of reaction AB and determines, therefore, the life of the battery under open circuit condition (shelf life). It is well to emphasize that the partial electronic conductivity of ionic compounds is not a constant of the material, but depends on impurities and on deviations from stoichiometry. There is no basic difference between the progress of the reaction in a solid state battery under open circuit conditions and tarnishing reactions. The importance of the electronic partial conductivity for tarnishing reactions (1) and the role of minute amounts of impurities (2) are well known.

For compound AB to be a suitable electrolyte for a solid state battery, the following requirements have to be fulfilled:

[1] Large free energy decrease, $-\Delta F$, of the reaction $A + B = AB$.

[2] Electronic transference number negligible: $\sigma_e \ll \sigma_i$.

[3] Ionic conductivity σ_i of high absolute value.

[4] Electronic conductivity σ_e of low absolute value. Conditions [1] and [2] are necessary for a high emf, since the emf at zero load is (1): $(\Delta F/e)\cdot \sigma_i/(\sigma_i + \sigma_e)$.[4] Condition [3] is necessary for a high short circuit current; condition [4] is necessary for a long shelf life.

Conditions for a good solid electrolyte have been formulated above in terms of its bulk properties only. There are further conditions which deal with ease of transfer of ions and electrons over the interphase boundaries A/AB and AB/B (3). Ions A^+ must be able to cross these boundaries easily in order to avoid polarization phenomena, when drawing current from the battery, i.e., the concentration of A^+ in AB at the boundaries A/AB and AB/B should not be modified by the current flow. On the

[1] Manuscript received August 27, 1952.

[2] Present address: Sprague Electric Company, North Adams, Massachusetts.

[3] Both the movement of electrons in the "empty energy band" and the movement of holes in the "filled energy band" may contribute to the electronic conduction.

[4] In the case that σ_i and σ_e are space dependent, average values are to be used.

other hand, harmful internal electron conduction can be decreased by presence of barrier layer effects at the electrode interfaces (4, 5).

High Current Density "Single-Shot" Battery

For a solid state battery capable of delivering a high current density, a compound of high ionic conductance has to be used as electrolyte. Ionic conductivity of the order of 1 $ohm^{-1}cm^{-1}$ is found in the high temperature modifications of AgI, Ag_2S, and of Ag_2HgI_4, among others. Their ionic conductivity compares favorably with that of strong liquid electrolytes. High ionic conductivity results from the peculiar lattice structure of these compounds: only the anion is bound to fixed lattice positions whereas the cations are distributed at random over a number of equivalent lattice positions, exceeding the number of cations available (6–8).

The authors experimented with systems involving the high temperature modification of AgI and Ag_2S. Tubandt and Lorenz (9) measured the conductivity of AgI both above and below the transition point (145°C) and found 1.31 $ohm^{-1}cm^{-1}$ above 145°C, and 3.4×10^{-4} $ohm^{-1}cm^{-1}$ just below 145°C. Conductivity is almost completely ionic. The emf of the combination Ag, AgI, I_2 has been reported as 0.7 volt (10). However, because of immediate difficulties associated with operation of an I_2 electrode at or above 145°C (the transition point above which AgI has a high ionic conductivity) this work was directed to an examination of the reaction $2Ag + S = Ag_2S$. The reaction product, Ag_2S, is a relatively good conductor above 179°C, but at this temperature a large portion of the conductivity is electronic. Thus, although the free energy change corresponds to an emf of 0.2 volt, Wagner (11) found that an Ag-Ag_2S-S cell above 179°C gave an emf of only 2–10 millivolts. In order to obtain the full 0.2 volt corresponding to the ΔF of formation of Ag_2S, it is necessary to suppress the electronic conduction. This is possible by inserting a layer of AgI (10), which is nearly a purely ionic conductor above 145°C.

A cell of composition Ag, AgI, Ag_2S, S was constructed as follows: an AgI-film of about 25 microns thickness was prepared on an Ag-sheet by tarnishing in iodine vapor. The sulfur electrode consisted of a sulfur-carbon mixture of composition 15%S–85%C by weight compressed into a pellet at 7000 atmospheres. The Ag_2S-layer was formed upon contact of the sulfur electrode with the AgI/Ag. The open circuit voltage of the cell at about 200°C was 0.2 volt, confirming Reinhold's value (10). Short circuit currents of 0.18 amp/cm^2 were obtained. Shelf life of the cell at operating temperature (200°C) was about 100 min.

Comparison of (*a*) the observed current density with ionic conductance of AgI (9) and of Ag_2S (12), and (*b*) of the shelf life of the cell with rate of tarnishing of AgI (13) suggests that there was considerable interface resistance present in these cells.

For a cell of high current density, which is useful at lower temperatures (and possibly at room temperature), other compounds, e.g., Ag_2HgI_4 and $Ag_xCu_{1-x}I_4$, appear to be promising.[5]

Low Current Density Long Life Cells

The authors have constructed cells of the composition Ag-AgI-I(+C) operating at room temperature with current densities of several hundred microamps/cm^2. The emf of this combination is 0.7 volt (10). Cells did not change during the period of this study.

Acknowledgment

The authors wish to express their gratitude to Dr. J. N. Mrgudich for his helpful discussion of and interest in this topic.

Any discussion of this paper will appear in a Discussion Section to be published in the December 1954 issue of the Journal.

References

1. C. Wagner, *Z. physik. Chem.*, **B21**, 25 (1933).
2. K. Hauffe, *Ann. Physik*, **18**, 201 (1950).
3. W. Schottky, *Wiss. Veröff. Siemens-werken*, **14**, 10 (1935), see for detailed treatment.
4. K. Hauffe and W. Pfeiffer, *Z. Elektrochem.*, **56**, 390 (1952).
5. H. J. Engell and K. Hauffe, *Metall*, **6**, 285 (1952).
6. L. W. Strock, *Z. physik. Chem.*, **B25**, 441 (1934).
7. J. A. A. Ketelaer, *Z. physik. Chem.*, **B26**, 327 (1934).
8. J. A. A. Ketelaer, *Trans. Faraday Soc.*, **34**, 875 (1938).
9. C. Tubandt and F. Lorenz, *Z. physik. Chem.*, **B7**, 513, 560 (1914).
10. H. Reinhold, *Z. Elektrochem.*, **40**, 361 (1934).
11. C. Wagner, *Z. physik. Chem.*, **B21**, 42 (1933).
12. H. Reinhold and K. Schmitt, *Z. physik. Chem.*, **B44**, 75 (1939).
13. C. Wagner, *Z. Elektrochem.*, **40**, 364 (1934), footnote 4.

[5] A paper on the preparation and properties of this compound will be published in the near future by Dr. L. Suchow of the Signal Corps Engineering Laboratory.

Quantitive or Qualitative Analyses
—Organic or Inorganic—

made rapidly and accurately
with the
FISHER ELECDROPODE

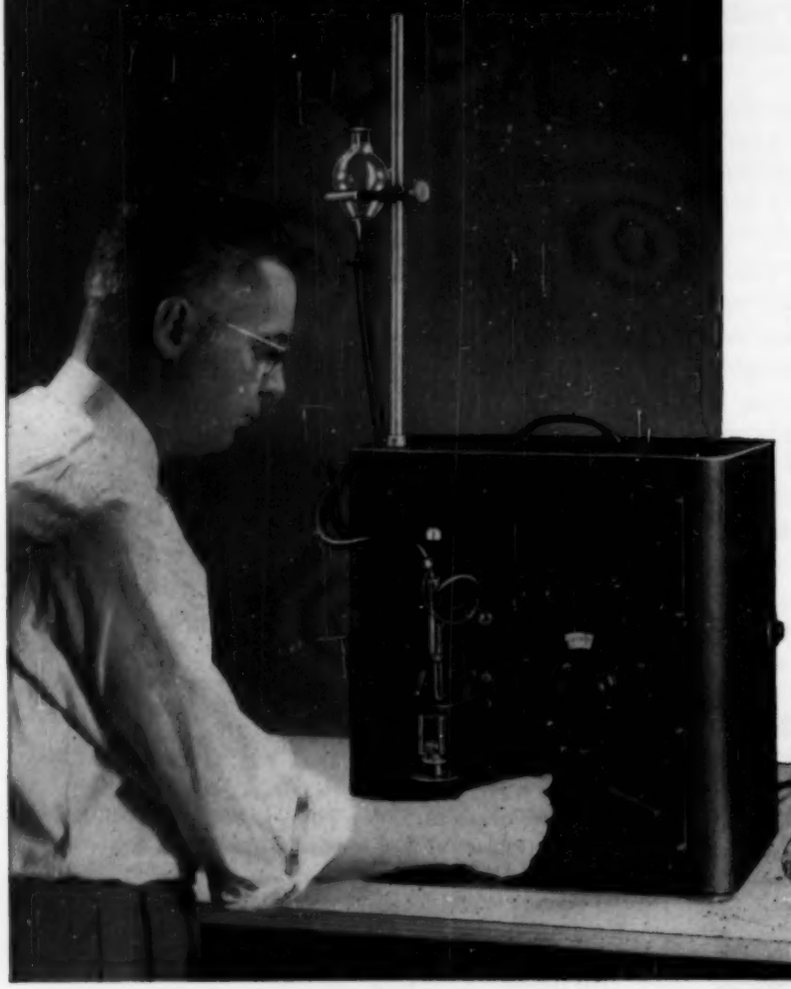

The Fisher Elecdropode employs the dropping mercury electrode system and is the leading analytical instrument for determining chemical composition by this rapidly growing technique.

It has been used very successfully in such analyses as lead in citric acid; copper lead and cadmium in commercial zinc; copper, nickel and cobalt in steels; oxygen in biological solutions; the many elements in the ash of plant tissue; traces of dyes, lyophilic colloids, fatty acids and alkaloids . . . and will perform any of the other analytical tasks that are possible with more expensive instruments.

It is a simple-to-operate instrument and analyses are accomplished in a few minutes. Only a small sample of solution is required (less than 10 ml). The sample is not altered during the analysis and may be recovered for further study.

It is a completely integrated unit . . . comes complete with cell . . . no additional accessories are needed.

Write for Booklet FS-236-11 for complete description and uses of this moderately priced instrument.

Each different ion causes a current increase at a particular voltage. Its concentration is denoted by the extent of increase.

FISHER SCIENTIFIC

PITTSBURGH (19) 717 Forbes St.
NEW YORK (14) 635 Greenwich St.
ST. LOUIS (18) 2850 S. Jefferson Ave.
MONTREAL (3) 904 St. James St
WASHINGTON 7722 Woodbury Dr. Silver Spring, Md.
TORONTO (8) 245 Carlaw Ave.

America's Largest Manufacturer-Distributor of Laboratory Appliances and Reagent Chemicals